INVESTIGATING THE ECOLOGICAL CONTROLS ON METHANE PRODUCTION IN A RIPARIAN COTTONWOOD FOREST AND ADJACENT RIVER

KRISTIAN SMITS
Bachelor of Science, Mount Royal University, 2019

A thesis submitted
in partial fulfilment of the
requirements for the degree of

MASTER OF SCIENCE

in

BIOLOGICAL SCIENCES

Department of Biological Sciences
University of Lethbridge
LETHBRIDGE, ALBERTA, CANADA

INVESTIGATING THE ECOLOGICAL CONTROLS ON METHANE PRODUCTION IN A RIPARIAN COTTONWOOD FOREST AND ADJACENT RIVER

KRISTIAN SMITS

Date of Defense: August 9, 2021

Dr. L. Flanagan Thesis Supervisor	Professor	Ph.D.
Dr. L. Selinger Thesis Examination Committee Member	Professor	Ph.D.
Dr. S. Rood Thesis Examination Committee Member	Professor Emeritus	Ph.D.
Dr. R. Golsteyn Chair, Thesis Examination Committee	Associate Professor	Ph.D.

Abstract:

This study explored how the chemical nature of organic matter may drive microbial communities and their metabolic processes of methane production in the Oldman River sediment and adjacent riparian cottonwood tree stems in southern Alberta. Carbon (C) and nitrogen (N) content in tree stems and river sediment environments were measured, while molecular genetic techniques and stable carbon isotope measurements were used to explore the microbial communities and methane production pathways. River sediment organic matter had lower C/N ratios than in tree stems, likely forming different substrates for microbial growth, resulting in contrasting microbial communities and greater microbial diversity observed in river sediments than in tree stems. The microbial communities differed in their metabolic pathways, with methane produced in tree stems occurring primarily through CO_2 reduction, while river sediments produced more methane through acetate fermentation. This study highlights distinct microbial communities and metabolic pathways contributing to net ecosystem methane emission.

Acknowledgments

I would like to extend my deepest gratitude to my thesis supervisor Dr. Larry Flanagan, who's expertise and guidance was the foundation for my growth throughout this project. I am also grateful to my committee members Dr. Brent Selinger, who was willing to offer assistance at the drop of a hat, and Dr. Stewart Rood, for his encouragement and insight. I also wish to thank Dr. Jenny McCune for letting me attend her ecology labs, and Dr. David Pearce for taking me to the field site and helping with tree identification. I would also like to thank Daniel Grant, who was integral in updating a DNA database used in this project.

I would like to acknowledge my late father Darren Smits, who saw my potential as limitless and pushed me to see his vision. I would not be the man I am today if not for his love and dedication. My success would not have been possible without my mother Larissa West, whose unwavering support allowed me to overcome failures and hardships. Thank you to my dog Noble, who kept me company in my first year, and sane in my second. Lastly, thank you to my friends and family who supported me over the last two years.

This study was made possible by research grant funds to L.B. Flanagan from the Natural Sciences and Engineering Research Council of Canada (NSERC), and Alberta Innovates grant to S.B. Rood and L.B. Flanagan.

Table of Contents

List of Tables

List of Figures

List of Abbreviations and Symbols

Acetoclastic = Acetate fermentation pathway of methane production

ASV = Amplicon sequence variant

CH_4 = Methane

CO_2 = Carbon dioxide

C_{Org} = Organic Carbon

C:N = Ratio of Carbon mass to Nitrogen mass

DBH = Tree diameter at breast height

H_2 = Molecular hydrogen

HSNR = Helen Schuler Nature Reserve

Hydrogenotrophic = CO_2 reduction pathway of methane production

mcrA =Methyl-coenzyme reductase α subunit

Methanogen = Methane producing obligate anaerobic Archaea

Methanogenic = The specific pathway of methane production performed

Methanogenesis = Metabolic process of methane production by methanogens

Methanotroph = Methane consuming aerobic bacteria

N_2 = Molecular nitrogen

NMDS = Non-metric multidimensional scaling

PCR = Polymerase chain reaction

PPB = Parts per billion (nmol mol^{-1})

PPM = Parts per million (μmol mol^{-1})

16s rRNA = Nucleotide sequence for the small subunit of ribosomal RNA

$\delta^{13}C$ = Carbon isotope ratio ($^{13}C/^{12}C$) in delta notation (see eq. 2)

‰ = Parts per thousand or per mil

ΔCH_4 = Change in CH_4 concentration

ΔCO_2 = Change in CO_2 concentration

1. INTRODUCTION

1.1 Natural methane production and emission

Forests and freshwater streams play an uncertain role in the global methane budget (Stanley *et al.*, 2016; Barba *et al.*, 2019; Saunois *et al.*, 2020). Natural ecosystems can harbour a consortium of anaerobic microorganisms whose metabolic activities decompose organic matter, with methane produced in the final stage by a diversity of Archaea known as methanogens (Conrad, 1999; Enzmann *et al.*, 2018; Lyu & Liu, 2018). Uncertainty in natural methane emissions stems from limited research into the microbial ecology and details of the methane production pathways (Barba *et al.*, 2019; Covey & Megonigal, 2019). A more nuanced understanding of the microbial community involved in methane production and their associated biogeochemical pathways are required for the creation of accurate mechanistic models, that can lead to the development of mitigation strategies to reduce net methane emissions to the atmosphere (Wang *et al.*, 2016; Barba *et al.*, 2019; Conrad, 2020a).

Decomposition of organic matter to methane has four main stages that operate in a complimentary fashion, which are performed by a diverse community of microorganisms in anaerobic environments (Whiticar, 1999; Conrad, 2020a). The first stage is performed by hydrolytic and fermenting bacteria, which break down complex polymeric substrates into simple monomers (Whiticar, 1999; Conrad, 2005). Hydrolytic and fermenting bacteria are highly diverse, with most known to belong to the phyla Bacteroidetes and Firmicutes (Nozhevnikova *et al.*,

2020). Second, acidogenic fermenting bacteria ferment the simple monomers into smaller compounds such as alcohols and volatile fatty acids (Whiticar, 1999; Nozhevnikova *et al.*, 2020). Acidogenic bacteria involved in anaerobic methane production belong to the phyla Bacteroidetes, Chloroflexi, Firmicutes and Proteobacteria (Nozhevnikova *et al.*, 2020). Next, syntrophic organisms such as *Syntrophomonas* degrade the products from previous stages to form the substrates (primarily H_2, CO_2, and acetate; discussed in following paragraph) required for methane production (Nozhevnikova *et al.*, 2020). Anaerobic fungi can also be present and are capable of breaking down many classes of molecules (Chapin *et al.*, 2011; Buresova *et al.*, 2019; Ma *et al.*, 2020). Methane production (methanogenesis) is the final stage of organic matter decomposition performed by Archaea known as methanogens (Whiticar, 1999; Lyu & Liu, 2018).

Methanogens are phylogenetically diverse obligate anaerobic methane producers belonging to Euryarchaeota*,* and possibly other archaeal phyla (Evans *et al.*, 2015; Lang *et al.*, 2015; Lyu & Liu, 2018). Methanogens are obligate anaerobes that fulfill a wide range of environmental niches and use a multitude of substrates for their metabolic pathways of methane production (H_2 + CO_2, acetate, formate, CO, methanol, secondary alcohols, methylamine and methoxylated aromatic compounds; Conrad, 2005; Lyu & Liu, 2018). Natural ecosystems can be dominated by methanogens, leading to methane emissions that were previously overlooked (Wang *et al.*, 2016; Pitz & Megonigal, 2017; Flanagan *et al.*, 2021). While our understanding of methanogens has grown

dramatically over recent years, the difficulty in culturing these microorganisms has hindered our understanding of their physiological and metabolic features (Lyu & Liu, 2018; Michal *et al.*, 2018). To improve our understanding of the drivers of natural methane emissions, we require further study of the methanogens present and their interactions with the environment and associated microbial community (Barba *et al.*, 2019; Covey & Megonigal, 2019; Yip *et al.*, 2019).

1.2 Riparian ecosystems and processes of methane production

Riparian zones contain a river channel and adjacent terrestrial ecosystem and have numerous processes that influence net methane exchange (Kemnitz *et al.*, 2004; Flanagan *et al.*, 2021). In southern Alberta, the Oldman River feeds the alluvial groundwater underneath the adjacent terrestrial plains, which is taken up by the deep roots of the cottonwood trees (*Populus spp*.) to supplement their water requirements (Flanagan *et al.*, 2019). Methane production, being an anaerobic process, has been identified in river sediment (Buriánková *et al.*, 2013; Mach *et al.*, 2015) and deep saturated soil in previously studied ecosystems (Kemnitz *et al.*, 2004; Covey & Megonigal, 2019). While freshwater streams generally contain high quantities of dissolved oxygen (Buriánková *et al.*, 2013; Flury & Ulseth, 2019), microbial O_2 demand for oxidation reactions often leads to the formation of anaerobic sediments and anoxic microsites (Megonigal & Guenther, 2008; Conrad, 2020a). The Oldman River was found to emit significant quantities of methane, indicating the sediments have active methanogens (Flanagan *et al.*, 2021).

Trees have also been found to be a source of methane (Bushong, 1907), with emission rates varying by tissue type with the greatest magnitude of methane emission coming from the stems (Barba *et al.*, 2019; Feng *et al.*, 2020). Methane emitted from tree stems can originate from one of two sources (Barba *et al.*, 2019; Covey & Megonigal, 2019). It has been demonstrated that plants and trees are able to act as a conduit for methane produced below ground by taking up water containing dissolved methane, which subsequently diffuses through the tree stem or is released from the leaves with water vapour (Nisbet *et al.*, 2009; Pangala *et al.*, 2013; Megonigal *et al.*, 2020). Second, tree stems with high internal water content are low-oxygen environments that can host methanogens (Zeikus & Ward, 1974; Wang *et al.*, 2017; Yip *et al.*, 2019). Cottonwood trees adjacent to the Oldman River were found to emit varying quantities of methane from their stems, and DNA analyses indicated that methanogens present in the stems contribute significantly to these emissions (Flanagan *et al.*, 2021).

Net ecosystem gas exchange measurements showed that the Oldman River and adjacent riparian cottonwood forest was a net source of methane emission over the 2017 growing season (Flanagan *et al*., 2021). Due to the complexity and limited knowledge of the processes of methane production, the relative contribution of tree stems and the river surface to net ecosystem methane emission is poorly understood (Flanagan *et al.*, 2021). Investigations into the microbial ecology and metabolic pathways of methane production in cottonwood tree stems and the adjacent river sediment are required to parse out

the contribution of these contrasting environments to net ecosystem methane emission (Barba *et al.*, 2019; Saunois *et al.*, 2020; Flanagan *et al.*, 2021).

1.3 Microbial ecology and pathways of methane production

It is not known whether the methanogen species within the cottonwood tree stems are the same as those in the adjacent river sediment. Water from the Oldman River feeds the alluvial groundwater, which is then taken up by the cottonwood trees (Flanagan *et al.*, 2019), providing a possible conduit for methanogens and their metabolic products (methane) in the river water to access the tree stems. Ecological conditions such as pH, oxygen content and the nature of organic matter; however, are the principal drivers of microbial community composition (Wen *et al.*, 2017; Cregger *et al.*, 2018; Lyu & Liu, 2018; Bertolet *et al.*, 2019). Therefore, differences in the characteristics between tree stem and river sediment environments are expected to lead to contrasting microbial communities and different methanogen species being present in the tree stems and river sediments.

While numerous methane production (methanogenic) pathways have been proposed, methanogens primarily use one of two metabolic pathways that can operate simultaneously in natural environments (Whiticar, 1999; Conrad, 2005). Methanogens obtain energy by reducing CO_2 using H_2 (hydrogenotrophic methanogenesis) or through acetate fermentation (acetoclastic methanogenesis) with methane formed as the end product (Conrad, 2005; Lyu & Liu, 2018).

Methanogen growth is often limited by substrate availability, so they are reliant on the associated microbial community to breakdown organic matter to form H_2/CO_2 and acetate (Worm *et al.*, 2010; Nazaries *et al.*, 2013; Conrad, 2020a). Syntrophic interactions between methanogens and the microbial community elicit strong control on methanogen growth (Worm *et al.*, 2010; Bertolet *et al.*, 2019; Conrad, 2020a), as exemplified by the increase in methane production with the abundance of bacteria and archaea present (Liu *et al.*, 2013). With methanogen growth largely limited by substrate availability (Conrad, 2020a), the relative abundance of CO_2 reducing and acetate fermenting methanogens in an environment should be mirrored by the relative contribution of these pathways to total methane produced (Buriánková *et al.*, 2012; Wang *et al.*, 2016; Barba *et al.*, 2019).

1.4 Influence of organic matter quality on microbial community composition and methane production

The extent to which each methane production pathway proceeds, limited by precursor substrate availability (H_2/CO_2 and acetate), is strongly regulated by the quality of organic matter decomposed (Hodgkins *et al.*, 2014; Bertolet *et al.*, 2019; Conrad, 2020a). The source organic matter can be solid, dissolved, or suspended particulate, and the nature of these compounds strongly dictates the rate and primary metabolic pathway of methane production (Hodgkins *et al.*, 2014; Bodmer *et al.*, 2020; Conrad, 2020a). Breakdown of high-quality organic matter such as glucan, typically produces acetate and H_2/CO_2 in a 2:1 ratio

(Conrad, 2020a). In contrast recalcitrant compounds resistant to decomposition such as cellulose, generally produce high levels of H_2 and CO_2 (Ji *et al.*, 2018; Conrad, 2020a). This leads to the dominance of acetate fermenting methanogens in environments with high quality organic matter, while CO_2 reducing methanogens dominate substrate-poor environments (Mach *et al.*, 2015; Finn *et al.*, 2020). The microbial community responsible for breaking down this organic matter to substrates for methane production also vary with organic matter quality (Chen *et al.*, 2018; Wu *et al.*, 2018). Properties commonly used to characterize organic matter quality include the molecule size, structure, and nutrient contents (Chapin *et al.*, 2011; Hodgkins *et al.*, 2014; Bodmer *et al.*, 2020).

An indicator of organic matter quality is the ratio of carbon mass to nitrogen mass (C:N), with low values (higher nitrogen content) equating to higher quality organic matter (Chapin *et al.*, 2011). Metabolic conversion of substrates is often limited by nitrogen availability (Chapin *et al.*, 2011), so organic matter with higher nitrogen content, or lower C:N ratios results in a significant increase the rate of methane production (Gebert *et al.*, 2006; Duc *et al.*, 2010; Bednařík *et al.*, 2019). High quality compounds are generally degraded first, leaving more recalcitrant matter to accumulate (Ji *et al.*, 2018; Wu *et al.*, 2018). This in turn results in the subsequent increase in the contribution of CO_2 reduction to total methane production, and decreased contribution of acetate fermentation (Ji *et al.*, 2018). While C:N ratio is important, additional organic matter characteristics strongly dictate the rate of decomposition and quantities of substrates formed

(Chapin *et al.*, 2011; García-Palacios *et al.*, 2015; Conrad, 2020a). Breakdown of large or irregularly shaped molecules, such as cellulose or lignin, requires the secretion of microbial enzymes (or involvement of additional microorganisms such as fungi) so they are resistant to full decomposition (Chapin *et al.,* 2011). The control of molecule size has also been suggested for dissolved organic matter, as high molecular weight compounds are often hydrolyzed into smaller molecules, leading to the accumulation of small recalcitrant compounds (Hodgkins *et al.*, 2014). Complete degradation of cellulose will produce high quantities of acetate (Conrad, 2020a); however, due to its recalcitrance, cellulose is expected to only be partially broken down, which yields H_2/CO_2 and little to no acetate (Harwood *et al.*, 1998). The quality of organic matter also strongly dictates the non-methanogen community composition (Wu *et al.*, 2018; Bertolet *et al.*, 2019; Buresova *et al.*, 2019). This leads to differing methanogen and bacterial communities observed for similar physical environments but with varying substrate quality, particularly nutrient contents (Finn *et al.*, 2020). Organic matter quality, thus, appears to play a dominant role on the microbial community composition, as well as the rate and relative contribution of each methanogenic pathway to total methane produced.

Aquatic systems rich in high-quality organic matter were believed to be dominated by acetoclastic methanogens (Conrad, 1999; Conrad, 2020a). However, recalcitrant organic matter, that can also be present in river sediments typically, produces H_2 and CO_2 at greater quantities than acetate (Flury & Ulseth,

2019; Conrad, 2020a). For example, previous studies of river sediments found that the abundance of both hydrogenotrophic (Methanomicrobiales and Methanobacteriales) and acetoclastic (Methanosarcinales) methanogen orders varied depending on sample location (Kemnitz *et al.*, 2004; Buriánková *et al.*, 2012; Mach *et al.*, 2015). Of importance, suspected members of the *Methanosaetaceae* family are obligate acetate consumers previously observed in river sediments, indicating steady-state quantities of acetate are present (Buriánková *et al.*, 2012; Mach *et al.*, 2015). Streams continuously erode, transport, and deposit surface sediment and microorganisms, leading to a mosaic pattern of microbial communities with increased methanogen and bacterial diversity in areas of high deposition (Braatne *et al.*, 1996; Febria *et al.*, 2012; Buriánková *et al.*, 2013). River sediments with greater flooding frequencies and sediment deposition were also found to contain greater quantities of acetate fermenting methanogens, presumably from increased amounts of high-quality organic matter inputs (Kemnitz *et al.*, 2004; Buriánková *et al.*, 2013). High variability in the microbial community composition and lack of knowledge regarding details of methane production pathways in river sediment and tree stem environments has contributed to uncertainty in the role freshwater streams play in the global methane budget (Stanley *et al.*, 2016; Saunois *et al.*, 2020).

In tree stems, the partial breakdown of wood cellulose produces the substrates CO_2 and H_2 (Zeikus & Ward, 1974; Conrad., 2020a), while acetate is formed during fermentation of glucose and pectin (Schink *et al.*, 1981). While

DNA analyses suggest both methane production pathways could be active (Yip *et al.*, 2019), the dominance of the hydrogenotrophic *Methanobacterium* (Zeikus & Ward, 1974;; Yip *et al.*, 2019) and *Methanobrevibacter* (Zieikus & Henning, 1975; Balch *et al.*, 1979) methanogen genera (Family *Methanobacteriaceae*) indicate that H_2 and CO_2 are the major substrates used in producing methane in tree stems. While the microbial community in tree stems has been investigated, the abundance of some microbes can vary significantly between tree species and tissue type (Cregger *et al.*, 2018; Yip *et al.*, 2019). To better understand natural methane production, the interactions among methanogens, the associated microbial community, and environmental variables must be further studied (Barba *et al.*, 2019; Saunois *et al.*, 2020). While there are presumably many forms of organic matter present in the tree stems and river sediments (Flury & Ulseth, 2019; Li *et al.*, 2019; Bogard *et al.*, 2014), the properties of river sediment organic matter were found to elicit stronger control on methane production than dissolved organic matter in the porewater (Bodmer *et al.*, 2020). This study will therefore focus on solid organic matter as a primary driver of microbial community composition and the methane production pathways.

1.5 Stable carbon isotope composition of methane

To study the relative contribution of different source and sink processes that affect the concentration of atmospheric methane, stable carbon isotope ($^{13}C/^{12}C$) compositions of methane can be analyzed (Whiticar, 1999; Conrad, 2005). The stable carbon isotope composition of methane is typically represented

using delta notation ($\delta^{13}C$, defined in the Methods section 2.3 - see equation 2). Currently, the global average $\delta^{13}C$ value of atmospheric methane is approximately -47.5‰, and this $\delta^{13}C$ value illustrates a latitudinal gradient (approximately 0.5‰ lower in the northern hemisphere than the southern hemisphere) and a seasonal cycle, with maximum seasonal changes of approximately 0.2 to 0.6‰ (lower $\delta^{13}C$ values in northern hemisphere summer and higher $\delta^{13}C$ values in winter; Quay *et al.*, 1999; Dlugokencky *et al.*, 2011). Methane's $\delta^{13}C$ value differs between sources, largely as a result of the production pathway (Whiticar, 1999). For example, methane produced by fermentation of acetate can have $\delta^{13}C$ values of methane depleted in ^{13}C by 5‰ to 35‰ relative to the source methyl carbon of acetate (Whiticar, 1999). In contrast, methane produced by CO_2 reduction can have $\delta^{13}C$ values of methane depleted in ^{13}C by 28‰ to 79‰ relative to the source carbon in CO_2 (Whiticar, 1999; Penger *et al.*, 2012). Acetate and carbon dioxide are the primary molecules that serve as substrates for methanogenesis during decomposition of plant organic matter (Conrad, 2005). Since there are only minor isotopic changes during decomposition and respiration processes that generate acetate and CO_2 from plant organic matter, the $\delta^{13}C$ values of these methanogenic substrates typically have values in the range -34‰ to -23‰ (Conrad, 2005). Of relevance to the current study, stem wood samples extracted from cottonwood trees in the Lethbridge Helen Schuler Nature Reserve (HSNR) have $\delta^{13}C$ values of -28‰ to -25‰ (Flanagan, unpublished data). Stable carbon isotope measurements of methane within *Populus* trees ($\delta^{13}C$: -78.3 to -89.1‰; Wang *et al.*, 2016) and river

sediment ($\delta^{13}C$: -19 to -70.9‰; Mach *et al*., 2015; Flury & Ulseth, 2019; Bednařík et al., 2019), are consistent with the suggestion for the dominance of CO_2 reduction in tree stems (Zeikus & Ward, 1974; Yip *et al.*, 2019) and greater contribution of acetate fermentation in freshwater streams (Kemnitz *et al.*, 2004; Buriánková *et al.*, 2013; Conrad, 2020a).

1.6 Primary research goal and hypotheses

The cottonwood tree stems and adjacent river sediment in the Oldman River riparian ecosystem, as connected by the supply of alluvial groundwater, offer a unique opportunity to investigate the ecological controls on methane production. The primary objective of this thesis was to study the microbial ecology and details of methane production pathways in the Oldman River sediment and adjacent *Populus* tree stems. To address these objectives, molecular genetic techniques allowed for characterization of the methanogen and bacterial community composition, and stable carbon isotope measurements of methane provided insight to the metabolic pathways of methane production.

While it is possible that the same methanogen species will be present in the tree stem and river sediment, because the alluvial groundwater provides a conduit for exchange of microbes between these linked environments, I hypothesize that significant differences in the environments and available substrates will result in distinct methanogen and bacterial community composition present in the tree stem and river sediments. More specifically, the chemical

composition of solid organic matter present in the river sediment is expected to lead to increased acetate availability (Buriánková *et al.*, 2013; Conrad, 2020a), and a greater abundance of the acetoclastic Methanosarcinales in the river sediment than in the tree stems. In contrast, tree stems will harbour the hydrogenotrophic family *Methanobacteriaceae*, because of the expected high quantities of H_2 and CO_2 substrates in the tree stem resulting from the partial decomposition of cellulose (Zeikus & Ward, 1974; Harwood *et al.*, 1998; Conrad, 2020a). The greater abundance of acetoclastic methanogens in the river sediment would lead to a greater portion of methane produced through acetate fermentation while CO_2 reduction is expected to be the primary methane production pathway in tree stems from the dominance of CO_2 reducing methanogens. Therefore, I hypothesize that distinctive stable carbon isotope composition of methane produced in the river sediment and tree stems will be observed, with river sediment producing methane more isotopically enriched in ^{13}C ($\delta^{13}C$: -45 to -65‰) than methane produced in the tree stems ($\delta^{13}C$: -70 to -110‰). Findings from this study will provide insight to the ecological controls on methane production pathways and provide information necessary for parsing out the contribution of these sources to net ecosystem methane emissions.

2. METHODS

2.1 Field site description

The experimental site was a riparian cottonwood forest located in the Helen Schuler Nature Reserve (HSNR) and the adjacent Oldman River in Lethbridge Alberta (49.702 N, 112.863 W, elevation 928 m; Fig. 2.1). This forest was primarily populated by the prairie cottonwood (*Populus deltoides* Bartr. Ex Marsh) and narrowleaf cottonwood (*Populus angustifolia* James) as well as their intersectional hybrids, known as lanceleaf cottonwoods (*P*. x *acuminata* Rydp.) (Kranjcec *et al.*, 1998). Some balsam poplar (*P. balsamifera* L.) trees, or the closely-related and phenotypically similar black cottonwood (*P. trichocarpa* T. & G.) are also present, and they do hybridize with the other cottonwood taxa (Gom & Rood, 1999). Poplar trees account for *c*. 50% of the total ecosystem leaf area index (1.8 ± 0.2 m^2 m^{-2}; measured in 2014), with understory plants making up the remaining fraction (Flanagan *et al.*, 2017). The Oldman River is fed by the meltwater from the Rocky Mountains, with water outflow through the streambed to the alluvial groundwater beneath the adjacent terrestrial plains, supplementing the water requirements of the cottonwood trees (Rood *et al.*, 2003; Flanagan *et al.*, 2019). The growing season (May to August) has a mean air temperature of 15.6°C, and precipitation of 211.8 mm (1981-2010) as recorded at the Lethbridge regional airport (Environment Canada, 2020).

Figure 2.1: Location of the HSNR field site within the city of Lethbridge in southern Alberta, Canada (Google Earth: Digital Globe 2020).

2.2 Molecular genetic analyses of microbial community composition

2.2.1 Field sample collection

Tree wood samples were collected (February 11, 13 & 18, 2020) from nine separate cottonwood trees using sterilized 9 mm diameter tree increment borers (Model 10- 100- 1018, Haglöf Inc., Långsele, Sweden) and immediately placed in sterile Whirl-Pak bags (S-22729, Whirl-Pak, Uline, Canada). Three cottonwood taxa (*P. deltoides*, *P. angustifolia*, and an intersectional hybrid) found in close proximity were sampled at each of the three locations along a transect of increasing distance perpendicular to the adjacent Oldman River (Cluster 1: 84 ± 16 m, Cluster 2: 145 ± 20 m, & Cluster 3: 205 ± 17 m; fig 2.2). To investigate possible relationships between tree characteristics and the microbial community composition, diameter at breast height (DBH, 1.3 m above the ground) and tree height were measured using a diameter tape and clinometer.

Six river bottom sediment samples (10 cm depth) were collected (July 24, 2020) along 2 transects across the width of the Oldman River at locations between the two bridges in Lethbridge that cross the river (Highway 3 bridge and Whoop-up Drive bridge), in areas that are adjacent to the HSNR (Fig. 2.2). Sediment samples were collected using a sterilized copper pipe (approximately 2 cm diameter) and pushed out into sterile 50 mL centrifuge tubes using a sterile solid copper rod. River column depth was recorded for each location sampled.

Groundwater samples were collected from 2 pre-installed wells made from 2.5 cm diameter PVC pipes that penetrate the groundwater table (approx. 2.5 m depth) below the HSNR cottonwood forest (Fig. 2.2). Standing water was pumped out and discarded, and the well was allowed to refill before collection in 50 mL centrifuge vials with a screw lid.

Before field sampling, instruments were cleaned, rinsed with bleach then sterile water, then autoclaved and sealed in individual autoclave bags for transport to the field site. Samples were held on ice for transport to the lab and stored at -80°C until DNA extraction. A small subset of each tree stem and river sediment sample was sacrificed for determination of pH. Tree stem pH was measured by mincing dried tissue, soaking 150 µL of finely minced wood in 1.2 mL sterile water and shaking (600 rpm) for 2 hours before centrifugation (1300 x *g* for 2 minutes) and measuring the pH of the supernatant (Yip *et al.*, 2019). River sediment was centrifuged (1300 x *g* for 2 minutes) and the pH of the supernatant was measured.

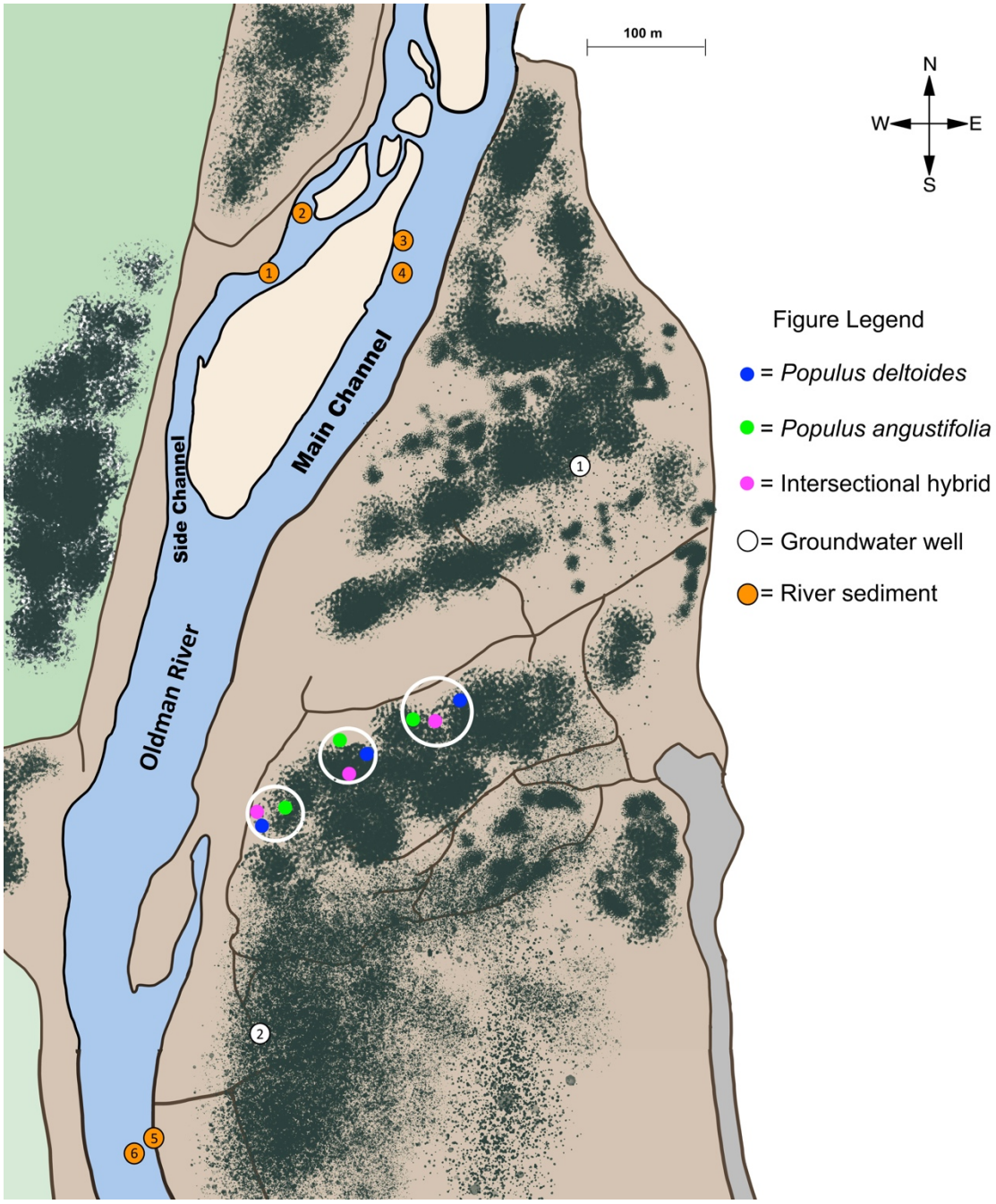

Figure 2.2: Diagram of river sediment, tree stem, and alluvial groundwater sampling locations within the HSNR in Lethbridge Alberta. In this diagram the dark green patches indicate forested areas, light brown is grassland, light green is grassland in the Elizabeth Hall Wetlands, brown lines are walking paths and the grey area is a roadway.

2.2.2 DNA extraction and Illumina sequencing

Environmental DNA (eDNA) was extracted from all field samples using a Powersoil DNA extraction kit according to protocol (Qiagen, Toronto, ON, Canada). Tree cores were minced (<2 mm) with a sterile razor blade (Cregger *et al.*, 2018; Yip *et al.*, 2019), while sediment samples were sieved (<2 mm). For wood samples, two technical replicates were combined to increase DNA yield (Yip *et al.*, 2019). River sediment was centrifuged (10,000 x *g* for 60s) and the supernatant and upper rock layers were discarded, using the fine sediment for DNA extraction (Buriánková *et al.*, 2013).

The eDNA from river sediment, groundwater and tree cores, as well as extraction buffer (blank control) were sent to Gènome Quèbec for shotgun metagenomic sequencing to characterize the methanogen community composition. River sediment and tree core eDNA were also sequenced to characterize the bacterial community composition. Sequencing was performed using a 2-step PCR approach using universal primers specific to bacterial 16s rRNA (515F: 5'- GTG CCA GCM GCC GCG GTA A-3' and 806R: 5'- GGA CTA CHV GGG TWT CTA AT; Walters *et al.*, 2016) and methanogen *mcrA* genes (*mcrA*fornew: GGT GTM GGD TTC ACH CAR TAY GC-3′ and *mcrA*revnew: 5′-TTC ATN GCR TAG TTH GGR TAG TT-3′ ;Gagnon *et al.*, 2011). Amplicons were sequenced using an Illumina MiSeq (PE 250).

2.2.3 Processing DNA sequencing data

Raw reads were processed using the DADA2 package (Callahan *et al.*, 2016) in R version 4.0.3 (R Project for Statistical Computing, Vienna, Austria) to create amplicon sequence variants (ASV's; Callahan *et al.*, 2017). Forward and reverse reads were trimmed (primers + 3 bases were removed, forward and reverse reads were truncated at 210 bases for 16s rRNA and 242 for *mcrA*) and filtered (no ambiguous bases, maximum expected error of 2 for 16s rRNA and 3 for *mcrA*) before dereplication. Filtered reads were pseudo-pooled for de-noising for better identification of rare taxa, then forward and reverse reads were merged (perfect overlap of ≥ 12 bases for 16s rRNA and ≥ 8 for *mcrA*) and chimeric reads were removed. Taxonomic classification of ASV's were conducted using the RDP Naïve Bayesian classifier (Wang *et al.*, 2007) with bootstrap values of 80% (Steinberg & Regan, 2008; Chen *et al.*, 2020). Bacterial ASV's were assigned taxonomy using the SILVA 138 database (Quast *et al.*, 2013), while *mcrA* sequences were assigned to the original *mcrA* database (Yang *et al.*, 2014) that was modified as follows. Following conversion to a DADA2 compatible format, redundant sequences with taxonomic classification of "Uncultured Archaeon" were removed (Chen *et al.*, 2020). Whole methanogen genome and entire methyl coenzyme reductase nucleotide sequences from pure cultures were pulled from Genbank (Clark *et al.*, 2016) using script written in Perl (Wall *et al.*, 2000) to pull and format their nucleotide sequence and taxonomic classifications appropriately. To extract the *mcrA* nucleotide region, the reference sequences were flanked and truncated using the *mcrA* (Steinberg & Regan, 2009), ML (Luton *et al.*, 2002),

*mcrA*159F/*mcrA*345R (Vaksmaa *et al.*, 2017), and *mcrA*NEW (Gagnon *et al.*, 2011) primer sets in Cutadapt V1.16 (Marcel, 2011) on the public server usegalaxy.org (Afgan *et al*., 2015). Additional script was written to merge only unique *mcrA* nucleotide sequences with the trimmed *mcrA* database (Yang *et al.*, 2014). ASV's that did not receive taxonomic classification were excluded from analyses.

For bacterial 16s rRNA sequences, taxa identified as "Mitochondria" (av. 0.15%) "Chloroplast" (av. 1.1%), or "Archaea" (av. 1.4%) were removed as possibly derived from plant material. Each tree stem and river sediment sample in the final rarefied (See Appendix 7.3) dataset contained 23, 647 *mcrA* sequences representing 664 ASV's, and 12,157 bacterial 16s rRNA sequences representing 5706 ASV's (See Appendix 7.1 for the number of ASV's per sample and sample type).

2.2.4 DNA sequence analyses

Statistical analyses of tree stem and river sediment sequence data were conducted individually for methanogen and bacterial datasets using vegan 2.4-2 (Oksanen et al., 2017) with figure generation using ggplot2 (Wickham, 2016) as part of the open source software Bioconductor (Huber *et al.*, 2015). Boxplots were generated using MATLAB software (R2020a, The Mathworks Inc., Natick, MA, USA). Alpha diversities were statistically evaluated between sample type and tree cluster/taxa based on species (ASV) richness and Shannon (Shannon-

Wiener) diversity index (Shannon & Weaver, 1949; eq. 1). In the Shannon diversity index (H'), p_i is the proportion of species i, *ln* is the natural logarithm and Σ indicates the sum for all species (S).

$$H' = -\sum^{S} P_i \, lnP_i \quad (1)$$

Relative abundance values for methanogen and bacteria taxa were determined by summing the sequence counts for ASV's corresponding to a given phylogeny, then dividing this by the total number of sequences in the sample and presented as a percentage (%).

Beta-diversity of the bacterial communities were calculated using the Bray-Curtis dissimilarity index and visualized by non-metric multidimensional scaling (NMDS) using *metaMDS*. River sediment and tree stem bacterial community compositions were compared using permutational ANOVA (PERMANOVA) models with 999 permutations using *adonis* in vegan. Pairwise PERMANOVA was used to determine whether bacterial community composition was significantly different for tree taxa or tree cluster (distance from the river) with FDR correction to account for type 1 errors.

2.3 Investigating the metabolic pathways of methane production

2.3.1 Tree stem and river sediment sample collection

Tree wood samples were collected (September 4, 2020) as previously described (See section 2.2.1; Fig. 2.2) and immediately placed in 50 mL centrifuge tubes filled with sterile water (Fisher Chemical, W7-4, Lot 172156).

Six river bottom sediment samples were collected (August 19, 2020) as previously described (See section 2.2.1; Fig. 2.2), with samples pushed out into Mason jars. The sediment samples were subsequently submerged in sterile water in the sealed Mason jars.

Before field sampling, instruments were cleaned, rinsed with sterile water then 95% ethanol, and individually wrapped in aluminum foil for transport to the field site. Tree and sediment samples were returned to the lab and stored in the dark at 4°C until incubation experiment preparation (<12 hours).

2.3.2 Anaerobic sample incubation and gas analysis

In vitro incubation experiments, constructed using a previously reported protocol (Conrad *et al.*, 2011; Mach *et al.*, 2015; Ji *et al.*, 2018), used river sediment and tree core samples held under anaerobic conditions to promote methane production, allowing for the analysis of methane and CO_2 concentration and their associated $\delta^{13}C$ values.

Tree cores (3.9 ± .15 g) were removed from sterile water and immediately broken into 8 pieces of similar size, and river sediment was sieved (<2 mm). Saturated tree cores or 30 mL of river sediment with 30 mL of sterile water were added to sterile 100 mL glass beakers. Beaker containing samples were placed in sterile 500 mL Mason jars with gas inlet and outlet connections made by inserting ~11 cm tubing (Bev-a-Line IV tubing, LABCOR, Concord, ON, Canada) through holes drilled in the lid and fitted with male and female (Masterflex fitting RK-45508-80 & RK-45512-82, Gelsenkirchen, DEU) adapters with one-way stopcock valves (Luer-Lok, 420163-0001, Franklin Lakes, NJ, USA), then sealed using Qubitac (Qubit, Kingston ON, Canada).

Mason jars were flushed with N_2 gas (Praxair, Lethbridge, AB, Canada) at a rate of 700 mL/min for ~10 minutes, with output gas passed though drying agent ($MgCl_2$) before the [CO_2] was measured (LI-820 CO_2 gas analyzer, LI-COR Biosciences, Lincoln, NE, USA). Flushed Mason jars, with [CO_2] lower than 12 ppm, were incubated in the dark at room temperature. At intervals, 50 mL gas samples were removed from the headspace of the jars, using syringes (SOFT-JEC, 1481757, Henke-Sass Wolfe, Tuttlingen, DEU) with one-way stopcock adapters, after 10, 20 and 45 hours (with an additional sample point of 64 hours for the tree cores).

Of the 50 mL gas sample, 20 mL was expelled before injecting the remaining 30 mL to measure [CH_{4dry}], [CO_{2dry}], $\delta^{13}C$ CH_4 and $\delta^{13}C$ CO_2 using a

small sample introduction module (A0314, Picarro, Santa Clara, CA, USA) attached to a gas analyzer (G2201-i analyzer, Picarro, Santa Clara, CA, USA). The carbon isotope composition of methane and CO_2 were reported using delta (δ) notation, which is the ratio of $^{13}C/^{12}C$ in a sample molecule compared to that of the VPDB standard and routinely expressed in parts per thousand or per mil [‰] (Coplen, 1994) (eq.2):

$$\delta^{13}C_{\text{VPDB}} = \left(\frac{\frac{^{13}C}{^{12}C}\text{sample}}{\frac{^{13}C}{^{12}C}\text{standard}} - 1\right) \times 1000\ ‰ \quad (2)$$

$\delta^{13}C$ values of CH_4 and CO_2 were calibrated to reference gas measurements taken prior to and following sample analyses (Environment Canada, Greenhouse Gas Lab). A standard curve was created to calibrate CH_4 and CO_2 concentration measurements using 5 reference gases previously calibrated by the Greenhouse Gas Lab at Environment Canada. Empty incubation chambers were flushed with each reference gas, then discrete gas samples were taken, analyzed, and plotted against the true values obtained from the 30-minute average of each reference gas measured by flowing through an Ultra-Portable Greenhouse Gas Analyzer (UGGA; Los Gatos Research, Mountain View, CA, USA). Predicted [CH_4] and [CO_2] differed from the actual values by <21.3 (ppb) and 0.91 (ppm) respectively. Precision of $\delta^{13}C$ CH_4 and $\delta^{13}C$ CO_2 values were ≤ 0.8 ‰ and 0.11 ‰, respectively, based on repeated measures of a reference gas taken prior to and following sample measurements.

2.4 Analysis of sample organic matter characteristics

Following incubation experiments, tree core and river sediment samples were oven-dried at 60°C. Dried tree core samples were first minced using a sterile razor blade and cutting board, then all samples were pulverized and homogenized in a ball mill (Retsch MM200, Haan, Germany). Inorganic carbon was removed from river sediment (5 g), by mixing with 1.2 N HCl (10 mL) in 50 mL falcon tubes sealed and wrapped with parafilm for 2 hours, shaking manually every 15 minutes followed by centrifugation (4000 RPM for 15 minutes; Eppendorf® Centrifuge 5804 R, Hamburg, Germany) and removal of the supernatant. In order to prevent organic carbon loss during sample drying, 3 DI H_2O washes (20 mL) were performed with centrifugation (4000 RPM for 15 minutes) and removal of the supernatant following each step. River sediment was re-dried at 60°C, then pulverized using a sterilized mortar and pestle.

Subsamples of tree and river sediment samples were analysed for their carbon and nitrogen content by weight (g C g^{-1} biomass, represented in %), and $^{13}C/^{12}C$ carbon isotope composition (expressed using delta-notation, $\delta^{13}C$ VPDB, ‰) by Continuous Flow-Elemental Analysis-Isotope Ratio Mass Spectrometry at the University of Calgary Isotope lab. Measurements were conducted on CO_2 and N_2 gas generated by sample combustion in an elemental analyzer (4100, Costech Analytical Technologies, Valencia, CA, USA) and quantified with a gas isotope ratio mass spectrometer (Delta Plus XL, Thermo Finnigan, San Jose, CA, USA) connected by a ConfloIV® device (Thermo Fisher Scientific, Waltham, MA,

USA). For river sediment, % C_{org} values were determined using acid washed samples, while non-acid washed samples were used for N measurements.

Individual C and N analyses were conducted for river sediment and tree core samples separately. Standardization by weight was determined using repeated measurements of internal lab standards (n=6) with different mass, and instrument drift was accounted for by re-measuring the internal lab standards following every 6 sample measurements. Standards used for river sediment (Mountain soil; % C=1.7; $\delta^{13}C_{org}$=-17.87 ‰; % N=0.1) and for tree cores (Peach Leaves; % C=45.8; $\delta^{13}C_{org}$=-25.23‰; Oak wood: % N=0.09) were characterized against international standards (USGS-40; $\delta^{13}C$=-26.39‰; USGS-41, $\delta^{13}C$=37.63‰), and re-checked by measuring both international standards (n=2) at the beginning and end of each analysis. Precision of % C, % N and $\delta^{13}C$ measurements (Table 2.1) were determined by repeated analysis (n=3) of each sample type. The mass of dried tree stem and river sediment samples from anaerobic incubations were used to approximate total carbon and nitrogen availability during incubation experiments.

Table 2.1: Precision of $\delta^{13}C$, % C and % N measurements of organic matter by Continuous Flow-Elemental Analysis-Isotope Ratio Mass Spectrometry. Precision was determined using the standard deviation for measures of each sample type (n=3).

Sample	$\delta^{13}C_{org}$ (‰)	% C_{org}	% N
Tree core	0.206	0.089	5.77×10^{-3}
River Sediment	0.203	0.046	5.30×10^{-4}

2.5 Statistical analyses

Value standardization and data organization was performed using Microsoft Excel (Version 16.3, Microsoft corporation., Redmond, WA, USA) with normality tests (Shapiro-Wilks), statistical analyses and figure generation performed using Matlab software (R2020a, The Mathworks Inc., Natick, MA, USA) unless stated otherwise. Within each boxplot, the center line represents the median, while the bottom and top of the box represent the 25th percentile (first quartile) and 75th percentile (third quartile) for the data set, respectively. The whiskers represent the smallest and largest measured values, and the red cross represents outliers.

3 RESULTS

3.1 Tree core and river sediment organic matter characteristics

Average organic carbon content (%) in tree stem (*Populus spp.)* samples were approximately 114 times greater than sediment from the Oldman River (Table 3.1). Nitrogen content (%) was an average of 2 times greater in tree stems than river sediment (Table 3.1) The amount of organic carbon available during incubation experiments was approximately 4.9 times greater for tree stems than river sediment, while river sediment samples had approximately 10 times greater nitrogen availability (Table 3.1). River sediment had $\delta^{13}C$ C_{org} values significantly more enriched than in the tree cores, by an average of 2.2‰ (Table 3.1). The C:N ratio for tree stem samples (average ± SD; 546.2 ± 199.6) was much greater than river sediment samples (9.9 ± 3.4).

Table 3.1: Differences in the organic matter characteristics of *Populus spp.* tree core (n=9) and Oldman River sediment (n=6) samples (mean ± SD). Tree stem samples had greater carbon and nitrogen content by weight (%), greater total C, less total N, and more isotopically depleted C_{org} than river sediment samples. These differences were statistically significant based on 1-way, unbalanced ANOVA for carbon content, $F_{(1,13)}=3.92x10^4$, $P<0.001$, nitrogen content, $F_{(1,13)}=11.7$, $P<0.01$, total carbon, $F_{(1,13)}=104$, $P<0.001$, and $\delta^{13}C$ C_{org}, $F_{(1,13)}=27.8$, $P<0.001$. $X^2_{(1,13)}=10.1$, $P<0.05$, and a Kruskal-Wallis test for total nitrogen $X^2_{(1,13)}=10.1$, $P<0.05$

Sample	$\delta^{13}C$ C_{org} (‰)	% C_{org}	% N	Total C (mg)	Total N (mg)
Tree stem	-27.0 ± 0.8	45.8 ± 0.5	0.09 ± 0.04	461.0 ± 74.6	0.94 ± 0.35
River sediment	-24.8 ± 0.8	0.4 ± 0.2	0.04 ± 0.02	92.5 ± 57.0	9.62 ± 5.84

3.2 Microbial community composition

3.2.1 Methanogen community composition

DNA sequencing identified *mcrA* nucleotide sequences with high genetic similarity to methanogens in the orders Methanobacteriales, Methanosarcinales, Methanomicrobiales, and Methanomassiliicoccales (Fig. 3.1). River sediment had significantly greater species richness and Shannon diversity index values than tree stems (Fig. 3.2). Methanogen species richness in tree stems did not differ significantly between tree cluster (location) ($X^2_{(2,6)}$=3.82, P=0.15) or cottonwood taxa ($X^2_{(2,6)}$=0.62, P=0.73), based on Kruskal-Wallis tests. Similarly, *mcrA* Shannon diversity index values did not differ significantly between tree cluster ($X^2_{(2,6)}$=0.62, P=0.73) or taxa ($X^2_{(2,6)}$=4.36, P=0.11) based on Kruskal-Wallis tests.

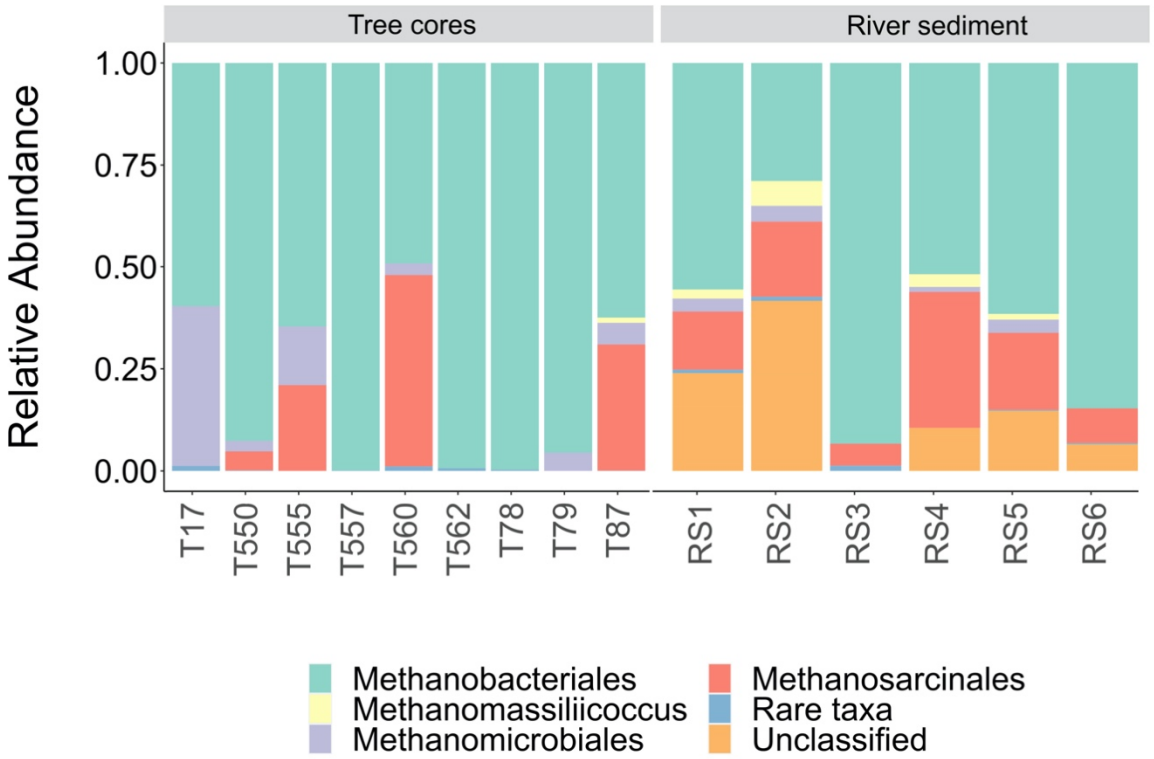

Figure 3.1: Relative abundance of dominant (>0.1%) methanogen orders in *Populus spp.* tree core and Oldman River sediment samples as classified by *mcrA* gene amplicons. Relative abundance is the sum of sequence counts for ASV's classified to a given methanogen order divided by the total number of sequences in the sample and presented as a percentage. Labels on the bottom indicate river sediment (RS) or tree core (T) sample type, and the associated number represents the sediment location (Fig. 2.2) and tree stem tag (See Appendix 7.5 for the associated taxa and cluster).

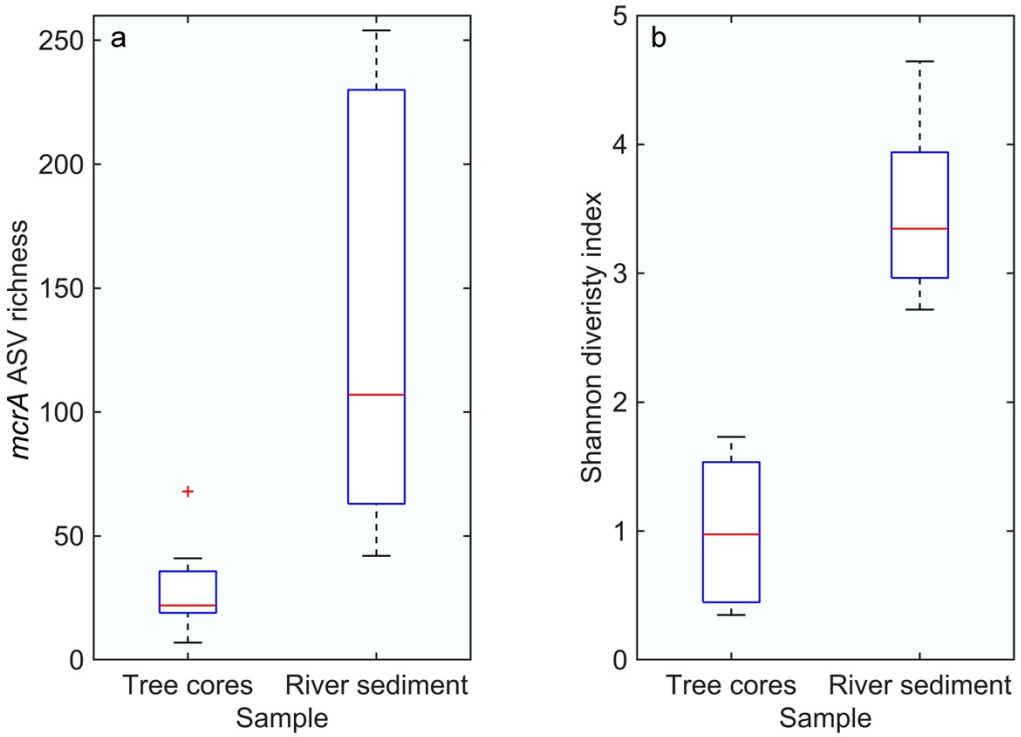

Figure 3.2: Differences in (a) the number of *mcrA* ASV's and (b) associated Shannon diversity index values from *Populus spp.* tree core (n=8) and Oldman River sediment (n=6) samples. The number of observed methanogens and Shannon diversity differed significantly for tree stem and river sediment samples based on Kruskal-Wallis tests. For observed methanogens, $X^2_{(1,13)}$=8.7, P<0.01, and for Shannon diversity, $X^2_{(1,13)}$=10.1, P<0.01

Considering all samples, tree stems (n=9) generally had a greater relative abundance (average ± SD) of Methanobacteriales sequences (78.3 ± 22.2%) than the river sediment samples (n=6; 60.8 ± 23.4%). Methanosarcinales ASV's had considerable relative abundance in all river sediment samples (5.74 to 34.5%) and were only significant (>1%) in four out of nine tree stem samples (5.30 to 45.9%; Fig. 3.3). The two alluvial groundwater samples had 12 and 15 *mcrA* ASV's representing 24 unique sequences, with most (93.2 & 97% relative abundance) classified as Methanobacteriales, and the remainder classified as Methanosarcinales (data not shown). Methanomicrobiales ASV's were present

(>1% relative abundance) in six out of nine tree stem samples, and four out of six river sediment samples, and were more abundant in tree stem (2.22 to 42.2%) than in river sediment samples (0.05 to 2.6%; Fig. 3.3). Methanomassiliicoccus had similar low relative abundance in all tree stem (0.23 to 5.69%) and river sediment samples (1.10 to 7.80%; Fig. 3.3). The relative abundance of each methanogen order did not differ significantly for tree cluster or taxa based on Kruskal-Wallis tests (P>0.08; data not shown), except for Methanomicrobiales ($X^2_{(1,13)}$=5.79, P=0.06), which were only absent in *P. angustifolia* tree stem samples.

Considering all Methanosarcinales sequences in tree stems, most belonged to one *Methanosarcinaceae* ASV (65% relative abundance) and one *Methanosaetaceae* ASV (29%). River sediment samples generally contained *Methanosaetaceae* at greater relative abundance (10.2 ± 3.90%; average ± SD) than *Methanosarcinaceae* (6.53 ± 7.81%). Methanobacteriales ASV's identified in all samples were the most genetically similar to the family *Methanobacteriaceae.* Methanobacteriales ASV's classified to genus level were primarily *Methanobacterium*, except for tree 87 which also contained the genus *Methanobrevibacter* in negligible relative abundance (<0.1%). Some unclassified *mcrA* ASV's from both tree stem and river sediment samples were assigned as *Methanobrevibacter* when bootstrap confidence was relaxed, so methanogens in this genus could be more abundant but had poor classification due to the limited reference database.

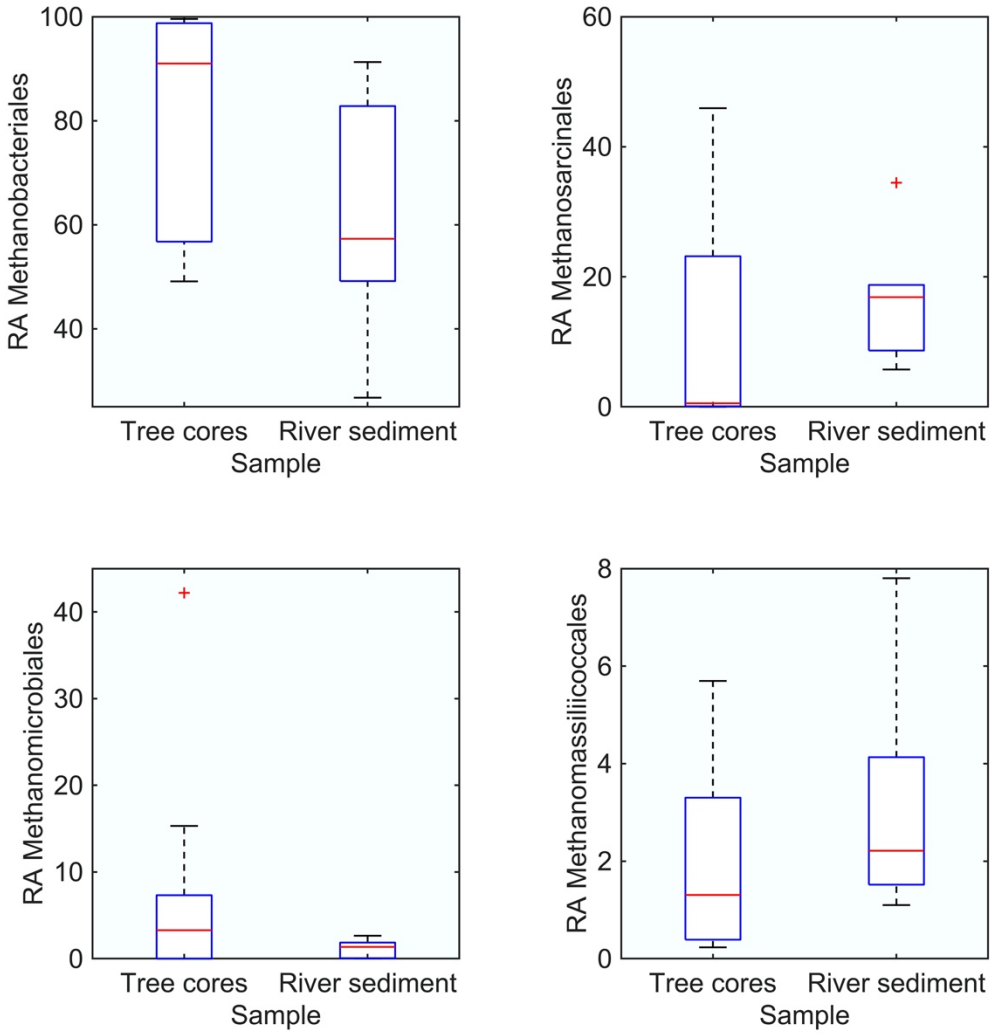

Figure 3.3: Comparison of the relative abundance (RA) of *mcrA* ASV's classified as the methanogen orders (a) Methanobacteriales, (b) Methanosarcinales, (c) Methanomicrobiales, and (d) Methanomassiliicoccales in tree stem (n=9) and river sediment samples (n=6). Relative abundance is the sum of sequence counts for ASV's classified to a given methanogen order divided by total sample sequences and presented in percentage. Differences in the relative abundance of Methanobacteriales, Methanosarcinales, Methanomicrobiales and Methanomassiliicoccus were not statistically significant based on Kruskal-Wallis tests. For Methanobacteriales, ($X^2_{(1,13)}$=4.5, P=0.19), for Methanosarcinales, (X^2(1,13)=2.0, P=0.16), for Methanomicrobiales, ($X^2_{(1,13)}$=0.9, P=0.34), and for Methanomassiliicoccus, ($X^2_{(1,13)}$=1.39, P=0.24).

3.2.2 Bacterial community composition in tree stems and river sediment

The average (± SD) relative abundance of dominant (>1%) bacterial phyla identified in tree stem (n=8; one tree stem sample was excluded due to high levels of plant contaminant) environments were Actinobacteria (30.8 ± 10.6%), Acidobacteria (15.5 ± 11.6%), Unclassified (10.1 ± 8.95%), Firmicutes (12.3 ± 5.96%), Bacteroidetes (11.7 ± 4.02%), Proteobacteria (8.04 ± 10.0%), Chloroflexi (5.78 ± 4.40%), Synergistetes (1.43 ± 3.49%), and Verrucomicrobia (1.00 ± 0.52%; Fig. 3.4).

The average (± SD) relative abundance of dominant (>1%) bacterial phyla in 6 river sediment samples were Proteobacteria (30.5 ± 5.6%), Acidobacteria (13.3 ± 4.5%), Verrucomicrobia (11.02 ± 2.65%), Bacteroidetes (9.46 ± 3.67%), Chloroflexi (7.37 ± 2.07%), Plantomycetes (7.15 ± 4.75%), Actinobacteria (4.03 ± 1.93%), Desulfobacterota (3.80 ± 3.23%), Nitrospirota (2.65 ± 0.79%), Myxococcota (1.74 ± 0.39%), unclassified Gemmatimonadetes (1.66 ± 0.36%), Myxococcota (1.74 ± 0.39%), and unclassified Armatimonadetes (1.00 ± 0.92%; Fig. 3.4).

Methanotrophic genera were present within tree stem samples belonged to *Crenothrix* (<3.8%), *Methylobacterium* (<0.65%), and *Methylocystis* (<0.03%; data not shown).

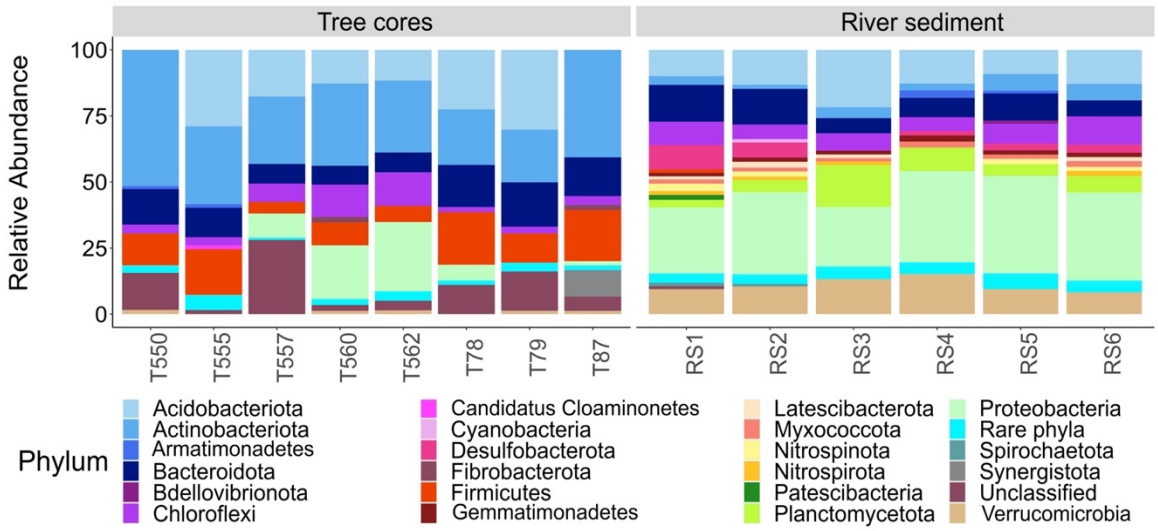

Figure 3.4: Relative abundance of dominant (>0.1%) bacterial phyla in *Populus spp.* tree core and Oldman River sediment samples classified by 16s rRNA amplicons. Relative abundance is the sum of sequence counts for ASV's classified to a given bacterial phyla divided by the total number of sequences in the sample and presented as a percentage. Labels on the bottom indicate river sediment (RS) or tree core (T) sample type, and the associated number represents the sediment location (Fig. 2.2) and tree stem tag (See Appendix 7.5 for the tags associated taxa and cluster).

River sediment samples had an average of 4.8 times as many bacterial 16s rRNA ASV's than tree stems, and river sediments had greater Shannon diversity index values (Fig. 3.5). The bacterial community compositions differed significantly for tree stem and river sediment samples, and within-group beta-diversity did not differ significantly for sample type (Fig. 3.6). In tree stem samples the bacterial community compositions did not differ significantly between cottonwood taxa or tree cluster (Fig. 3.7).

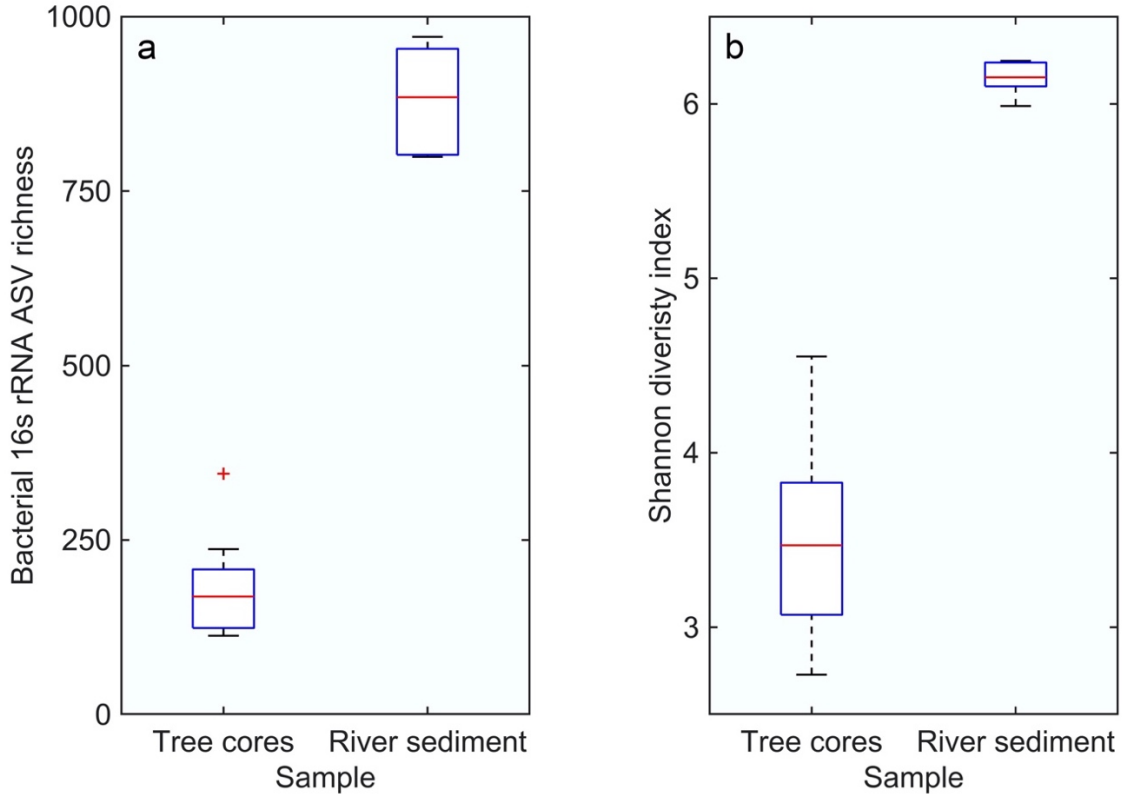

Figure 3.5: Differences in (a) the number of bacterial 16s rRNA ASV's and (b) associated Shannon diversity index values from *Populus spp.* tree core (n=8) and Oldman River sediment (n=6) samples. The number of observed bacterial ASV's and Shannon diversity differed significantly for tree stem and river sediment samples based on Kruskal-Wallis tests. For observed bacterial ASV's, $X^2_{(1,12)}$=9.60, P<0.01, and for Shannon diversity, $X^2_{(1,12)}$=9.60, P<0.01.

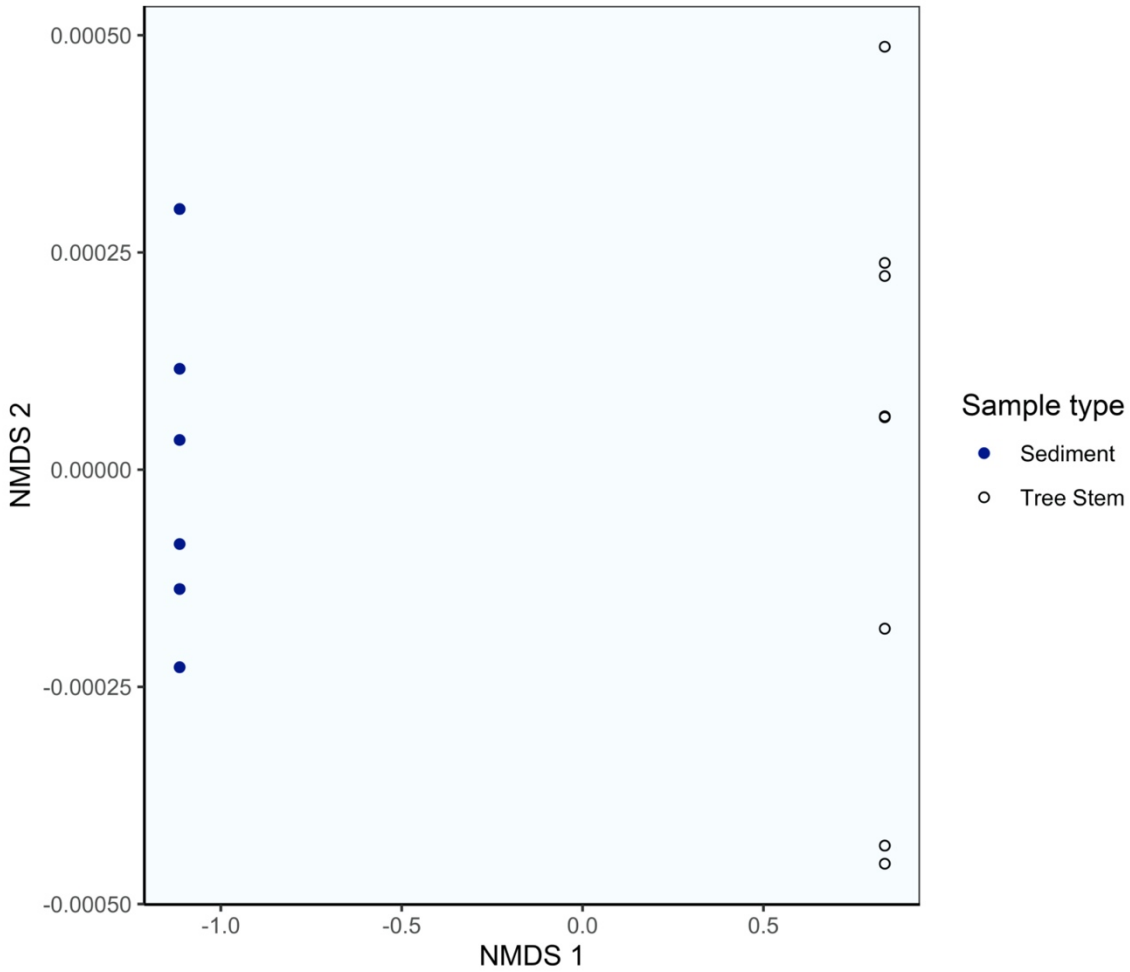

Figure 3.6: Non-metric multidimensional scaling (NMDS) with Bray-Curtis distance for bacterial 16s rRNA ASV counts in *Populus spp*. tree core (T; n=8) and Oldman River sediment (RS; n=6) samples. River sediment and tree stem bacterial community compositions differed significantly based on permutational multivariate analysis of variance (PERMANOVA) with 999 permutations $F_{(1,12)}$=2.68, P<0.01. Within-group beta diversity did not differ significantly for tree stem and river sediment samples based on PERMANOVA with 9,999 permutations $F_{(1,12)}$=0.01, P=0.92. Tree core and river sediment dissimilarities are expanded in figures 3.7 & 3.8. The ordination stress is 8.70×10^{-5}

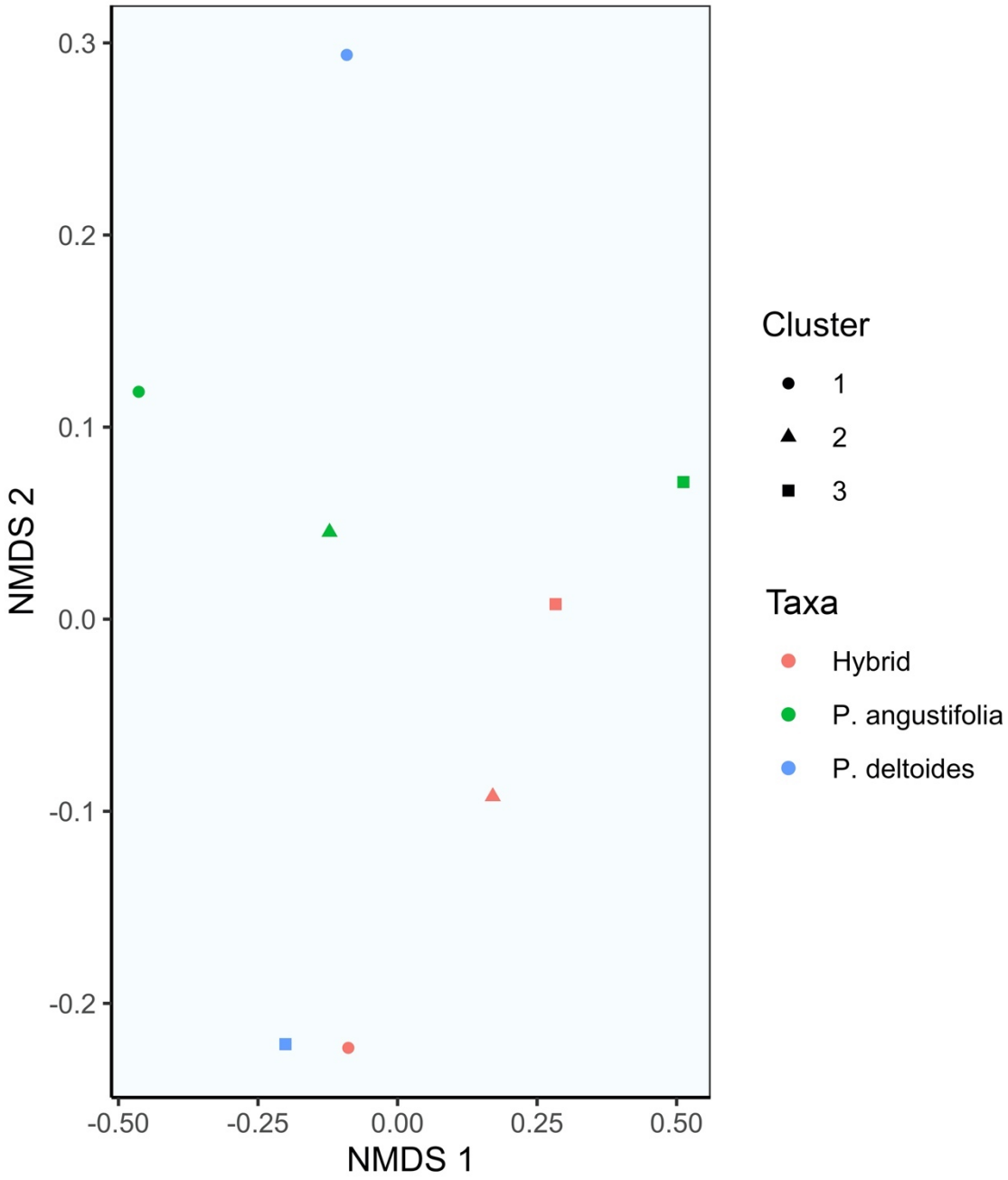

Figure 3.7: Non-metric multidimensional scaling (NMDS) with Bray-Curtis distance for bacterial 16s rRNA ASV counts in *Populus spp*. tree core samples. Bacterial community composition in tree stems did not differ significantly between taxa ($F_{(2,5)}$=1.04, P=0.44) or cluster ($F_{(2,5)}$=1.13, P=0.21) based on PERMANOVA tests with 999 permutations. The ordination stress is 0.11

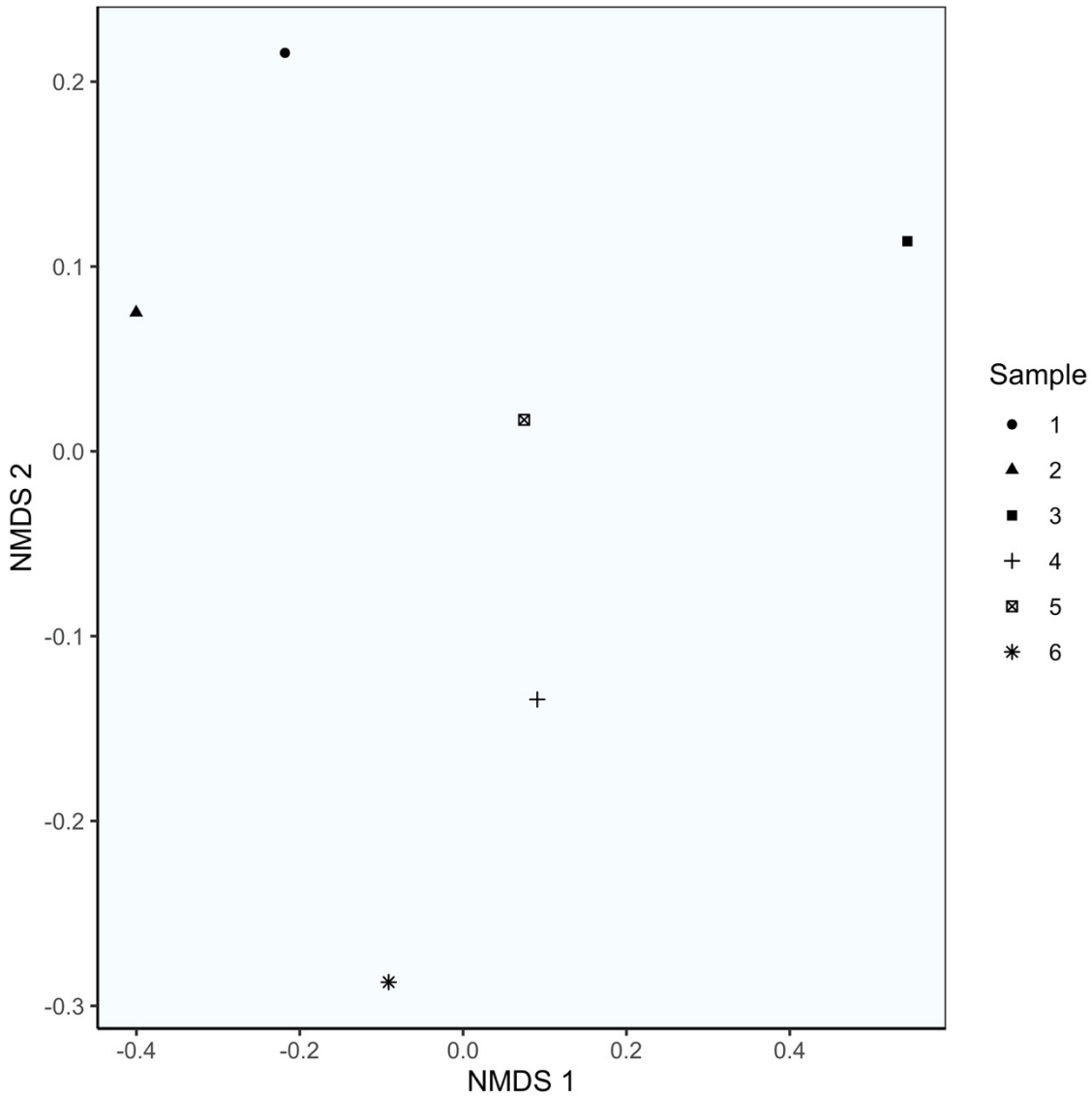

Figure 3.8: Non-metric multidimensional scaling (NMDS) with Bray-Curtis distance for bacterial 16s rRNA ASV counts in Oldman River sediment (RS) samples. The ordination stress is 0.03

3.3 Metabolic pathways of methane production

3.3.1 Methane and carbon dioxide gas production

Each river sediment and tree core sample had significant increases in the concentration of CO_2 and CH_4 in the chamber headspace over the course of anaerobic incubation experiments (Fig. 3.9; Fig. A.1.1 – A.1.14). River sediment sample 1 was lost during the experiment. Concentrations of methane in the headspace did not differ significantly for sample type (Fig. 3.9a). Tree core samples produced significantly greater quantities of CO_2 than the river sediment (Fig. 3.9b), with tree core samples having greater than twice the average [CO_2] of river sediment at every time point.

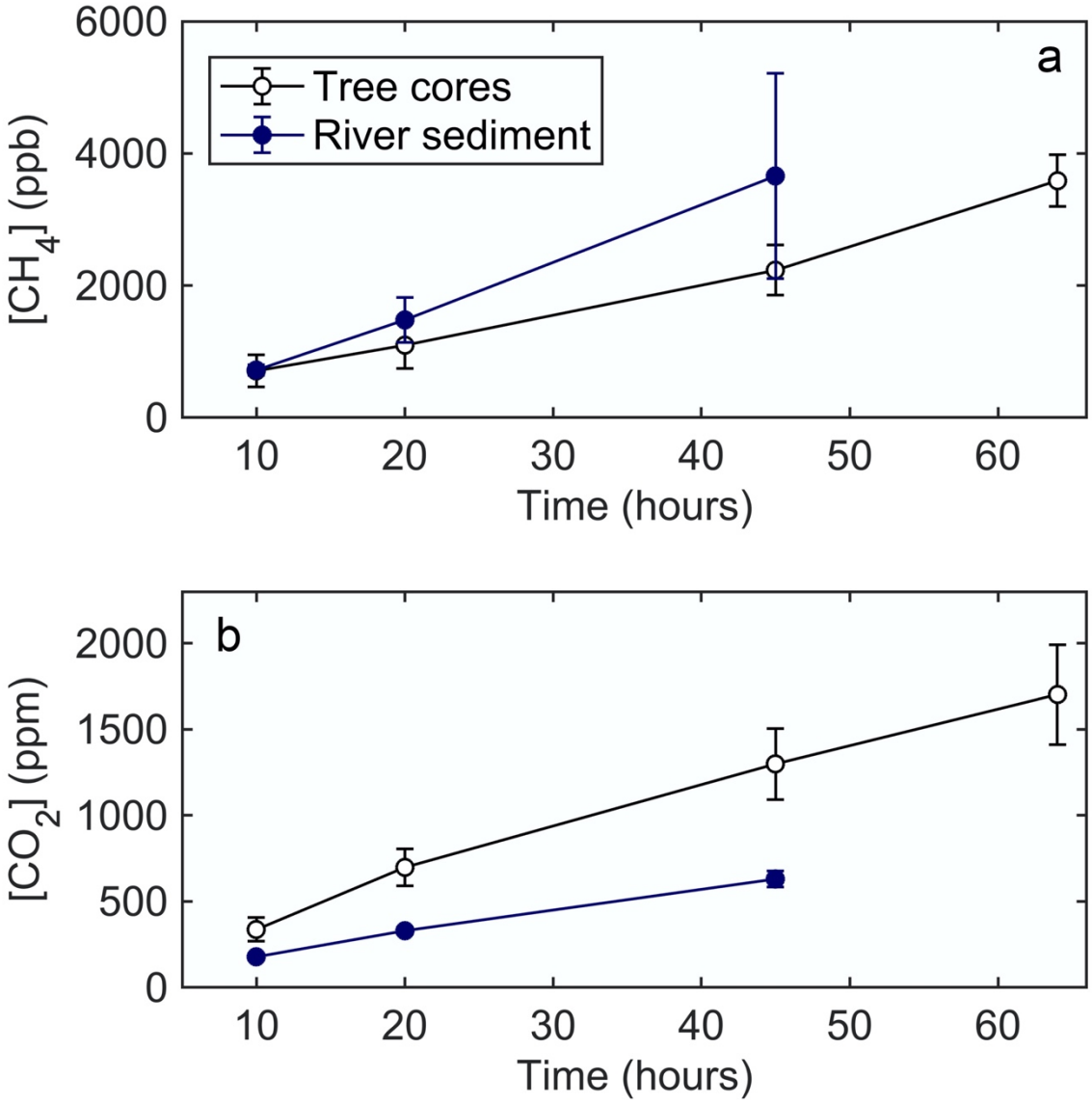

Figure 3.9: Comparison of (a) methane and (b) carbon dioxide gas production by tree cores (*Populus spp.;* n=9) and Oldman River sediment (n=5) during anaerobic incubation, represented as the mean ± SE. Sample type and time were statistically significant effects for $[CO_2]$, while only time was a significant effect for $[CH_4]$, based on 2-way, unbalanced, repeated measure ANOVA on $[CO_2]$ and $\ln([CH_4])$ values (time is repeated factor). Methane values were transformed due to non-normal distribution at 20 and 45 hours, and because of a significant increase in variance for the river sediment measures. For $\ln([CH_4])$ values, time effect was significant, $F_{(2,24)}=40.36$, $P<0.001$, whereas sample type, $F_{(1,12)}=2.62$, $P=0.13$, and interaction $F_{(2,24)}=0.77$, $P=0.47$, were not. For $[CO_2]$ values, sample effect, $F_{(1,12)}=7.66$, $P<0.05$, and time effect, $F_{(2,24)}=15.7$, $P<0.001$, were significant, while their interaction was not, $F_{(2,24)}=2.03$, $P<0.05$.

3.3.2 Stable carbon isotope analyses

Methane initially produced by tree cores was relatively enriched in ^{13}C (-20‰), but its stable carbon isotope composition became more depleted with increasing accumulation of methane, leveling off with $\delta^{13}C$ CH_4 values near -84‰ at high methane concentrations (Fig. 3.10b). The largest change in tree core $\delta^{13}C$ CH_4 values was seen from 2000 to 3000 ppb, which showed depletion in ^{13}C by ~20‰ (Fig. 3.10b). This contrasts with trends observed for river sediment incubations, which had no significant change in methane $\delta^{13}C$ values as methane accumulated in the chamber headspace (Fig. 3.11).

At the end of the incubation experiment, the average stable carbon isotope composition of methane from the river sediment (-52.2 ‰) was enriched in ^{13}C by an average of 35.4‰ compared to methane produced by tree cores (-87.6 ‰; Fig. 3.12). Methane $\delta^{13}C$ values from river sediment (-48.4 to -55.1‰) showed less variation than from tree cores (-70.6 to -103.7‰; Fig. 3.12).

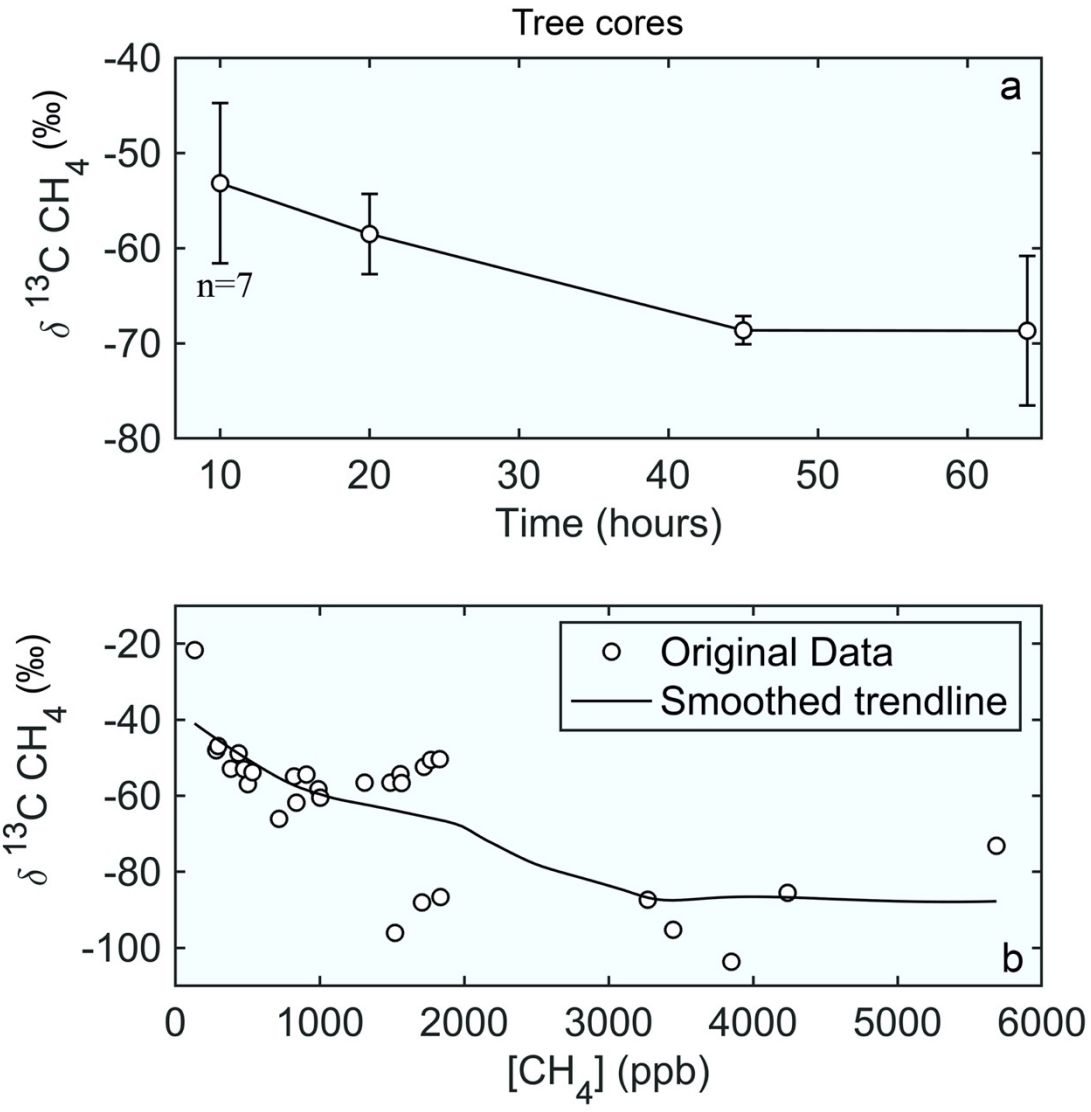

Figure 3.10: Trends in the stable carbon isotope composition of accumulated methane produced by tree cores (*Populus spp.)* during anaerobic incubation, expressed as (a) time course of the average isotopic signature (n=9 unless denoted where sample size was reduced due to methane concentrations being below the limit of detection for $\delta^{13}C$ values) ± SE, and (b) a combination of all [CH_4] versus $\delta^{13}C$ data points (n=30), excluding one outlier with [CH_4] > twice the average [CH_4] at the end of incubation. The black line is a smoothed trendline from a linear LOESS model (Cleveland & McGill., 1984), with a smoothing parameter of 0.7 (See Fig. 7.8 for model comparisons) using MATLAB functions written by W. L & A. R Martinez (2002).

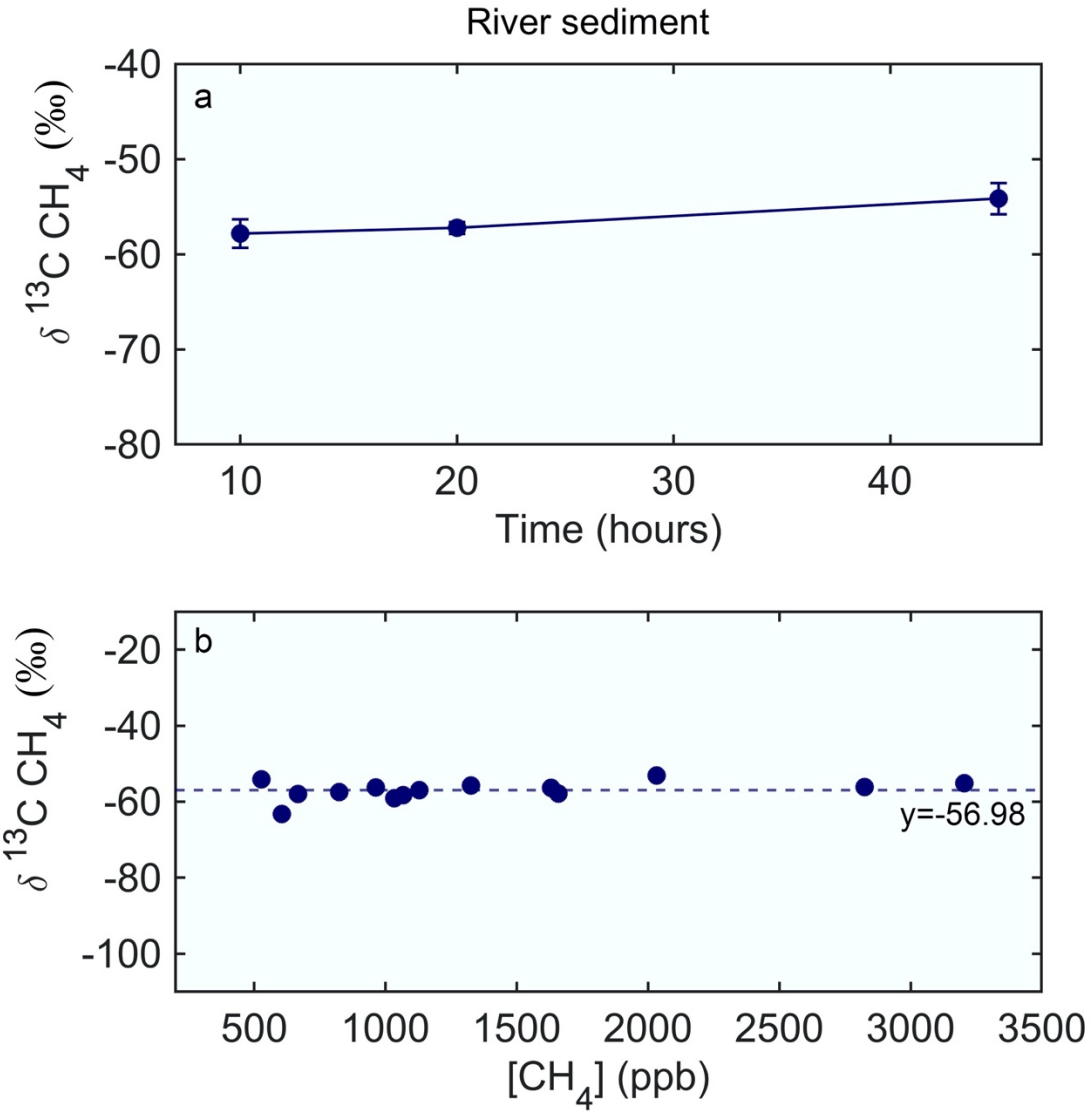

Figure 3.11: Trends in the stable carbon isotope composition of accumulated methane produced by Oldman River sediment during anaerobic incubations. Values are represented as (a) time course of the average isotopic signature (n=5) ± SE, and (b) combination of all [CH_4] versus $\delta^{13}C$ CH_4 data points (n=14), excluding one outlier with [CH_4] > twice the average [CH_4]. The dashed line shows the median value as $\delta^{13}C$ CH_4 did not change significantly with [CH_4], based on an F test of the linear regression model, $F_{(1,13)}$=2.84, P=0.12.

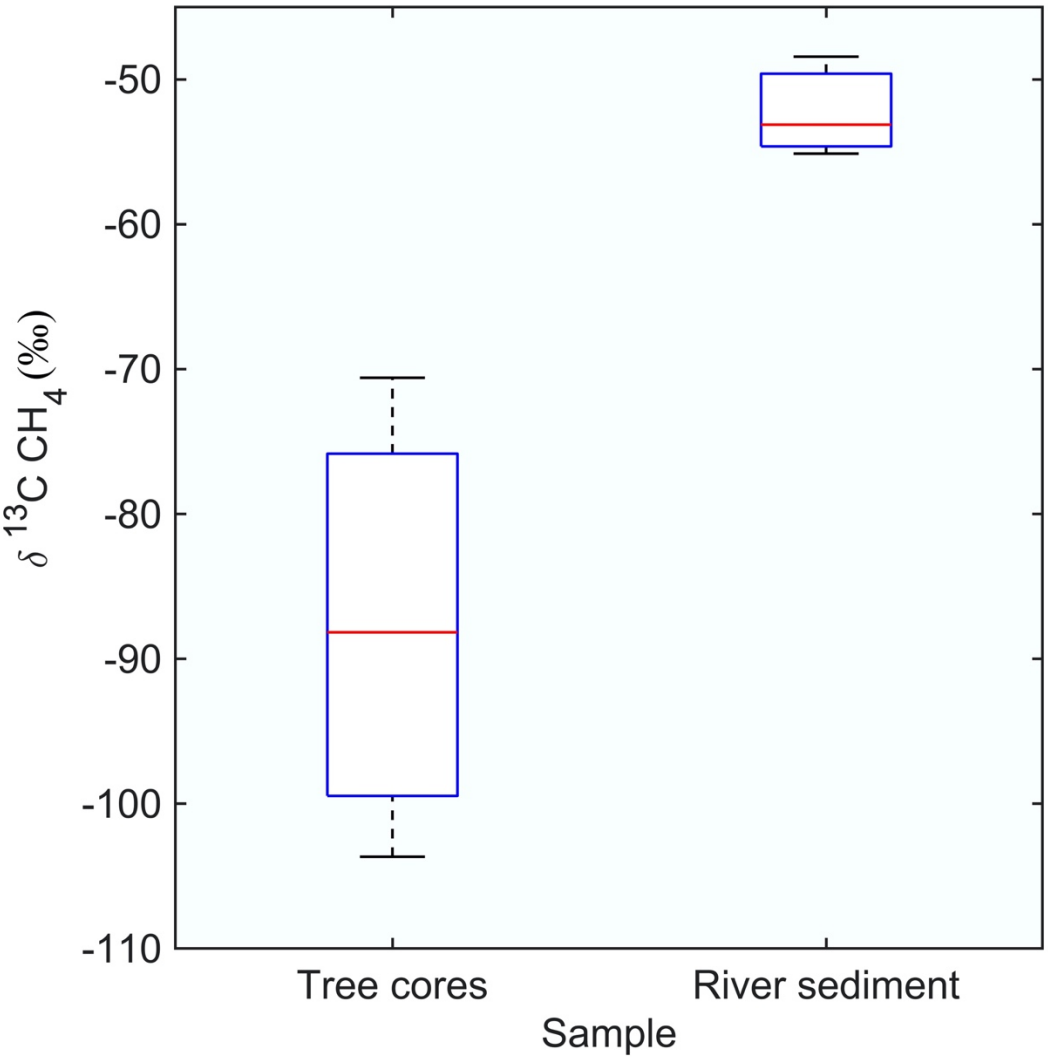

Figure 3.12: Box and whisker plots for the stable carbon isotope composition ($\delta^{13}C$ values) of methane produced by tree stem (*Populus spp.)* and Oldman River sediment samples following anaerobic incubation. $\delta^{13}C$ CH_4 changed with [CH_4] as methane accumulated, so river sediment (n=3) and tree core (n=4) values represent samples with significant [CH_4] (>>2000 ppb) at the end of the incubation period. $\delta^{13}C$ values of methane produced by tree cores and river sediment at the end of incubation were significantly different, based on a Kruskal-Wallis test ($X^2_{(1,5)}$=4.5, P<0.05)

4. DISCUSSION

4.1 Methanogen community composition

Oldman River sediment, alluvial groundwater and *Populus* tree stems in the adjacent riparian forest harboured different methanogen communities (Fig. 3.1). As expected, the relative abundance of ASV's classified as CO_2 reducing Methanobacteriales was significantly greater in tree stems (89.7 to 99.6%) than in the river sediment (28.2 to 98.4%; Fig. 3.1). Predictably, Methanosarcinales had significant (>1%) relative abundance in all river sediment samples (average ± SD; 16.9 ± 10.1%), and they were only in four out of nine tree stems (11.5 ± 17.1%; Figs. 3.1 & 3.2). Methanogen communities in the river sediment were more diverse than in tree stems, as ~3 times as many methanogen ASV's were detected, and Shannon's diversity index values were significantly greater in the river sediment (2.72 to 4.64) than tree stems (0.34 to 1.73; Fig. 3.2). Methanogens in the alluvial groundwater may change seasonally with flooding events and subsequent organic matter supply as demonstrated for bacterial communities (Xia *et al.*, 2020), so the identification of primarily (>93%) Methanobacteriales in the alluvial groundwater could be a result of the date sampling was conducted.

Most (>99.9%) Methanobacteriales ASV's classified to genus were *Methanobacterium*, and their high abundance observed in the cottonwood tree stems aligns with previous studies (Zeikus & Ward, 1974; Yip *et al.*, 2019). Similarly, *Methanobrevibacter* classified ASV's were only identified in one tree stem in low abundance (<0.1%), which is consistent with a previous study of

poplar tree stems (Yip *et al.*, 2019). The presence of methanogen orders Methanosarcinales, Methanobacteriales, Methanomicrobiales and Methanomassiliicoccales in the river sediments was also consistent with previous reports (Kemnitz *et al.*, 2004; Buriánková *et al.*, 2013; Mach *et al.*, 2015; Cozannet *et al.*, 2020). Nearly 1/3 of *mcrA* nucleotide sequences variants identified in the cottonwood trees were present in the river sediment, and phylogenetic analyses of the remaining amplicons suggested they were genetically similar (See Appendix 7.2). While the same methanogen species could be present in each environment, contrasting abundance of different methanogen species in the tree stems and river sediment demonstrate the environmental pressures driving methanogen growth and community composition in the two environments (Wen *et al.*, 2017; Lyu & Liu, 2018).

ASV's classified as the methanol-reducing order Methanomassiliicoccales had similar relative abundance in cottonwood tree stems (0.23 to 5.70%) and the Oldman River sediment (1.52 to 7.80%; Fig. 3.3). While a previous study of cottonwood trees found the bacterial and archaeal community contained Methanomassiliicoccales in low relative abundance (<1%; Yip *et al.,* 2019), these results suggest they can account for a considerable portion of the methanogen community (Fig. 3.3). Methanol is often formed through pectin degradation, so this pathway has been suggested to be more important in environments with high quantities of pectin (Schink *et al.*, 1981; Conrad, 2020a). The breakdown of pectin to methanol generally produces the substrates H_2/CO_2 and acetate (Schink

et al., 1981; Conrad, 2020a), which may contribute to the greater abundance of Methanobacteriales and Methanosarcinales (Fig. 3.3). Contrary to expectations and previous studies of cottonwood trees (Zeikus & Ward, 1974; Balch *et al.*, 1979; Wang *et al.*, 2016; Yip *et al.*, 2019), Methanosarcinales were identified in tree stems up to relative abundance of 45.9%, suggesting acetate fermentation could occur to some extent in tree stems (Lyu & Liu, 2018). This was supported by functional gene mapping within cottonwood trees that suggested both CO_2 reduction and acetate fermentation pathways could be active simultaneously (Yip *et al*., 2019). Of importance, a majority of Methanosarcinales sequences in tree stems belonged to *Methanosarcinaceae*, which can also perform hydrogenotrophic methanogenesis (Lyu & Liu, 2018). Consistent with previous studies (Cregger *et al.*, 2018; Yip *et al.*, 2019), the relative abundance of each methanogen order, and methanogen alpha diversity, did not differ significantly between cottonwood taxa or distance from the river, except for Methanomicrobiales, which were absent from *P. angustifolia* samples. The absence of Methanomicrobiales in *P. angustifolia* could be due to them being missed during sampling, differences in Populus biochemical products within the stem, or microbial interactions such as differing abundance of bacterial/fungal pathogens between tree species (Cregger *et al.,* 2018).

River sediments contained the acetoclastic family *Methanosaetaceae* at greater relative abundance (10.2 ± 3.90%; average ± SD) than *Methanosarcinaceae* (6.53 ± 7.81%). Buriánková *et al.* (2013) found

Methanosaetaceae spp. present in river sediments with consistently high concentrations of acetate in the porewater, suggesting that significant quantities of acetate were present the Oldman River sediment. These results differ significantly from previous studies that reported a greater abundance of *Methanosarcinaceae* in river surface sediments, while *Methanosaetaceae* were absent or rare in surface layers but increased with sediment depth (Buriánková *et al.*, 2013; Mach *et al.*, 2015). *Methanosaetaceae* have a high affinity for acetate and dominate in low concentrations (<30 μM; Kemnitz *et al*., 2004), while *Methanosarcinaceae* generally use acetate when it is in high quantities (~1 mM; Lyu & Liu, 2018). Additionally, *Methanosarcinaceae* sp. are generally more tolerant of oxygen than *Methanosaetaceae* sp. (Kemnitz *et al.*, 2004; Conrad, 2020b). The greater abundance of *Methanosaetaceae* observed in this study could thus be indicative of differences in O_2 content or acetate availability.

4.2 Bacterial community composition

The bacterial community associated with methanogens has been suggested to strongly regulate methanogen growth by controlling the formation of precursor methanogenic substrates (Bertolet *et al.*, 2019; Conrad, 2020a). River sediment and tree stem bacterial community compositions differed significantly (Fig. 3.6), which likely contributed to the dominance of different methanogen species.

Differences in the abundance and activity of bacteria involved in breaking down organic matter could yield H_2/CO_2 and acetate in differing quantities (Conrad, 2020a; Nozhevnikova *et al.*, 2020), resulting in the dominance of different methanogen species. The bacterial community composition in tree stems did not differ significantly between cottonwood taxa or location, which is consistent with previous reports (Cregger *et al.*, 2018; Yip *et al.*, 2019). Bacterial diversity in river sediments has been found to increase with sediment accumulation, leading to a mosaic pattern of microbial communities (Leff *et al.*, 1992; Besemer, 2015; Chen *et al.*, 2018). River sediment locations with greater organic matter inputs and bacterial diversity may support the growth of more methanogens. This is consistent with the large variation in the number of *mcrA* ASV's observed among river sediment samples (Fig. 3.2).

In alignment with previous studies (Yip et al., 2019), methane consuming bacteria (methanotrophs) were found in low relative abundance in some tree stem samples and belonged to the genera *Crenothrix* (<3.8%), *Methylobacterium* (<0.65%), and *Methylocystis* (<0.03%; data not shown). Of importance, some oxygen rich tree bark can harbour methanotrophs (Iguchi *et al.*, 2012; Iguchi *et al.*, 2015; Jeffrey *et al.*, 2021), so it is possible methanotroph DNA detected in tree stem samples originated from the tree bark and contaminated samples during collection (Yip et al., 2019). Regardless, their observed presence highlights the potential for methane consumption processes to occur within tree stems or in the bark, reducing net methane emission from tree stems (Jeffrey *et al.*, 2021). Further studies should test for the presence of methanotrophs in bark

and determine the extent to which they reduce methane flux from cottonwood tree stems.

4.3 Effect of organic matter on microbial community composition

The methanogen species present in an environment depends largely on the availability of substrates used to support their growth (Lyu & Liu, 2018; Conrad, 2020a), indicating that greater quantities of H_2/CO_2 were produced in the tree stems, while more acetate was formed in the river sediment. The nature of organic matter has been suggested to strongly dictate the quantities of precursor methanogenic substrates (Ji *et al.*, 2018; Conrad, 2020a), and river sediment and tree stem samples differed significantly as observed by their unique $\delta^{13}C$ C_{org}, % C, % N values (Table 2.1). High quality organic matter often has greater nitrogen content and a lower C:N ratio, and is suggested to produce greater quantities of acetate than H_2/CO_2 (Conrad, 2020a) and strongly control microbial community composition (Wu *et al.*, 2018; Grasset *et al.*, 2019; Xia *et al.*, 2020). Cottonwood tree stems had greater nitrogen content per gram biomass (0.09 ± 0.04%) than the river sediment (0.04 ± 0.02%; Table 3.1), however the tree stems high C:N ratio (546.2 ± 199.6) suggests this nitrogen was incorporated into recalcitrant structural components such as cellulose (Cowling & Merrill, 1996; Chapin *et al.*, 2011). This is supported by the estimated total carbon and nitrogen available during incubation experiments, as tree stems had significantly greater carbon but approximately 9 times less available nitrogen than river sediments (Table 3.1). The partial breakdown of cellulose has been found to form high

quantities of H_2/CO_2 (Harwood *et al.*, 1998; Conrad, 2020a), which likely supported the dominance of Methanobacteriales in the cottonwood tree stems (Fig. 3.3). This conclusion is supported by the greater abundance of ASV's belonging to the class Clostridia observed in trees (See section 7.4; Fig. 7.4.1), whose metabolic processes are suggested to degrade cellulose (Amin *et al.*, 2021). *Clostridium* have also been proposed to break down pectin to form H_2/CO_2 and acetate (Schink *et al.*, 1981; Amin *et al.*, 2021), which could support the growth of Methanosarcinales observed in tree stems (Fig. 3.1). The abundance of Methanosarcinales in tree stems was not associated with any organic matter or tree characteristic measured; however, cottonwood trees have been found to vary in the abundance of fungal pathogens (Cregger *et al.*, 2018), which could alter microbial interactions or the quantities of H_2/CO_2 and acetate substrates produced (Ma *et al.*, 2020).

Organic carbon content in the river sediment (0.4 ± 0.24) was within the range previously reported for methanogen-inhabited river sediments (0.5 to 3.1; Mach *et al.*, 2015; Bednařík *et al.,* 2019), with C:N ratio (9.9 ± 3.4) lower than previously reported (12.6 ± 1.8; Flury & Ulseth, 2019; 16.5 ± 5.8; Chen *et al*., 2018; 10.2 ± 0.2; Bednařík *et al*., 2019). These previous studies showed that river sediments harboured a large number of Methanosarcinales, indicating organic matter present in the Oldman River sediment breaks down to form significant quantities of acetate. This assumption is supported by the presence of stress

intolerant *Methanosaetaceae* in each sediment sample that obligately utilize acetate for metabolism (Buriánková *et al.*, 2013; Lyu & Liu, 2018).

Microbial diversity and metabolic processes have been shown to increase in river sediment with higher organic matter inputs (Chen *et al.*, 2018; Bednařík *et al.*, 2019). Species richness and Shannon diversity index were both greater in river sediment environments than in tree stems (Fig. 3.5), likely due to greater organic matter inputs supporting the growth of a wider range of microorganisms (Chen *et al.*, 2018; Xia *et al.*, 2020). While not explored in this study, greater quantities of dissolved labile (lipid-like) and recalcitrant (lignin-like) organic matter can increase the complexity of bacterial metabolism (Flury & Ulseth, 2019). Dissolved organic matter is typically present in freshwater streams (Flury & Ulseth, 2019; Bodmer *et al.*, 2020), and presumably contributed to the greater bacterial diversity observed in the river sediments than tree stem (Fig. 3.5)

4.4 Primary metabolic pathways of methane production

Investigation into methane production in river sediment (Oldman River) and *Populus* tree stems in the adjacent riparian forest revealed striking differences in their metabolic pathways of methane production. As expected, at the end of incubation experiments the stable carbon isotope composition of methane produced by tree stems (-70.6 to -103.6‰) were more depleted in ^{13}C than methane from the river sediment (-48.4 to -55.1‰) (Fig. 3.12). Methane produced by tree core samples had $\delta^{13}C$ values indicative of methane production

dominated CO_2 reduction (-70 to -110‰), while river sediment $\delta^{13}C$ CH_4 values indicated a greater contribution of acetate fermentation (-45 to -65‰; Whiticar 1999).

Methane produced by tree cores had an average $\delta^{13}C$ value (-87.6‰) in the range of previous measurements in upland forest cottonwood tree stems (-78.3 to 89.1‰; Wang *et al*., 2016), where values were consistent with CO_2 reduction being the primary metabolic pathway (Whiticar, 1999). In this study river sediment produced methane with $\delta^{13}C$ values (-52.2‰) that were slightly more enriched in ^{13}C than river sediments environments studied previously (-59 to -68‰; Mach *et al*., 2015; -67.1 to -70.9‰; Bednařík *et al*., 2019). In these previous studies, the relative contribution of acetate fermentation to total methane produced in sediment ranged from 25-59%, indicating significant contribution of acetate fermentation to total methane production in the Oldman River sediment (Mach et al., 2015; Bednařík *et al*., 2019). These previous reports were also consistent with additional studies noting the dominance of CO_2-reducing methanogens in tree stems (Zeikus & Ward, 1974; Zieikus & Henning, 1975; Wang *et al.*, 2016; Yip *et al.*, 2019), and the high diversity of both CO_2 reducing and acetate fermenting methanogens in river sediments (Kemnitz *et al.*, 2004; Buriánková *et al.*, 2013; Mach *et al.*, 2015).

Methane produced by the river sediment had little variation in $\delta^{13}C$ values (Fig. 3.11), whereas methane from tree cores was initially enriched in ^{13}C but

became more depleted over the course of anaerobic incubation (Fig. 3.10). Ji *et al.* (2018) observed significant changes in methane's $\delta^{13}C$ value during anaerobic incubation as organic matter became more recalcitrant and the contribution of CO_2 reduction increased; a mechanism not anticipated in this study due to the short incubation time (64 h) in comparison to the Ji *et al.* (2018) study (120 days). The observed changing $\delta^{13}C$ values of methane from tree cores were thus consistent with non-steady-state conditions such as decreased substrate availability (Whiticar, 1999) and methanogen growth phase eliciting varying levels of isotope fractionation (Valentine *et al.*, 2004; Okumura *et al.*, 2016). Once steady-state was reached, the $\delta^{13}C$ values were representative of the primary methane production pathway (Conrad, 1999; Conrad, 2005; Bednařík *et al.*, 2019), with the accumulation of methane trending towards these steady-state values (Fig. 3.10b).

4.5 Organic matter characteristics driving methane production

The primary metabolic pathway for methane production and the associated microbial community necessary for organic matter decomposition are driven by ecological conditions (Lyu & Liu, 2018; Yip *et al.*, 2019; Xia *et al.*, 2020). The rate at which each methanogenic pathway proceeds is limited by substrate availability (Conrad, 2005; Conrad, 2020a), indicating greater quantities of acetate are produced in the Oldman River sediment, while more H_2/CO_2 is produced in cottonwood tree stems. Quantities of H_2/CO_2 and acetate produced depend on the nature of organic matter decomposed (Conrad, 2020a; Bertolet *et*

al., 2019), implying different organic matter types were present in the river sediment and tree stem environments, which were supported by their distinct $\delta^{13}C$ C_{org} values (Table 3.1). The available carbon in cottonwood tree stem samples during anaerobic incubations was an average of 4.9 times greater than river sediment samples (Table 3.1), which is attributed to the high abundance of the structural components, lignin and cellulose (Sannigrahi *et al.*, 2010; Chapin *et al.*, 2011). The highly recalcitrant nature of these compounds hinders their full decomposition (Chapin *et al.*, 2011), with the partial breakdown of cellulose yielding high quantities of the substrates H_2 and CO_2 and no acetate (Harwood *et al.*, 1998; Conrad, 2020a). Partial cellulose decomposition likely explains the greater CO_2 production by tree cores than the river sediment, a trend that is not attributed to differences in overall metabolic activity as rates of methane production were similar (Fig. 3.9). Organic carbon content (%) in the river sediment (0.4 ± 0.24) was similar to values reported for river sediments with methanogens by Mach *et al*. (2015; 0.55 ± 0.06) and less than values reported by Bednařík *et al.* (2019) in surface sediment (0-10 cm; 2.5 ± 0.6) and in deeper sediment layers (10-20 cm; 1.1 ± 0.6). Of importance, Bednařík *et al.* (2019) found the contribution of acetate fermentation to total methane produced was lower in the surface sediment with greater organic carbon content. These findings suggest the primary metabolic pathway of methane production is more strongly controlled by organic matter quality than quantity.

River sediment organic matter had a C:N ratio (9.9 ± 3.4) lower than previously reported in riparian sediments (12.6 ± 1.8; Flury & Ulseth, 2019; 16.5 ± 5.8; Chen *et al*., 2018; 10.2 ± 0.2; Bednařík *et al*., 2019), indicating high quality organic matter was present. Methane production in lake sediment was previously found to be greatest when the C:N ratio was <10 (Duc *et al.*, 2010), further supporting the assumption of relatively high nitrogen contents in the organic matter in the Oldman River sediment. Sediment C:N ratio had no significant correlation with methane production ($[CH_4]$ or $\delta^{13}C$ CH_4), however there was a strong correlation between % N *(x)* and $[CH_4]$ *(y)* at the end of the incubation period ($y = 262794x - 3699.2$, $r^2 = 0.973$, $P < .01$; data not shown). Previous studies found rates of methane production were more strongly correlated to total nitrogen content than to organic carbon content or C:N ratio (Gebert *et al.*, 2006; Duc *et al.*, 2010; Bednařík *et al.*, 2019). Poplar tree stems generally have a high C:N ratio (84 to 621; Sannigrahi *et al.*, 2010) as observed in this study (265 to 930), which likely provide insufficient nutrients (N) for complete microbial degradation (Chapin *et al.*, 2011). This is supported by the approximately 9 times greater available nitrogen in river sediment incubation samples than tree stem samples (Table 3.1). Rates of tree stem methane production were not correlated to carbon or nitrogen content but increased significantly when stem samples were fully submerged in water (See chapter 7.7; Fig. 7.7). Tree stem water content has been found to significantly increase rates of methane production (Wang *et al.*, 2017; Wang *et al.*, 2021), but showed no effect on the abundance of methanogens within the tree stem (Yip *et al.*, 2019). Significant differences in tree

stem and river sediment solid organic matter highlights the strong control organic matter quality elicits on the pathways of methane production.

CHAPTER 5. CONCLUSION

In southern Alberta, the Oldman River and adjacent riparian cottonwood trees harbour a consortium of microorganisms that break down organic matter and produce methane. Organic matter quality, which strongly controls microbial community composition and their metabolic processes (Wen *et al.*, 2017; Ji *et al.*, 2018; Conrad, 2020a), differed significantly for tree stem and river sediment environments. In tree stems, high quantities of H_2/CO_2 formed during the partial breakdown of cellulose is the suggested mechanism for dominance of CO_2 reducing methanogens. Acetate fermenting methanogens belonging to the family *Methanosaetaceae* were more abundant in the river sediment than tree stems, presumably due to higher quality organic matter breaking down to form greater quantities of acetate (Conrad, 2020a). Similarly, the bacterial community required to break down organic matter to form precursor methanogenic substrates also differed significantly for tree stem and river sediment environments. High-quality organic matter present in the river sediment also likely supported microbial growth, resulting in greater methanogen and bacterial diversity than in tree stems. Differences in substrate availability and microbial community composition in tree stems and river sediment were mirrored by striking differences in their metabolic pathways of methane production. Low $\delta^{13}C$ values of methane produced in tree cores were indicative of CO_2 reduction being the dominant methane production pathway, while the high $\delta^{13}C$ values of methane from the

river sediment suggest a greater contribution of acetate fermentation to total methanogenesis.

Methanogen communities appear relatively stable over long periods when anaerobic conditions are maintained (Mach *et al.*, 2015; Conrad, 2020b), so their composition in river sediment and tree stems are not expected to change significantly over the growing season. While the microbial community composition may remain stable, their pathways of methane production should change with substrate availability (Ji *et al.*, 2018; Conrad, 2020a). This thesis research provided a simplified investigation into the microbial community and metabolic pathways of methane production in tree stems and river sediment. For example, methanogens can be associated with algae (Bogard *et al.*, 2014) and freshwater biofilms (Besemer, 2015), which can be hotbeds for methanogen activity (Buriánková *et al.*, 2013; Grasset *et al.*, 2019). Additionally, microbial biofilms can consume acetate, and in turn increase the contribution of CO_2 reduction to total methane produced (Conrad 2020a). Dissolved organic matter, with such proxies as molecular weight, aromaticity, and quantities of lipid and lignin-like compounds, can strongly influence the microbial community (Wu *et al.*, 2018), as well as the rate and primary pathway of methane production (Fellman *et al.*, 2010; Hodgkins *et al.*, 2014; Bodmer *et al.*, 2020).

The effect of tree stem tissue type (heartwood and sapwood) on methane production was explored (See Appendix section 7.7), with no significant

difference in the rate of gas production or stable carbon isotope composition of methane. Additional compounds could be present within tree stems that elicit changes to the metabolic pathway of methane production (Li *et al.*, 2019). For example, lignin is highly recalcitrant in anaerobic environments, but can be partially decomposed to produce methanol (Conrad, 2020a); and methanol consuming methanogens were observed in this study. Fungi are primary lignin degraders (Chapin *et al.*, 2011) that have previously been identified within *Populus* tree stems (Cregger *et al.*, 2018) and freshwater streams (Besemer, 2015), and their inclusion in methanogen incubation experiments with lignocellulose significantly increased methane production (Ma *et al.*, 2020). Non-structural carbohydrates are also present in trees and vary in abundance between species (Covey & Megonigal, 2019), with their degradation forming greater quantities of acetate than H_2 and CO_2 (Conrad, 2020a). Now that the microbial community composition and primary metabolic pathways of methane production in tree stems and river sediment have been explored, future studies can delve further into the ecological conditions eliciting change on the rate and primary metabolic pathways of methane production.

Uncertainty in the magnitude of natural methane emissions are being met head-on by ambitious models that predict methane emission rates (Saunois *et al.*, 2020), and changes to methanogen activity (Michal *et al.*, 2018) with different environmental conditions. While rich in potential, these models rely on interdisciplinary studies exploring the microbial community, their metabolic

pathways, and ecological controls on these microorganisms (Barba *et al.*, 2019; Conrad, 2020a). Characterization of these aspects in upland forest tree stems addresses a largely understudied aspect of natural methane emissions (Barba *et al.*, 2019). Increasing knowledge of the distinct microbial communities dominating river sediment and tree stems and differences in methane production pathways will provide insight into the ecological controls on these processes. $\delta^{13}C$ measurements of methane can be used as a reference to explore additional methane source, sink, or transport processes eliciting change to methane's isotopic signature in these environments (Whiticar, 1999; Conrad, 2005). Methane's $\delta^{13}C$ value from these sources can also be used to explore the relative contribution of the river and tree stems to net ecosystem methane emission (Flanagan *et al.*, 2021), and for incorporation into mechanistic models using isotopic compositions (Saunois *et al.*, 2020).

CHAPTER 6. REFERENCES

Afgan E, Baker D, Batut B, van den Beek M, Bouvier D, Cech M, Chilton J, Clements D, Coraor N, Gruning BA, et al. 2018. The Galaxy platform for accessible, reproducible and collaborative biomedical analyses: 2018 update. *Nucleic Acids Research* **46**(W1): W537-W544.

Amin FR, Khalid H, El-Mashad HM, Chen C, Liu G, Zhang R. 2021. Functions of bacteria and archaea participating in the bioconversion of organic waste for methane production. *Science of the Total Environment* **763**: 143007.

Balch WE, Fox GE, Magrum LJ, Woese CR, Wolfe RS. 1979. Methanogens: reevaluation of a unique biological group. *Microbiology Reviews* **43**(2): 260-296.

Barba J, Bradford MA, Brewer PE, Bruhn D, Covey K, van Haren J, Megonigal JP, Mikkelsen TN, Pangala SR, Pihlatie M, et al. 2019.

Methane emissions from tree stems: a new frontier in the global carbon cycle. *New Phytologist* **222**(1): 18-28.

Bednařík A, Blaser M, Rulik M. 2019. Methane formation and consumption by sediments in a cross-channel profile of a small river impoundment. *Journal of Limnology* **78**(2): 233-242.

Bertolet BL, West WE, Armitage DW, Jones SE. 2019. Organic matter supply and bacterial community composition predict methanogenesis rates in temperate lake sediments. *Limnology and Oceanography Letters* **4**(5): 164-172.

Besemer K. 2015. Biodiversity, community structure and function of biofilms in stream ecosystems. *Research in Microbiology* **166**(10): 774-781.

Bodmer P, Wilkinson J, Lorke A. 2020. Sediment properties drive spatial variability of potential methane production and oxidation in small streams. *Journal of Geophysical Research: Biogeosciences* **125**: e2019JG005213

Bogard MJ, del Giorgio PA, Boutet L, Chaves MC, Prairie YT, Merante A, Derry AM. 2014. Oxic water column methanogenesis as a major component of aquatic CH4 fluxes. *Nature Communications* **5**: 5350.

Braatne JH, Rood SB, Heilman PE. 1996. Life history, ecology, and conservation of riparian cottonwoods in North America. *Biology of Populus and its Implications for Management and Conservation*. Ottawa, ON, Canada: NRC Research Press, 57-85.

Buresova A, Kopecky J, Hrdinkova V, Kamenik Z, Omelka M, Sagova-Mareckova M. 2019. Succession of microbial decomposers is determined by litter type, but site conditions drive decomposition rates. *Applied Environmental Microbiology* **85**(24): e01760-01719.

Buriánková I, Brablcova L, Mach V, Dvorak P, Chaudhary PP, Rulik M. 2013. Identification of methanogenic archaea in the hyporheic sediment of Sitka stream. *PLoS One* **8**(11): e80804.

Buriánková I, Brablcová L, Mach V, Hýblová A, Badurová P, Cupalová J, áp L, Rulík M. 2012. Methanogens and methanotrophs distribution in the hyporheic sediments of a small lowland stream. *Fundamental and Applied Limnology* **181**(2): 87-102.

Bushong FW. 1907. Composition of gas from Cottonwood trees. *Transactions of the Kansas Academy of Science* **21**: 53.

Callahan BJ, McMurdie PJ, Holmes SP. 2017. Exact sequence variants should replace operational taxonomic units in marker-gene data analysis. *ISME Journal* **11**(12): 2639-2643.

Callahan BJ, McMurdie PJ, Rosen MJ, Han AW, Johnson AJ, Holmes SP. 2016. DADA2: High-resolution sample inference from Illumina amplicon data. *Nature Methods* **13**(7): 581-583.

Chapin SF, Matson PA, Vitousek P. 2011. *Principles of terrestrial ecosystem ecology*. New York: Springer. pp. 186-276

Chen J, Wang P, Wang C, Wang X, Miao L, Liu S, Yuan Q. 2018. Bacterial communities in riparian sediments: A large-scale longitudinal distribution pattern and response to dam construction. *Frontiers in Microbiology* **9**: 999.

Chen S, Wang P, Liu H, Xie W, Wan XS, Kao SJ, Phelps TJ, Zhang C. 2020. Population dynamics of methanogens and methanotrophs along the salinity gradient in Pearl River Estuary: implications for methane metabolism. *Applied Microbiology and Biotechnology* **104**(3): 1331-1346.

Clark K, Karsch-Mizrachi I, Lipman DJ, Ostell J, Sayers EW. 2016. GenBank. *Nucleic Acids Research* **44**(D1): D67-72

Cleveland W, McGill R. 1984. Graphical Perception: Theory, Experimentation, and Application to the Development of Graphical Methods. *Journal of the American Statistical Association* **79**(387): 531-554.

Conrad R. 1999. Contribution of hydrogen to methane production and control of hydrogen concentrations in methanogenic soils and sediments. *FEMS Microbiology Ecology* **28**(3): 193-202.

Conrad R. 2005. Quantification of methanogenic pathways using stable carbon isotopic signatures: a review and a proposal. *Organic Geochemistry* **36**(5): 739-752.

Conrad R. 2020a. Importance of hydrogenotrophic, aceticlastic and methylotrophic methanogenesis for methane production in terrestrial, aquatic and other anoxic environments: A mini review. *Pedosphere* **30**(1): 25-39.

Conrad R. 2020b. Methane production in soil environments-anaerobic biogeochemistry and microbial life between flooding and desiccation. *Microorganisms* **8**(6): 881.

Conrad R, Noll M, Claus P, Klose M, Bastos WR, Enrich-Prast A. 2011. Stable carbon isotope discrimination and microbiology of methane formation in tropical anoxic lake sediments. *Biogeosciences* **8**(3): 795-814.

Coplen TB. 1994. Reporting of stable carbon, hydrogen, and oxygen isotopic abundances. *International Union of Pure and Applied Chemistry* **66**(2): 31–34.

Covey KR, Megonigal JP. 2019. Methane production and emissions in trees and forests. *New Phytologist* **222**(1): 35-51.

Cowling, E. B., & Merrill, W. 1966. Nitrogen in Wood and Its Role in Wood Deterioration. *Canadian Journal of Botany,* **44**(11): 1539-1554.

Cozannet, M., Borrel, G., Roussel, E., Moalic, Y., Allioux, M., Sanvoisin, A., et al. 2020. New Insights into the Ecology and Physiology of Methanomassiliicoccales from Terrestrial and Aquatic Environments. *Microorganisms,* **9:** 1.

Cregger MA, Veach AM, Yang ZK, Crouch MJ, Vilgalys R, Tuskan GA, Schadt CW. 2018. The Populus holobiont: dissecting the effects of plant niches and genotype on the microbiome. *Microbiome* **6**: 31.

Dlugokencky EJ, Nisbet EG, Fisher R, Lowry D. 2011. Global atmospheric methane: budget, changes and dangers. *Philosophical Transactions of The Royal Society A: Mathematical Physical and Engineering Sciences* **369**(1943): 2058-2072.

Duc NT, Crill P, Bastviken D. 2010. Implications of temperature and sediment characteristics on methane formation and oxidation in lake sediments. *Biogeochemistry* **100**(1-3): 185-196.

Enzmann F, Mayer F, Rother M, Holtmann D. 2018. Methanogens: biochemical background and biotechnological applications. *AMB Express* **8**(1): 1.

Evans PN, Parks DH, Chadwick GL, Robbins SJ, Orphan VJ, Golding SD, Tyson GW. 2015. Methane metabolism in the archaeal phylum Bathyarchaeota revealed by genome-centric metagenomics. *Science* **350**(6259): 434-438.

Environment Canada. 2020. Climate Data Online. Available at: http://climate.weather.gc.ca/climate_normals/index_e.html. (accessed 10 April 2020).

Febria CM, Beddoes P, Fulthorpe RR, Williams DD. 2012. Bacterial community dynamics in the hyporheic zone of an intermittent stream. *ISME Journal* **6**(5): 1078-1088.

Fellman JB, Hood E, Spencer RGM. 2010. Fluorescence spectroscopy opens new windows into dissolved organic matter dynamics in freshwater ecosystems: A review. *Limnology and Oceanography* **55**(6): 2452-2462.

Feng H, Guo J, Han M, Wang W, Peng C, Jin J, Song X, Yu S. 2020. A review of the mechanisms and controlling factors of methane dynamics in forest ecosystems. *Forest Ecology and Management* **455**: 117702

Finn DR, Ziv-El M, van Haren J, Park JG, Del Aguila-Pasquel J, Urquiza-Munoz JD, Cadillo-Quiroz H. 2020. Methanogens and methanotrophs show nutrient-dependent community assemblage patterns across tropical peatlands of the Pastaza-Maranon Basin, Peruvian Amazonia. *Frontiers in Microbiology* **11**: 746.

Flanagan LB, Nikkel DJ, Scherloski LM, Tkach RE, Smits KM, Selinger LB, Rood SB. 2021. Multiple processes contribute to methane emission in a riparian cottonwood forest ecosystem. *New Phytologist* **229**(4): 1970-1982.

Flanagan LB, Orchard TE, Logie GSJ, Coburn CA, Rood SB. 2017. Water use in a riparian cottonwood ecosystem: Eddy covariance measurements and scaling along a river corridor. *Agricultural and Forest Meteorology* **232**: 332-348.

Flanagan LB, Orchard TE, Tremel TN, Rood SB. 2019. Using stable isotopes to quantify water sources for trees and shrubs in a riparian cottonwood ecosystem in flood and drought years. *Hydrological Processes* **33**(24): 3070-3083.

Flury S, Ulseth AJ. 2019. Exploring the sources of unexpected high methane concentrations and fluxes from alpine headwater streams. *Geophysical Research Letters* **46**(12): 6614-6625.

Gagnon N, Barret M, Topp E, Kalmokoff M, Masse D, Masse L, Talbot G. 2011. A novel fingerprint method to assess the diversity of methanogens in microbial systems. *FEMS Microbiology Letters* **325**(2): 115-122.

García-Palacios P, McKie BG, Handa IT, Frainer A, Hättenschwiler S, Jones H. 2015. The importance of litter traits and decomposers for litter decomposition: a comparison of aquatic and terrestrial ecosystems within and across biomes. *Functional Ecology* **30**(5): 819-829.

Gebert J, Köthe H, Gröngröft A. 2006. Prognosis of methane formation by river sediments (9 pp). *Journal of Soils and Sediments* **6**(2): 75-83.

Gom LA, Rood SB. 1999. The discrimination of cottonwood clones in a mature grove along the Oldman River in southern Alberta. *Canadian Journal of Botany* **77**(8): 1084-1094.

Grasset C, Abril G, Mendonca R, Roland F, Sobek S. 2019. The transformation of macrophyte-derived organic matter to methane relates to plant water and nutrient contents. *Limnology Oceanography* **64**(4): 1737-1749.

Harwood H, Caspari D, Fiebig K, Gottschalk G. 1998. Anaerobic metabolism of aromatic compounds via the benzoyl-CoA pathway. *FEMS Microbiology Reviews* **22**: 439-458.

Hodgkins SB, Tfaily MM, McCalley CK, Logan TA, Crill PM, Saleska SR, Rich VI, Chanton JP. 2014. Changes in peat chemistry associated with permafrost thaw increase greenhouse gas production. *Proceedings of the National Acadamy of Science USA* **111**(16): 5819-5824.

Huber W, Carey VJ, Gentleman R, Anders S, Carlson M, Carvalho BS, Bravo HC, Davis S, Gatto L, Girke T, et al. 2015. Orchestrating high-throughput genomic analysis with Bioconductor. *Nature Methods* **12**(2): 115-121.

Iguchi H, Sato I, Sakakibara M, Yurimoto H, Sakai Y. 2012. Distribution of methanotrophs in the phyllosphere. *Bioscience, Biotechnology and Biochemistry* **76**(8): 1580-1583.

Iguchi H, Yurimoto H, Sakai Y. 2015. Interactions of methylotrophs with plants and other heterotrophic bacteria. *Microorganisms* **3**(2): 137-151.

Jeffrey LC, Maher DT, Chiri E, Leung PM, Nauer PA, Arndt SK, Tait DR, Greening C, Johnston SG. 2021. Bark-dwelling methanotrophic bacteria decrease methane emissions from trees. *Nature Commun* **12**(1): 2127.

Jeffrey LC, Maher DT, Tait DR, Johnston SG. 2020. A Small Nimble In Situ Fine-Scale Flux Method for Measuring Tree Stem Greenhouse Gas Emissions and Processes (S.N.I.F.F). *Ecosystems* **23**(8): 1676-1689.

Ji Y, Liu P, Conrad R. 2018. Change of the pathway of methane production with progressing anoxic incubation of paddy soil. *Soil Biology and Biochemistry* **121**: 177-184.

Kemnitz D, Chin KJ, Bodelier P, Conrad R. 2004. Community analysis of methanogenic archaea within a riparian flooding gradient. *Environmental Microbiology* **6**(5): 449-461.

Kranjcec J, Mahoney JM, Rood SB. 1998. The responses of three riparian cottonwood species to water table decline. *Forest Ecology and Management* **110**(1-3): 77-87.

Lang K, Schuldes J, Klingl A, Poehlein A, Daniel R, Brunea A. 2015. New mode of energy metabolism in the seventh order of methanogens as revealed by comparative genome analysis of "*Candidatus methanoplasma termitum*". *Applied Environmental Microbiology* **81**(4): 1338-1352.

Leff LG, Vaun McArthur J, Shimkets LJ. 1992. Information spiraling: Movement of bacteria and their genes in streams. *Microbial Ecology* **24**(1): 11-24.

Li H-L, Zhang X-M, Deng F-D, Han X-G, Xiao C-W, Han S-J, Wang Z-P. 2019. Microbial methane production is affected by secondary metabolites in the heartwood of living trees in upland forests. *Trees* **34**(1): 243-254.

Liu Y, Yao T, Gleixner G, Claus P, Conrad R. 2013. Methanogenic pathways,^{13}C isotope fractionation, and archaeal community composition in lake sediments and wetland soils on the Tibetan Plateau. *Journal of Geophysical Research: Biogeosciences* **118**(2): 650-664.

Luton PE, Wayne JM, Sharp RJ, Riley PW. 2002. The *mcrA* gene as an alternative to 16S rRNA in the phylogenetic analysis of methanogen populations in landfill. *Microbiology* **148**: 3521-3530.

Lyu Z, Liu Y. 2018. Diversity and Taxonomy of Methanogens. In: Stams A., Sousa D, eds. *Biogenesis of Hydrocarbons. Handbook of Hydrocarbon and Lipid Microbiology*: Springer International Publishing, 19-77

Ma Y, Li Y, Li Y, Cheng Y, Zhu W. 2020. The enrichment of anaerobic fungi and methanogens showed higher lignocellulose degrading and methane producing ability than that of bacteria and methanogens. *World Journal of Microbiology and Biotechnology* **36**(9): 125.

Mach V, Blaser MB, Claus P, Chaudhary PP, Rulik M. 2015. Methane production potentials, pathways, and communities of methanogens in vertical sediment profiles of river Sitka. *Frontiers in Microbiology* **6**: 506.

Marcel, M. 2011. Cutadapt removes adapter sequences from high-throughput sequencing reads. *EMBnet.Journal*, **17**(1): 10-12

Martinez WR, Martinez A, R. 2002. *Computational Statistics Handbook with MATLAB*. Boca Raton, FL: Chapman & Hall/CRC.

Megonigal JP, Brewer PE, Knee KL. 2020. Radon as a natural tracer of gas transport through trees. *New Phytologist* **225**(4): 1470-1475.

Megonigal JP, Guenther AB. 2008. Methane emissions from upland forest soils and vegetation. *Tree Physiology* **28**(4): 491-498.

Michal B, Gagat P, Jablonski S, Chilimoniuk J, Gaworski M, Mackiewicz P, Marcin L. 2018. PhyMet^2 : a database and toolkit for phylogenetic and metabolic analyses of methanogens. *Environmental Microbiology Reports* **10**(3): 378-382.

Nazaries L, Murrell JC, Millard P, Baggs L, Singh BK. 2013. Methane, microbes and models: fundamental understanding of the soil methane cycle for future predictions. *Environmental Microbiology* **15**(9): 2395-2417.

Nisbet RE, Fisher R, Nimmo RH, Bendall DS, Crill PM, Gallego-Sala AV, Hornibrook ER, Lopez-Juez E, Lowry D, Nisbet PB, et al. 2009. Emission of methane from plants. *Proceedings of the Royal Society B: Biological Sciences* **276**(1660): 1347-1354.

Nozhevnikova AN, Russkova YI, Litti YV, Parshina SN, Zhuravleva EA, Nikitina AA. 2020. Syntrophy and interspecies electron transfer in methanogenic microbial communities. *Microbiology* **89**(2): 129-147.

Oksanen, J., and others. 2017. Vegan: Community ecology package. R package version 2.4-2.

Okumura T, Kawagucci S, Saito Y, Matsui Y, Takai K, Imachi H. 2016. Hydrogen and carbon isotope systematics in hydrogenotrophic methanogenesis under H2-limited and H2-enriched conditions: implications for the origin of methane and its isotopic diagnosis. *Progress in Earth and Planetary Science* **3**(1).

Pangala SR, Moore S, Hornibrook ERC, Gauci V. 2013. Trees are major conduits for methane egress from tropical forested wetlands. *New Phytologist* **197**(2): 524-531.

Penger, J., Conrad, R., Blaser, M. 2012. Stable carbon isotope fractionation by methylotrophic methanogenic archaea. *Applied Environmental Microbiology, **78***(21): 7596-7602.

Pitz S, Megonigal JP. 2017. Temperate forest methane sink diminished by tree emissions. *New Phytologist* **214**(4): 1432-1439.

Quast C, Pruesse E, Yilmaz P, Gerken J, Schweer T, Yarza P, Peplies J, Glockner FO. 2013. The SILVA ribosomal RNA gene database project: improved data processing and web-based tools. *Nucleic Acids Research* **41**(Database issue): D590-596.

Quay P, Stutsman J, Wilbur D, Snover A, Dlugokencky E, Brown T. 1999. The isotopic composition of atmospheric methane. *Global Biogeochemical Cycles* **13**(2): 445-461.

Rood SB, Braatne JH, Hughes FM. 2003. Ecophysiology of riparian cottonwoods: stream flow dependency, water relations and restoration. *Tree Physiology* **23**(16): 1113-1124.

Sannigrahi P, Ragauskas AJ, Tuskan GA. 2010. Poplar as a feedstock for biofuels: A review of compositional characteristics. *Biofuels, Bioproducts and Biorefining* **4**(2): 209-226.

Saunois M, Stavert AR, Poulter B, Bousquet P, Canadell JG, Jackson RB, Raymond PA, Dlugokencky EJ, Houweling S, Patra PK, et al. 2020.

The Global Methane Budget 2000–2017. *Earth System Science Data* **12**(3): 1561-1623.

Schink B, Ward JC, Zeikus JG. 1981. Microbiology of wetwood: importance of pectin degradation and *clostridium* species living in trees. *Applied and environmental microbiology* **42**: 526-532.

Shannon C, Weaver W. 1949. *The Mathematical Theory of Communication*: University of Illinois Press, Urbana.

Stanley EH, Casson NJ, Christel ST, Crawford JT, Loken LC, Oliver SK. 2016. The ecology of methane in streams and rivers: patterns, controls, and global significance. *Ecological Monographs* **86**(2): 146-171.

Steinberg LM, Regan JM. 2008. Phylogenetic comparison of the methanogenic communities from an acidic, oligotrophic fen and an anaerobic digester treating municipal wastewater sludge. *Applied Environmental Microbiology* **74**(21): 6663-6671.

Steinberg LM, Regan JM. 2009. mcrA-targeted real-time quantitative PCR method to examine methanogen communities. *Applied Environmental Microbiology* **75**(13): 4435-4442.

Vaksmaa A, Jetten MS, Ettwig KF, Luke C. 2017. McrA primers for the detection and quantification of the anaerobic archaeal methanotroph '*Candidatus Methanoperedens nitroreducens*'. *Applied Microbiology and Biotechnology* **101**(4): 1631-1641.

Valentine DL, Chidthaisong A, Rice A, Reeburgh WS, Tyler SC. 2004. Carbon and hydrogen isotope fractionation by moderately thermophilic methanogens 1 1Associate editor: N. E. Ostrom. *Geochimica et Cosmochimica Acta* **68**(7): 1571-1590.

Wall L, Christiansen T, Orwant J. 2000. *Programming perl*: O'Reilly Media Inc.

Walters W, Hyde ER, Berg-Lyons D, Ackermann G, Humphrey G, Parada A, Gilbert JA, Jansson JK, Caporaso JG, Fuhrman JA, et al. 2016. Improved bacterial 16S rRNA gene (V4 and V4-5) and fungal internal transcribed spacer marker gene primers for microbial community Surveys. *mSystems* **1**(1): e00009-15

Wang Q, Garrity GM, Tiedje JM, Cole JR. 2007. Naive Bayesian classifier for rapid assignment of rRNA sequences into the new bacterial taxonomy. *Applied Environmental Microbiology* **73**(16): 5261-5267.

Wang ZP, Han SJ, Li HL, Deng FD, Zheng YH, Liu HF, Han XG. 2017. Methane production explained largely by water content in the heartwood of

living trees in upland forests. *Journal of Geophysical Research: Biogeosciences* **122**(10): 2479-2489.

Wang ZP, Li HL, Wu HH, Han SJ, Huang JH, Zhang XM, Han XG. 2021. Methane concentration in the heartwood of living trees and estimated methane emission on stems in upland forests. *Ecosystems* DOI: 10.1007/s10021-020-00596-3

Wang ZP, Gu Q, Deng FD, Huang JH, Megonigal JP, Yu Q, Lu XT, Li LH, Chang S, Zhang YH, et al. 2016. Methane emissions from the trunks of living trees on upland soils. *New Phytologist* **211**(2): 429-439.

Wen X, Yang S, Horn F, Winkel M, Wagner D, Liebner S. 2017. Global Biogeographic Analysis of Methanogenic Archaea Identifies Community-Shaping Environmental Factors of Natural Environments. *Frontiers in Microbiology* **8**: 1339.

Whiticar MJ. 1999. Carbon and hydrogen isotope systematics of bacterial formation and oxidation of methane. *Chemical Geology* **161**(1-3): 291-314.

Wickham H. 2016. ggplot2: Elegant Graphics for Data Analysis. New York: Springer-Verlag.

Worm P, Müller N, Plugge CM, Stams AJM, Schink B. 2010. Syntrophy in methanogenic degradation. In: Hackstein J, eds. *(Endo)symbiotic Methanogenic* Archaea*. Microbiolgy Monographs* **19.** Springer, Berlin, Heidelberg, 143-173.

Wu X, Wu L, Liu Y, Zhang P, Li Q, Zhou J, Hess NJ, Hazen TC, Yang W, Chakraborty R. 2018. Microbial Interactions With Dissolved Organic Matter Drive Carbon Dynamics and Community Succession. *Frontiers in Microbiology* **9**: 1234.

Xia X, Stewart DI, Cheng L, Wang K, Li J, Zhang D, Ding A. 2020. Changes in groundwater bacterial community during cyclic groundwater-table variations. *Hydrological Processes* **34**(25): 4973-4984.

Yang S, Liebner S, Alawi M, Ebenhoh O, Wagner D. 2014. Taxonomic database and cut-off value for processing mcrA gene 454 pyrosequencing data by MOTHUR. *Journal of Microbiological Methods* **103**: 3-5.

Yip DZ, Veach AM, Yang ZK, Cregger MA, Schadt CW. 2019. Methanogenic Archaea dominate mature heartwood habitats of Eastern Cottonwood (Populus deltoides). *New Phytologist* **222**(1): 115-121.

Zeikus JG, Ward JC. 1974. Methane formation in living trees: a microbial origin. *Science* **184**(4142): 1181-1183.

Zieikus JG, Henning DL. 1975. *Methanobacterium arbophilicumsp.nov*. An obligate anaerobe isolated from wetwood of living trees. *Antonie van Leeuwenhoek* **41**: 543-552.

CHAPTER 7: APPENDICES

7.1 Number of methanogen and bacterial ASV's detected for individual samples

Table 7.1: Number of *mcrA* and bacterial 16s rRNA ASV's for each tree stem and river sediment sample, as well as the total number of ASV's observed for each sample type and for all samples.

Sample	# of *mcrA* ASV's	# of bacterial 16s rRNA ASV's
RS1	230	799
RS2	250	866
RS3	42	903
RS4	79	802
RS5	132	954
RS6	63	971
T17	21	N/A
T550	7	122
T555	22	179
T557	20	113
T560	68	237
T562	25	345
T78	41	126
T79	16	175
T87	34	163
Tree stem	120	1229
River sediment	588	4514
Total	664	5706

7.2 Phylogenetic tree construction of *mcrA* nucleotide sequences:

All *mcrA* nucleotide sequences found in tree stem and river sediment samples were aligned by codons using MUSCLE (Edgar, 2004) in Mesquite v3.61 (Maddison & Maddison, 2019) to reference sequences pulled from GenBank (Accession numbers in brackets on phylogenetic tree; Fig. 7.2; Clark *et al*., 2016). Reference sequences from the methanogen order Methanocellales were excluded from analyses as none were detected in this study (Fig. 3.1), and their inclusion in phylogenetic analyses can cause unresolved clades (Lyu & Liu, 2018). Inferred amino acid sequences were run through IQ-TREE (Nguyen *et al.*, 2014) on the public server usegalaxy.eu (Afgan *et al.*, 2018), and the best maximum-likelihood tree model was predicted using the Akaike information criterion implemented in Modelfinder (Kalyaanamoorthy *et al.*, 2017). IQ-TREE was then used to create a phylogenetic tree using the maximum likelihood method (LG + F + R4) with perturbation strength set to 0.1 and statistical evaluation with 100 bootstrap replicates. This tree was used to select ASV's from both tree stems and river sediment that were placed in different clades to generate a smaller representative tree as previously described. Figure generation was performed in FigTree v1.4.4 (Rambaut, 2014).

Of the 120 *mcrA* ASV's found in tree stems, 39 were also found in river sediment samples. Many inferred *mcrA* amino acid sequences were identical between unique ASV's, as indicated by branch lengths of 0, signifying non-functional changes to the nucleotide sequence (Fig. 7.2). *mcrA* phylotypes in the

river sediment formed clades separate from those found in tree stems, while *mcrA* amplicons from tree stems were consistently found in poorly resolved clades with those found in the river (Fig. 7.2). The origin of methanogens within the cottonwood trees in the HSNR is believed to be from the groundwater, which is fed by the Oldman River. This hypothesis is supported by the high genetic similarity of *mcrA* gene sequences identified in the tree stems and river sediment. This phylogenetic analysis is representative of the *mcrA* gene region, so it may reflect establishment and differentiation of methanogens, but may not accurately reflect species-level evolutionary trends. River sediment ASV's grouped with Methanococcales were BLAST searched (Altschul *et al.*, 1990) in NCBI (Fassler *et al.*, 2000) and were genetically similar to this order (79%), but more genetically similar (97%) to unclassified *mcrA* clone amplicons, so they remained labeled as unclassified in this study.

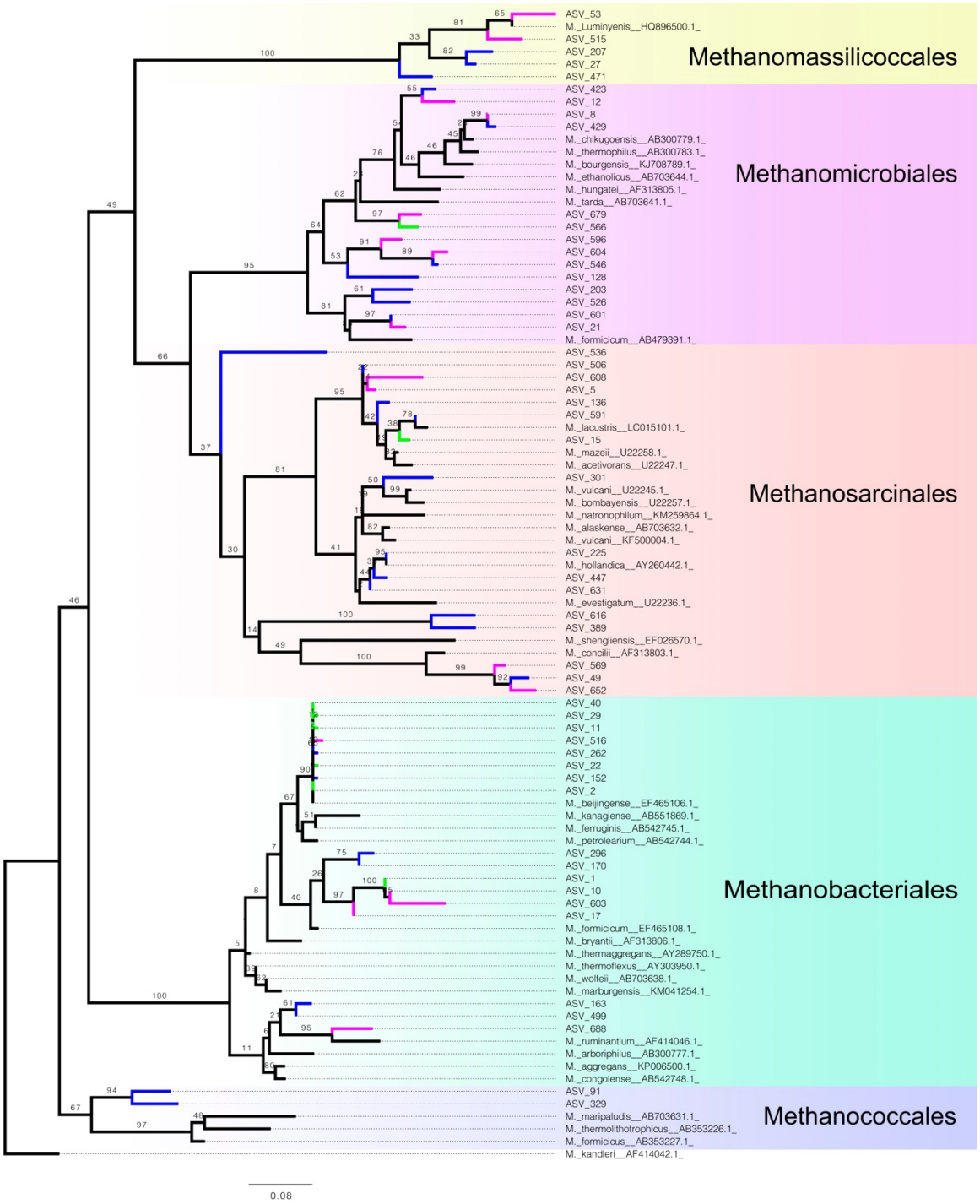
ASV_53
M._Luminyenis__HQ896500.1_
ASV_515
ASV_207
ASV_27
ASV_471
Methanomassiliicoccales
ASV_423
ASV_12
ASV_8
ASV_429
M._chikugoensis__AB300779.1_
M._thermophilus__AB300783.1_
M._bourgensis__KJ708789.1_
M._ethanolicus__AB703644.1_
M._hungatei__AF313805.1_
M._tarda__AB703641.1_
ASV_679
ASV_566
ASV_596
ASV_604
ASV_546
ASV_128
ASV_203
ASV_526
ASV_601
ASV_21
M._formicicum__AB479391.1_
Methanomicrobiales
ASV_536
ASV_506
ASV_608
ASV_5
ASV_136
ASV_591
M._lacustris__LC015101.1_
ASV_15
M._mazeii__U22258.1_
M._acetivorans__U22247.1_
ASV_301
M._vulcani__U22245.1_
M._bombayensis__U22257.1_
M._natronophilum__KM259864.1_
M._alaskense__AB703632.1_
M._vulcani__KF500004.1_
ASV_225
M._hollandica__AY260442.1_
ASV_447
ASV_631
M._evestigatum__U22236.1_
ASV_616
ASV_389
M._shengliensis__EF026570.1_
M._concilii__AF313803.1_
ASV_569
ASV_49
ASV_652
Methanosarcinales
ASV_40
ASV_29
ASV_11
ASV_516
ASV_262
ASV_22
ASV_152
ASV_2
M._beijingense__EF465106.1_
M._kanagiense__AB551869.1_
M._ferruginis__AB542745.1_
M._petrolearium__AB542744.1_
ASV_296
ASV_170
ASV_1
ASV_10
ASV_603
ASV_17
M._formicicum__EF465108.1_
M._bryantii__AF313806.1_
M._thermaggregans__AY289750.1_
M._thermoflexus__AY303950.1_
M._wolfeii__AB703638.1_
M._marburgensis__KM041254.1_
ASV_163
ASV_499
ASV_688
M._ruminantium__AF414046.1_
M._arboriphilus__AB300777.1_
M._aggregans__KP006500.1_
M._congolense__AB542748.1_
Methanobacteriales
ASV_91
ASV_329
M._maripaludis__AB703631.1_
M._thermolithotrophicus__AB353226.1_
M._formicicus__AB353227.1_
M._kandleri__AF414042.1_
Methanococcales
0.08

Figure 7.2: Phylogenetic tree based on inferred amino acid sequences of *mcrA* genes obtained from *Populus* tree cores and Oldman River sediment. The tree was constructed from 159 deduced amino acid sites using the maximum likelihood model (LG + F +R4) with perturbation strength set to 0.1 and statistical support with 1000 bootstrap replicates. Reference sequences are abbreviated to their species name with accession numbers in brackets, and *Methanopyrus kandleri* was used as the outgroup (Luton et al., 2002; Lyu & Liu, 2018). The scalebar represents 0.1 substitutions per amino acid position. Branch colours indicate whether the ASV was present in tree stems (pink), river sediment (blue) or both (green). One Methanobacteriales branch was collapsed for better visualization.

REFERENCES (cited in this section and absent from main text)

Altschul SF, Gish W, Miller W, Myers EW, Lipman DJ. 1990. Basic local alignment search tool. *Journal of Molecular Biology* **215:** 403–410.

Edgar RC. 2004. MUSCLE: multiple sequence alignment with high accuracy and high throughput. *Nucleic Acids Research* **32**(5): 1792-1797.

Fassler J, Nadel C, Richardson N, McEntyre J, Schuler G, McGinnis S, Pongor S. 2000. NCBI website from http://www.ncbi.nlm.nih.gov/

Kalyaanamoorthy S, Minh BQ, Wong TKF, von Haeseler A, Jermiin LS. 2017. ModelFinder: fast model selection for accurate phylogenetic estimates. *Nature Methods* **14**(6): 587-589.

Maddison WP, Maddison DR. 2019. Mesquite: a modular system for evolutionary analysis. Version 3.61.

Nguyen LT, Schmid MC, von Haeseler A, Minh BQ. 2014. IQ-TREE: A Fast and Effective Stochastic Algorithm for Estimating Maximum-Likelihood Phylogenies. *Molecular Biology and Evolution* **32**: 268-274.

Rambaut A 2014. FigTree v1.4.4.

7.3 Rarefaction curves for genetic analyses

Rarefying was performed to ensure equal sampling depth across sample types for accurate comparisons. The number of observed *mcrA* and bacterial 16s rRNA ASV's plateaued for each sample type with increasing sequencing depth, indicating only rare species remain unsampled (Fig. 7.3).

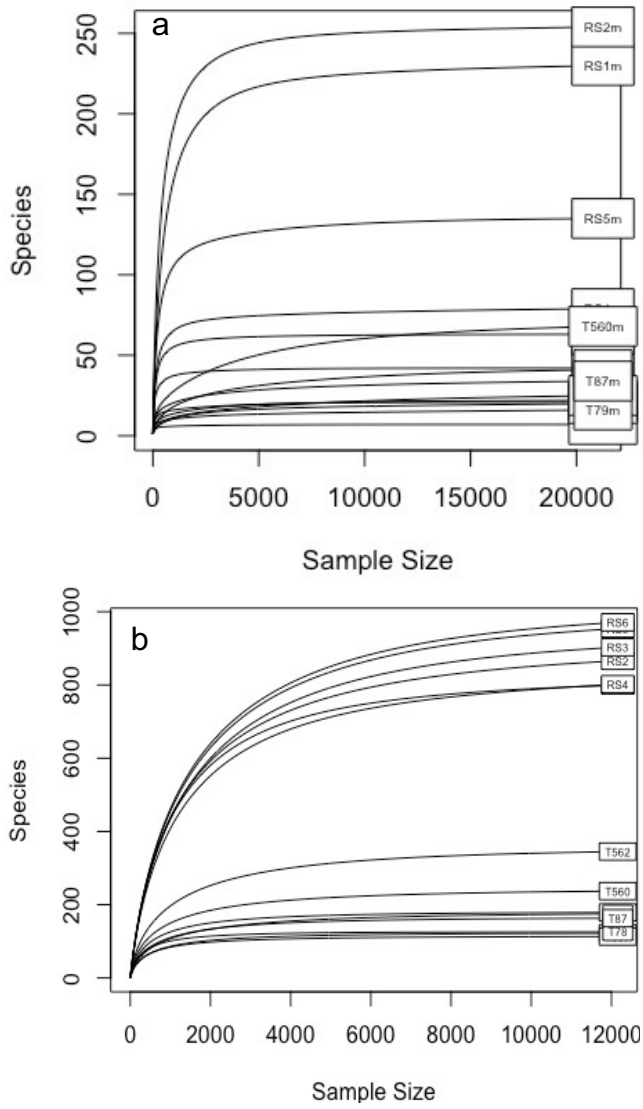

Figure 7.3: Rarefaction curves for (a) methanogen and (b) bacterial genetic sequence markers identified from tree stem and river sediment samples. Codes on each line indicate river sediment (RS) or tree core (T) sample type, and the associated number represents the sediment location (Fig. 2.2) and tree stem tag (See appendix 7.5 for the associated taxa and cluster).

7.4 Relative abundance of Clostridia in river sediment and tree stems

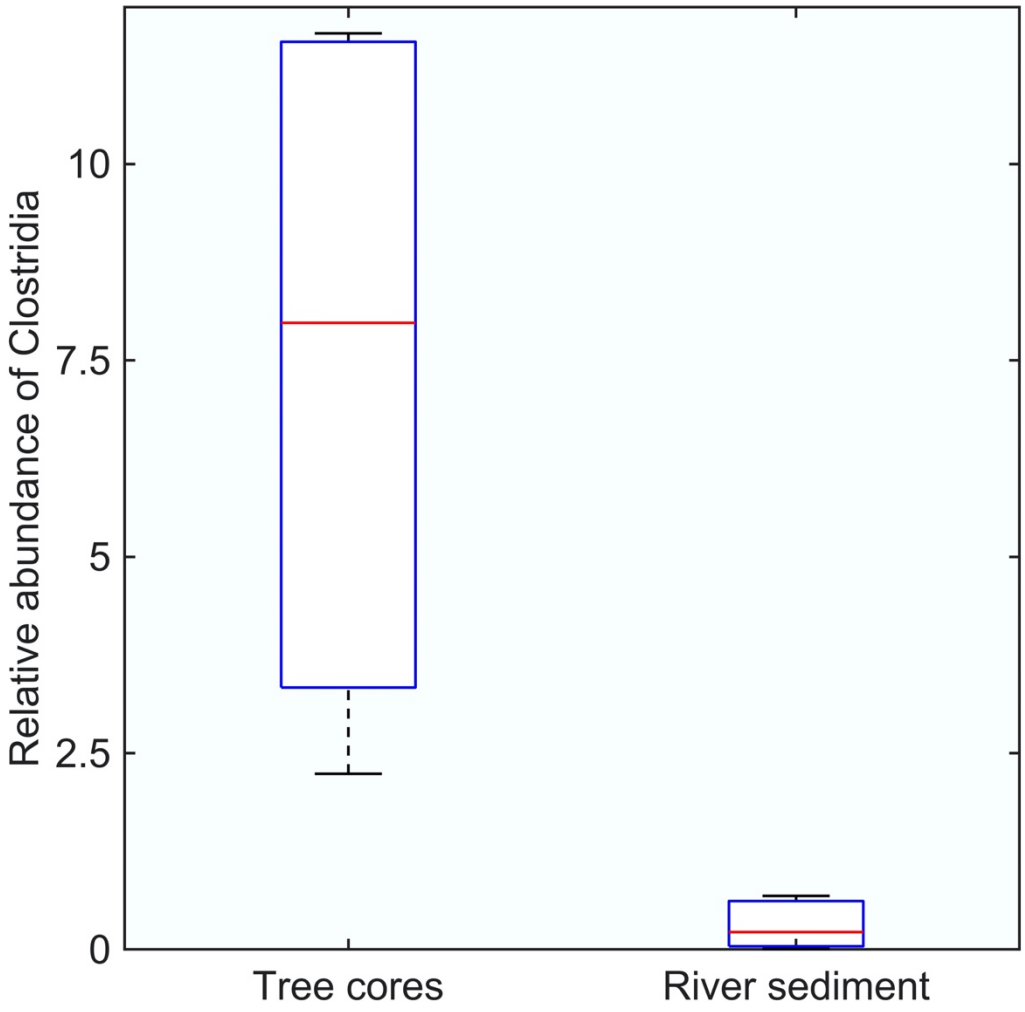

Figure 7.4.1: Relative abundance of ASV's in the class Clostridia within *Populus spp.* tree core (n=8) and Oldman River sediment (n=6) samples. The number of observed Clostridia differed significantly for tree stem and river sediment samples based on a Kruskal-Wallis test, $X^2_{(1,12)}$=9.60, P<0.01

7.5 Trends in gas production for individual *Populus* tree core and Oldman River sediment incubation experiments.

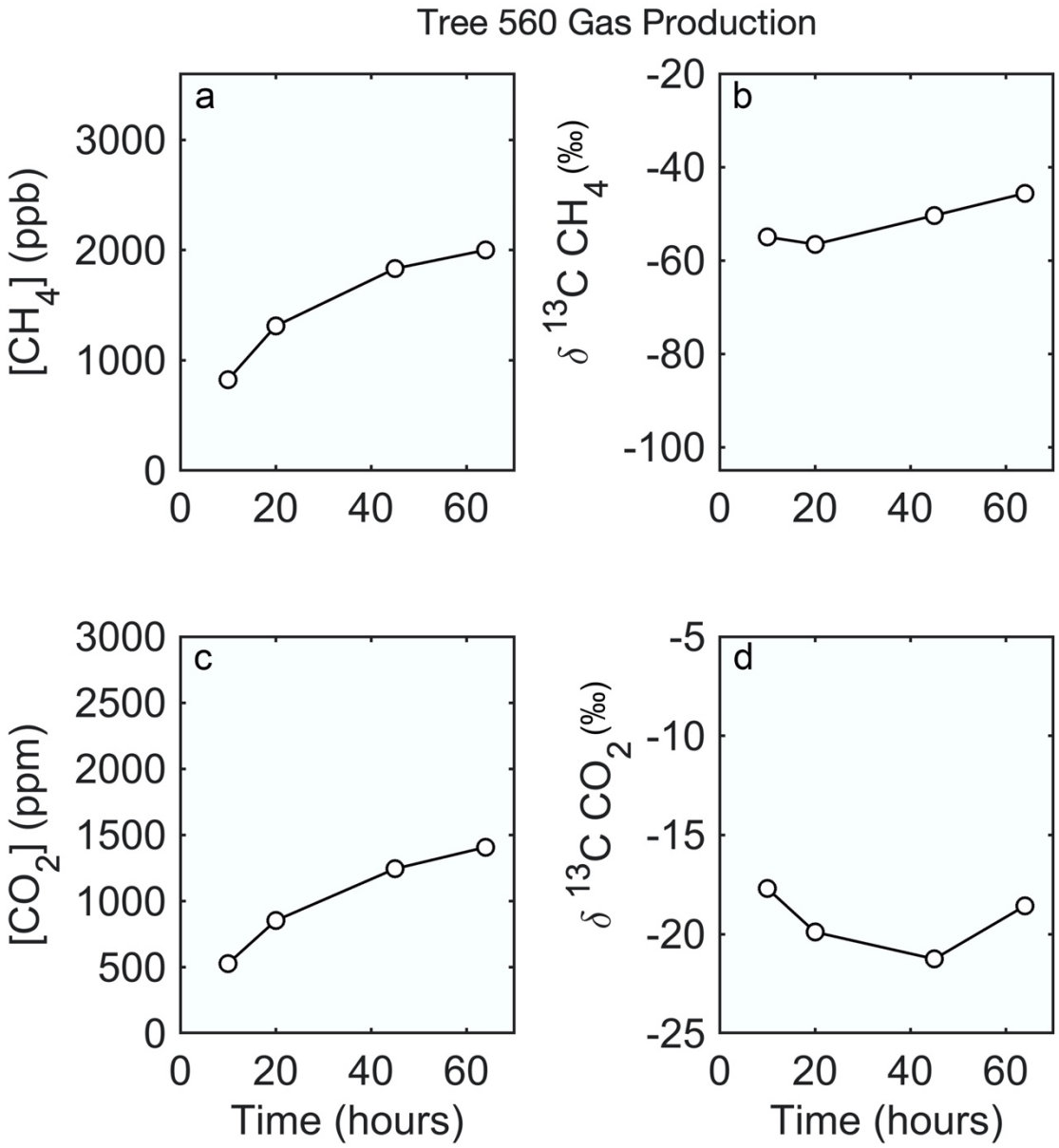

Figure 7.5.1: Gas production by tree core sample 560 (*Populus acuminata* in cluster 1) during anaerobic incubation, measuring (a) the concentration of methane and (b) its stable carbon isotope composition ($\delta^{13}C$), as well as (c) the concentration of carbon dioxide and (d) its stable carbon isotope composition over 64 hours.

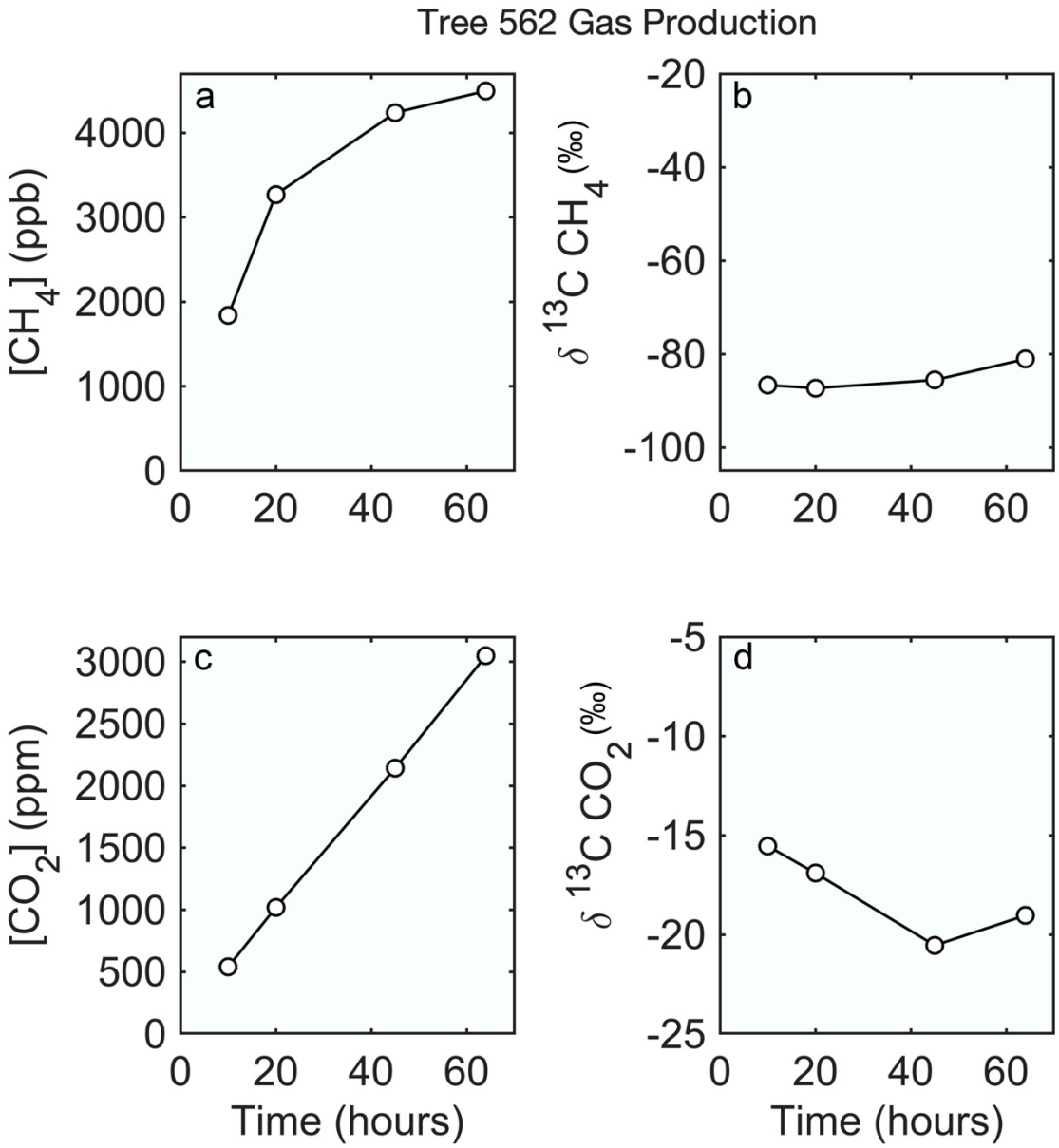

Figure 7.5.2: Gas production by tree core sample 562 (*Populus angustifolia* in cluster 1) during anaerobic incubation, measuring (a) the concentration of methane and (b) its stable carbon isotope composition ($\delta^{13}C$), as well as (c) the concentration of carbon dioxide and (d) its stable carbon isotope composition over 64 hours. Note the y-axes on (a) & (b) differ from other individual sample figures.

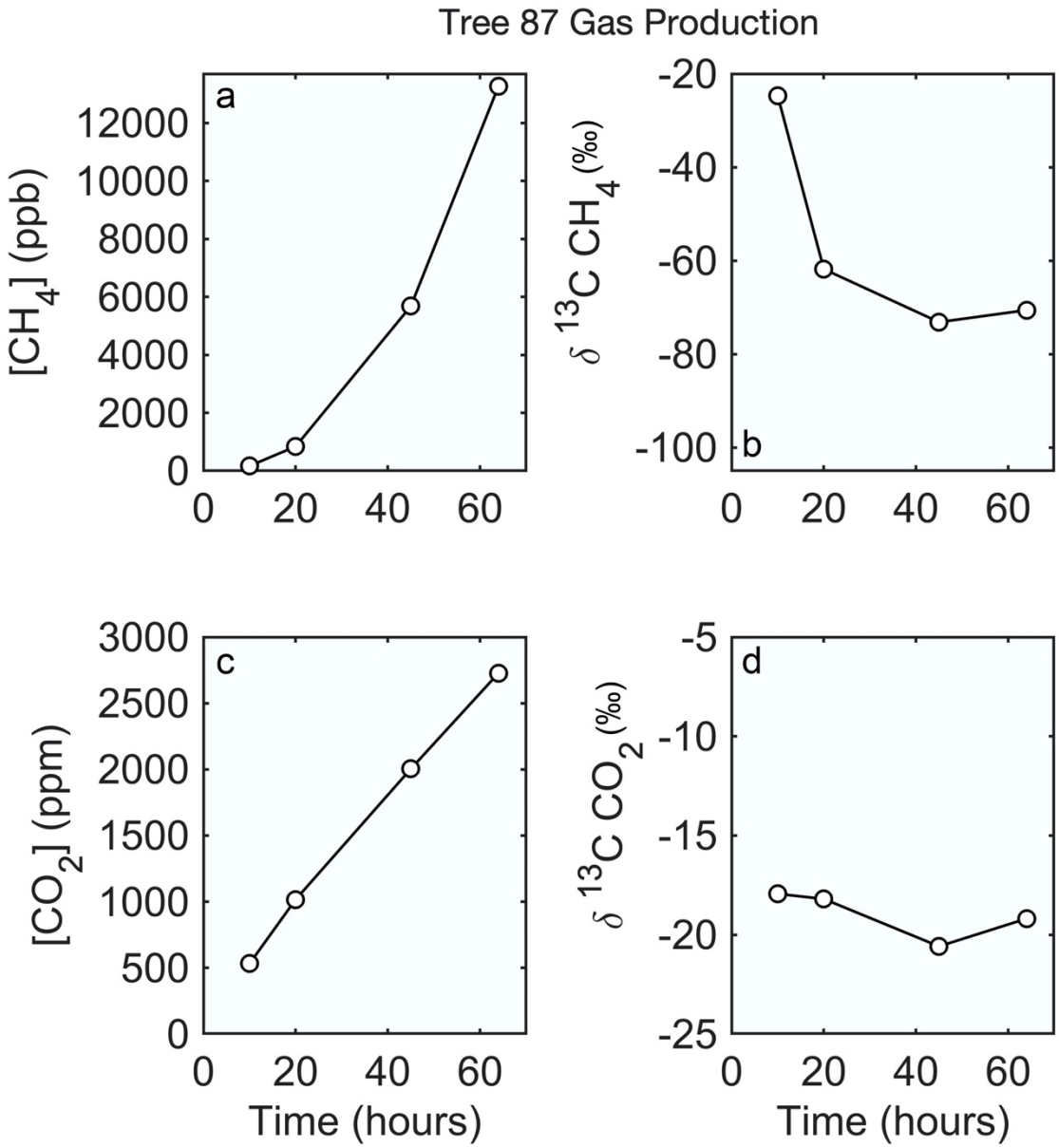

Figure 7.5.3: Gas production by tree core sample 87 (*Populus deltoides* in cluster 1) during anaerobic incubation, measuring (a) the concentration of methane and (b) its stable carbon isotope composition ($\delta^{13}C$), as well as (c) the concentration of carbon dioxide and (d) its stable carbon isotope composition over 64 hours. Note the y-axes on (a) & (b) differ from other individual sample figures

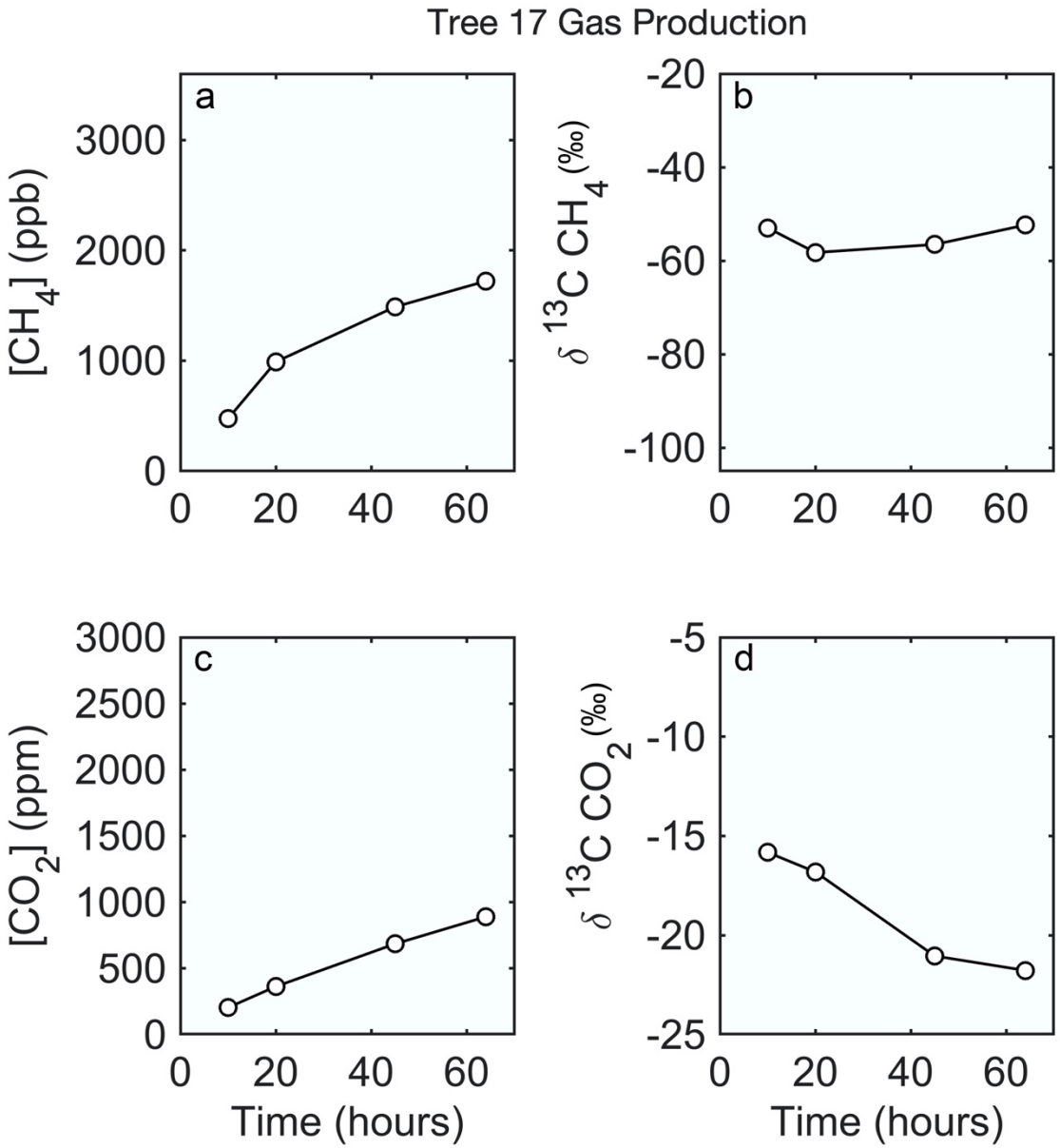

Figure 7.5.4: Gas production by tree core sample 17 (*Populus deltoides* in cluster 2) during anaerobic incubation, measuring (a) the concentration of methane and (b) its stable carbon isotope composition ($\delta^{13}C$), as well as (c) the concentration of carbon dioxide and (d) its stable carbon isotope composition over 64 hours.

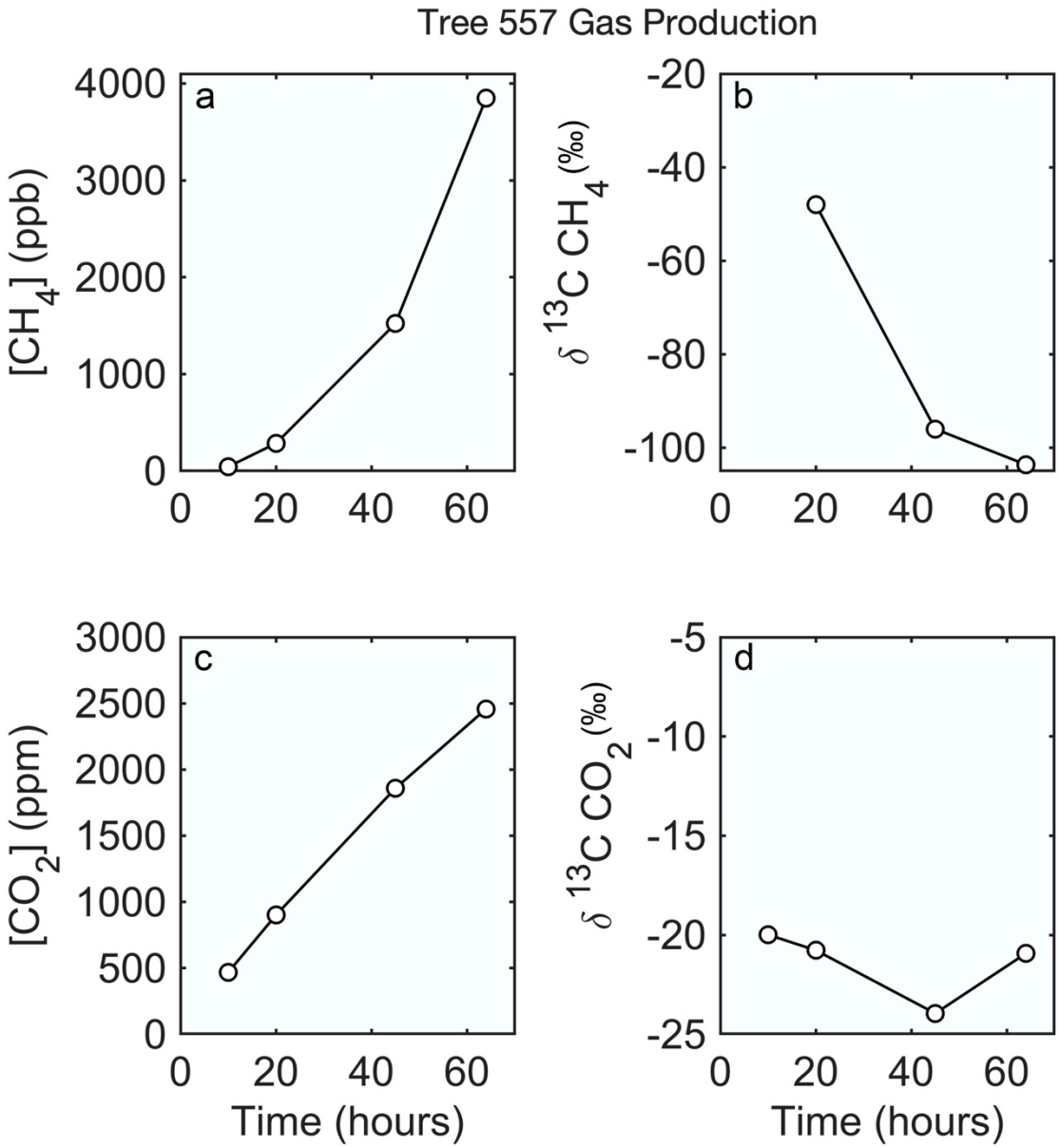

Figure 7.5.5: Gas production by tree core sample 557 (*Populus angustifolia* in cluster 2) during anaerobic incubation, measuring (a) the concentration of methane and (b) its stable carbon isotope composition ($\delta^{13}C$), as well as (c) the concentration of carbon dioxide and (d) its stable carbon isotope composition over 64 hours. Note the y-axis on (a) differs from other individual sample figures

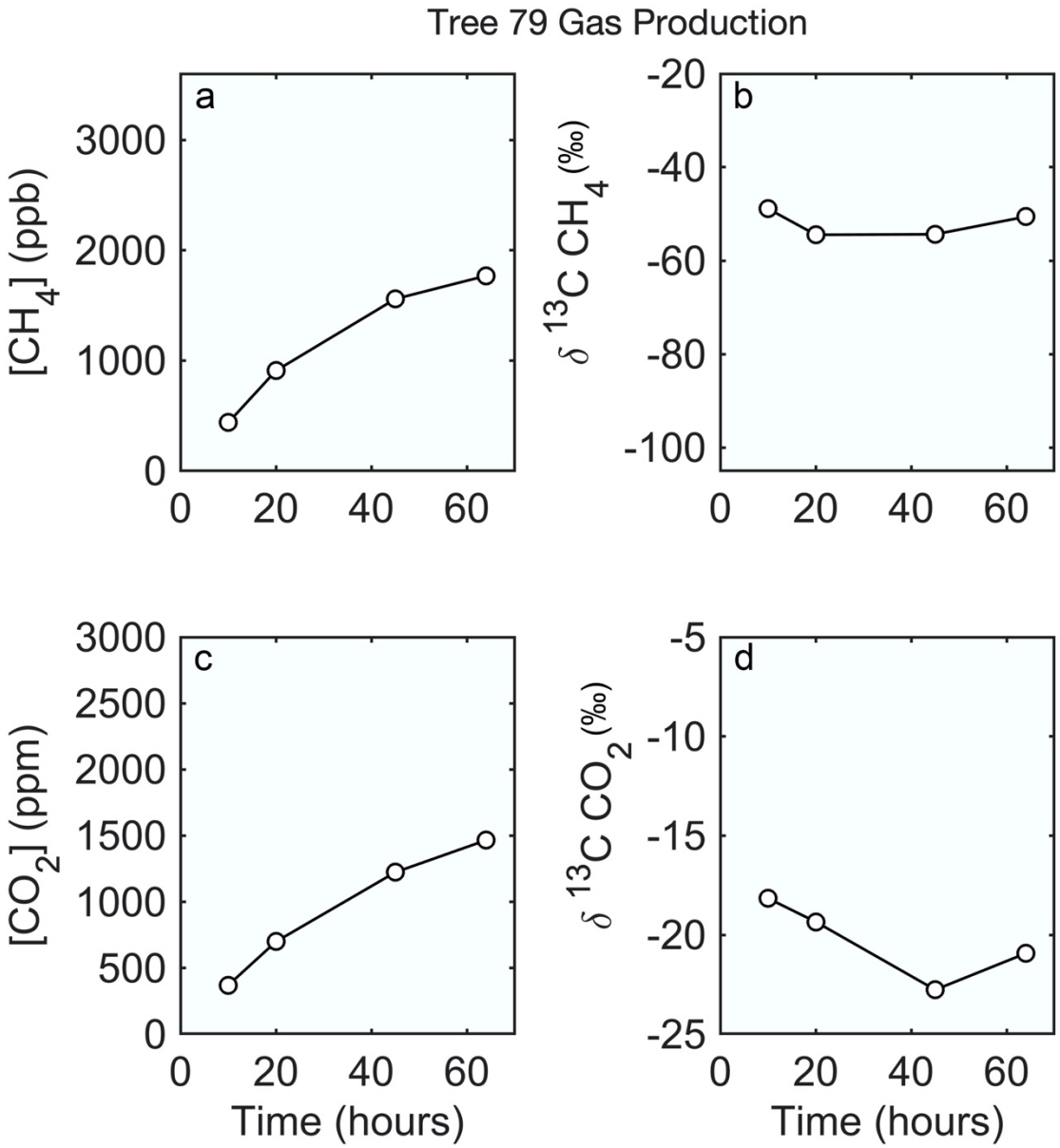

Figure 7.5.6: Gas production by tree core sample 79 (*Populus acuminata* in cluster 2) during anaerobic incubation, measuring (a) the concentration of methane and (b) its stable carbon isotope composition ($\delta^{13}C$), as well as (c) the concentration of carbon dioxide and (d) its stable carbon isotope composition over 64 hours.

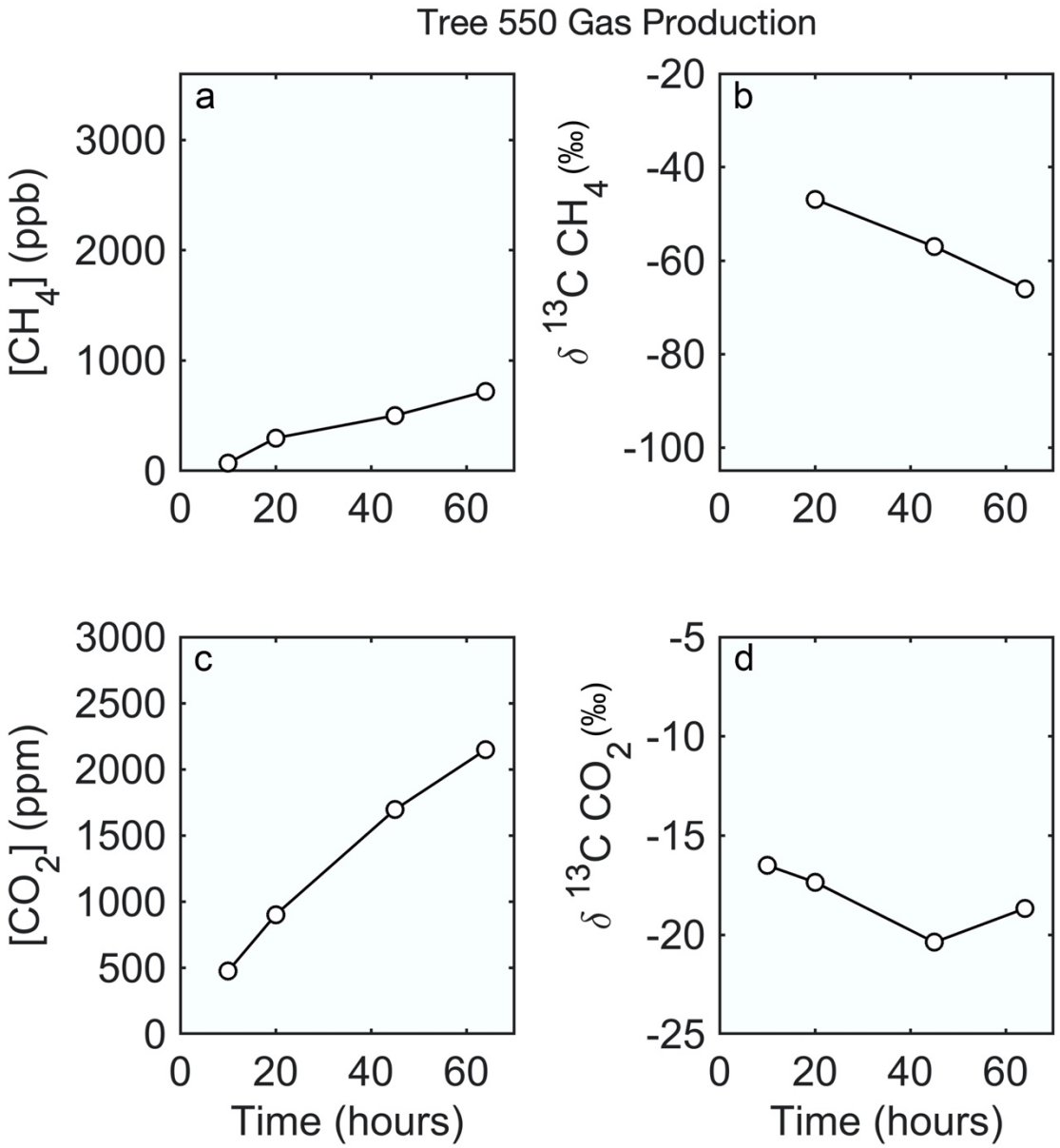

Figure 7.5.7: Gas production by tree core sample 550 (*Populus deltoides* in cluster 3) during anaerobic incubation, measuring (a) the concentration of methane and (b) its stable carbon isotope composition ($\delta^{13}C$), as well as (c) the concentration of carbon dioxide and (d) its stable carbon isotope composition over 64 hours.

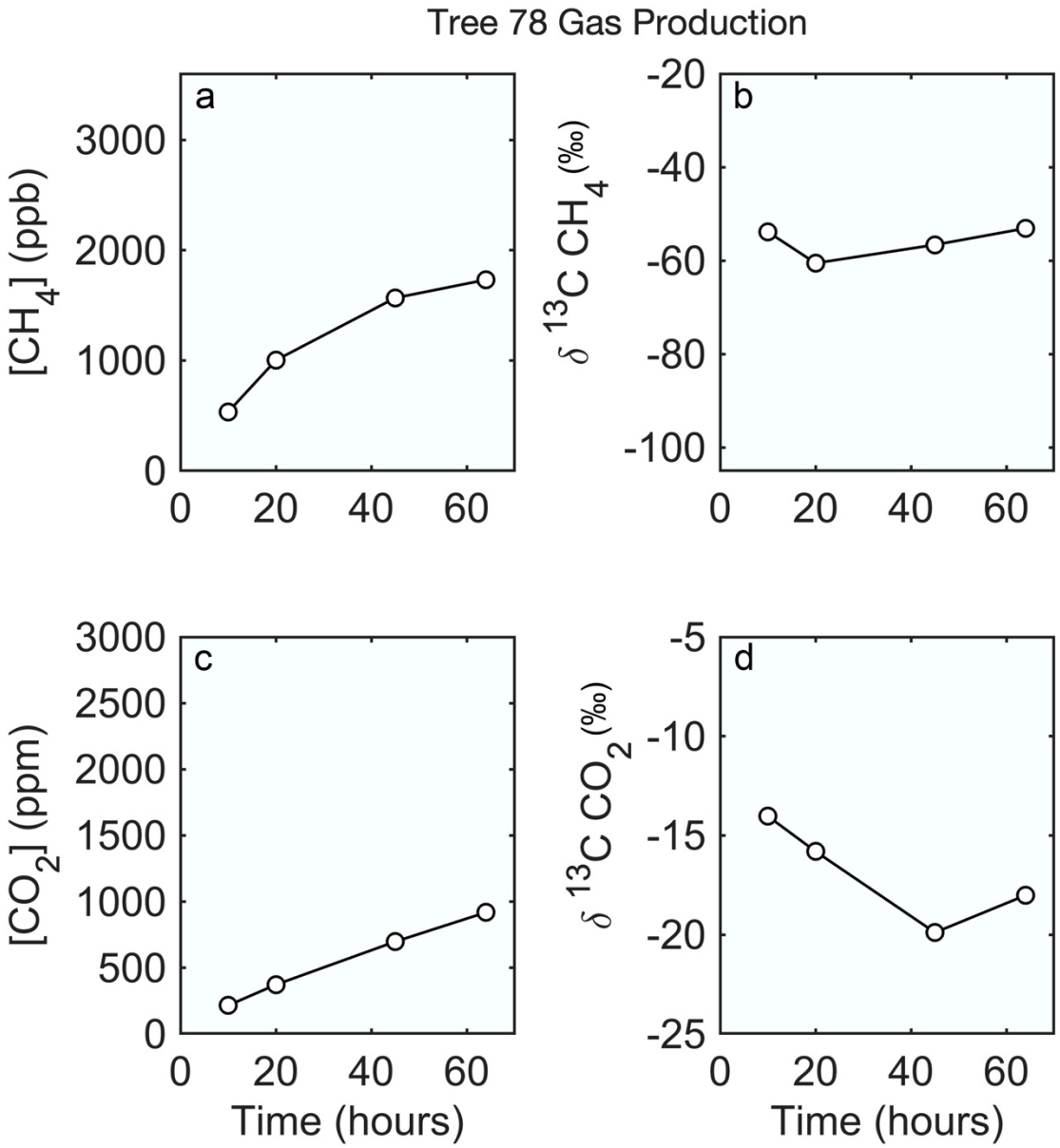

Figure 7.5.8: Gas production by tree core sample 78 (*Populus angustifolia* in cluster 3) during anaerobic incubation, measuring (a) the concentration of methane and (b) its stable carbon isotope composition ($\delta^{13}C$), as well as (c) the concentration of carbon dioxide and (d) its stable carbon isotope composition over 64 hours.

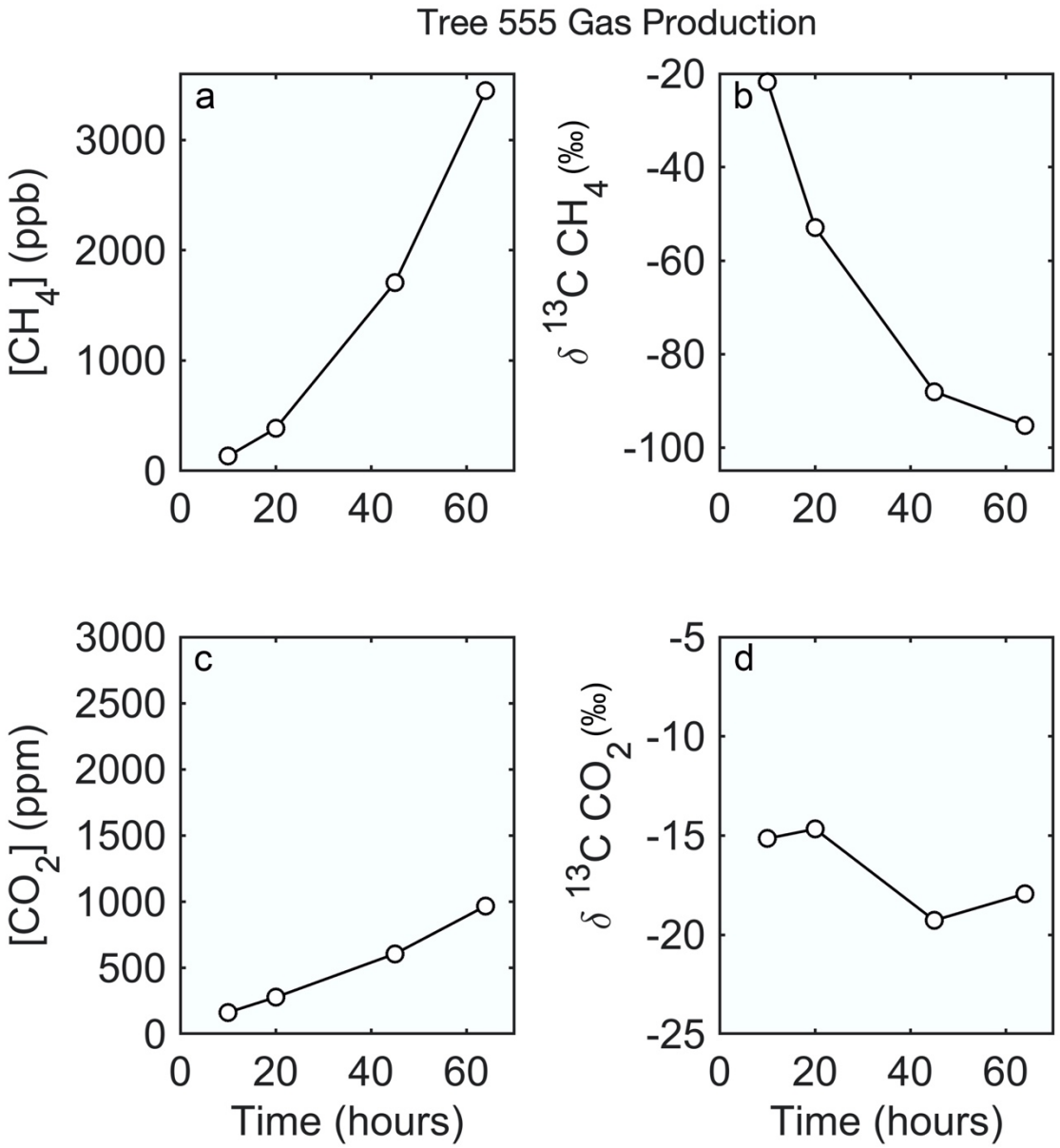

Figure 7.5.9: Gas production by tree core sample 555 (*Populus acuminata* in cluster 3) during anaerobic incubation, measuring (a) the concentration of methane and (b) its stable carbon isotope composition ($\delta^{13}C$), as well as (c) the concentration of carbon dioxide and (d) its stable carbon isotope composition over 64 hours.

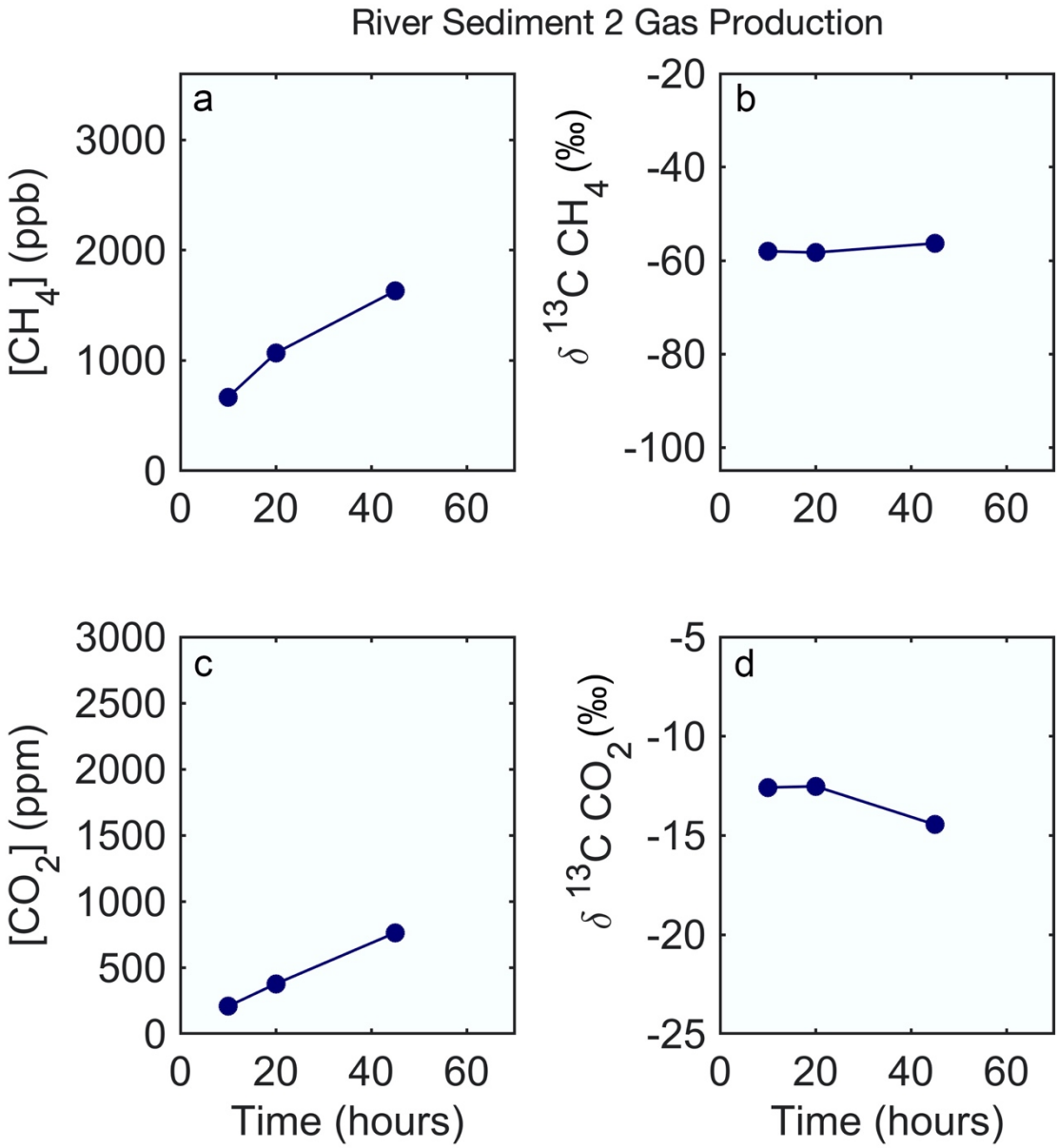

Figure 7.5.10: Gas production by Oldman River sediment sample 2 during anaerobic incubation, measuring (a) the concentration of methane and (b) its stable carbon isotope composition ($\delta^{13}C$), as well as (c) the concentration of carbon dioxide and (d) its stable carbon isotope composition over 45 hours

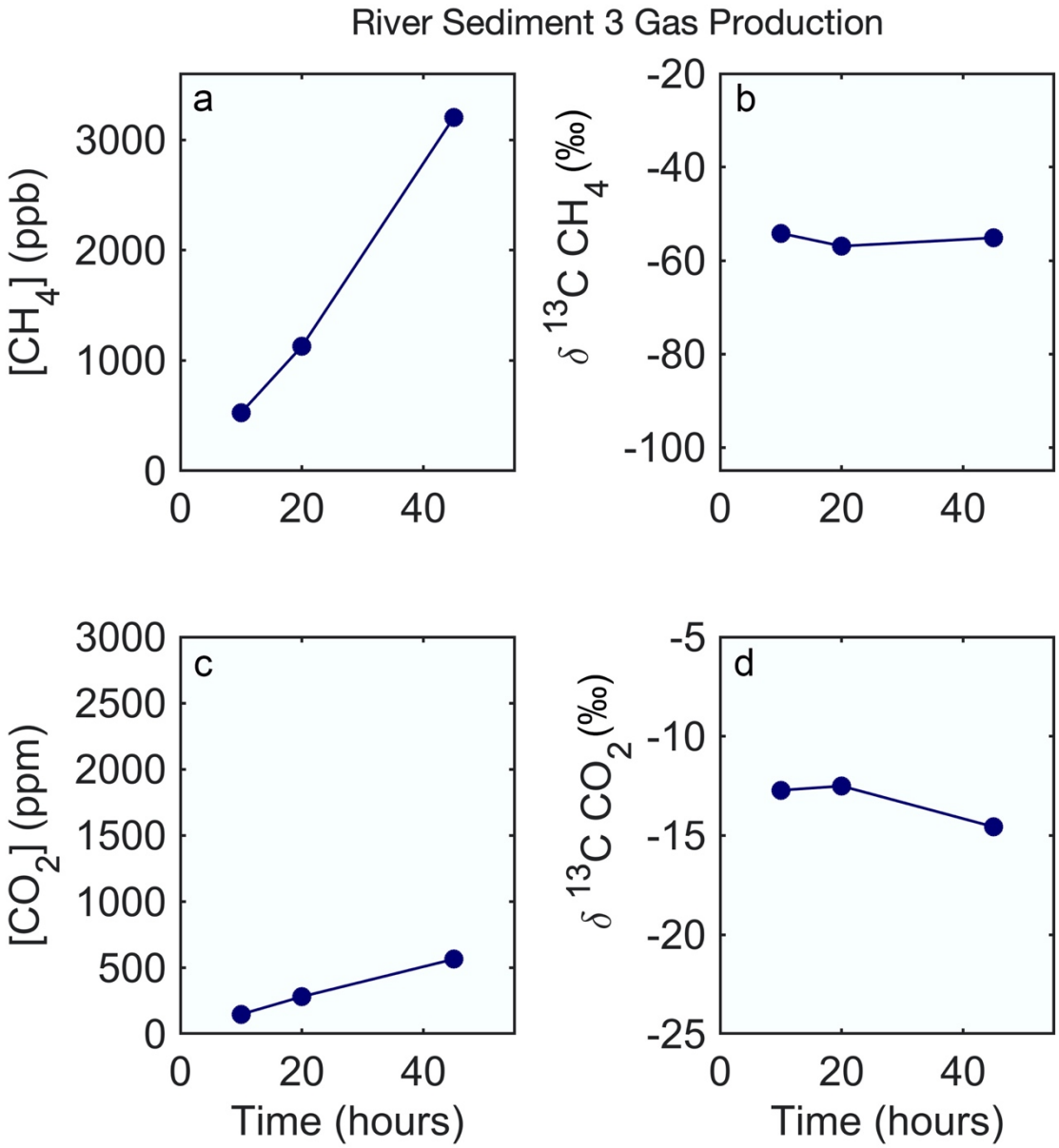

Figure 7.5.11: Gas production by Oldman River sediment sample 3 during anaerobic incubation, measuring (a) the concentration of methane and (b) its stable carbon isotope composition ($\delta^{13}C$), as well as (c) the concentration of carbon dioxide and (d) its stable carbon isotope composition over 45 hours

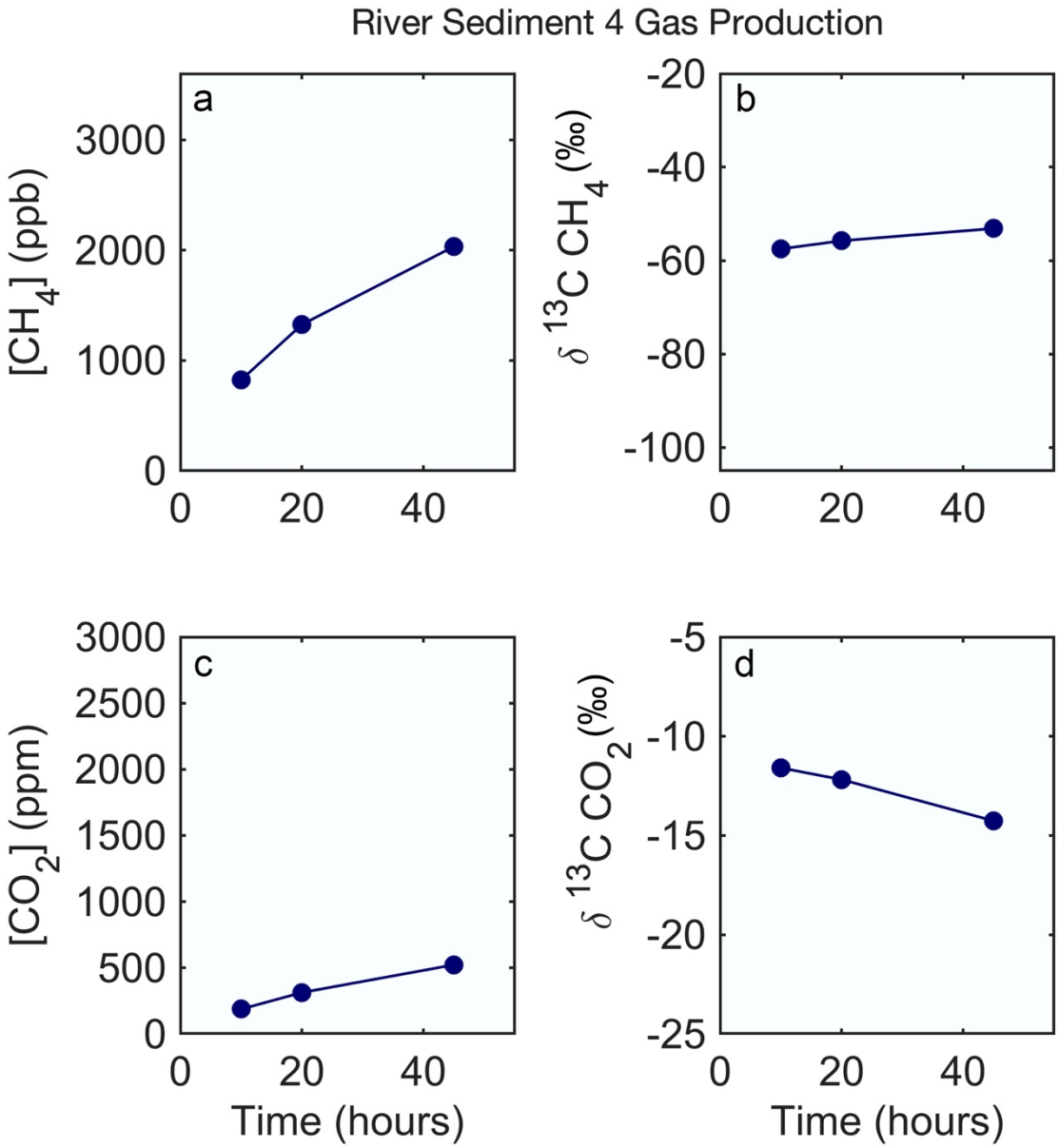

Figure 7.5.12: Gas production by Oldman River sediment sample 4 during anaerobic incubation, measuring (a) the concentration of methane and (b) its stable carbon isotope composition ($\delta^{13}C$), as well as (c) the concentration of carbon dioxide and (d) its stable carbon isotope composition over 45 hours

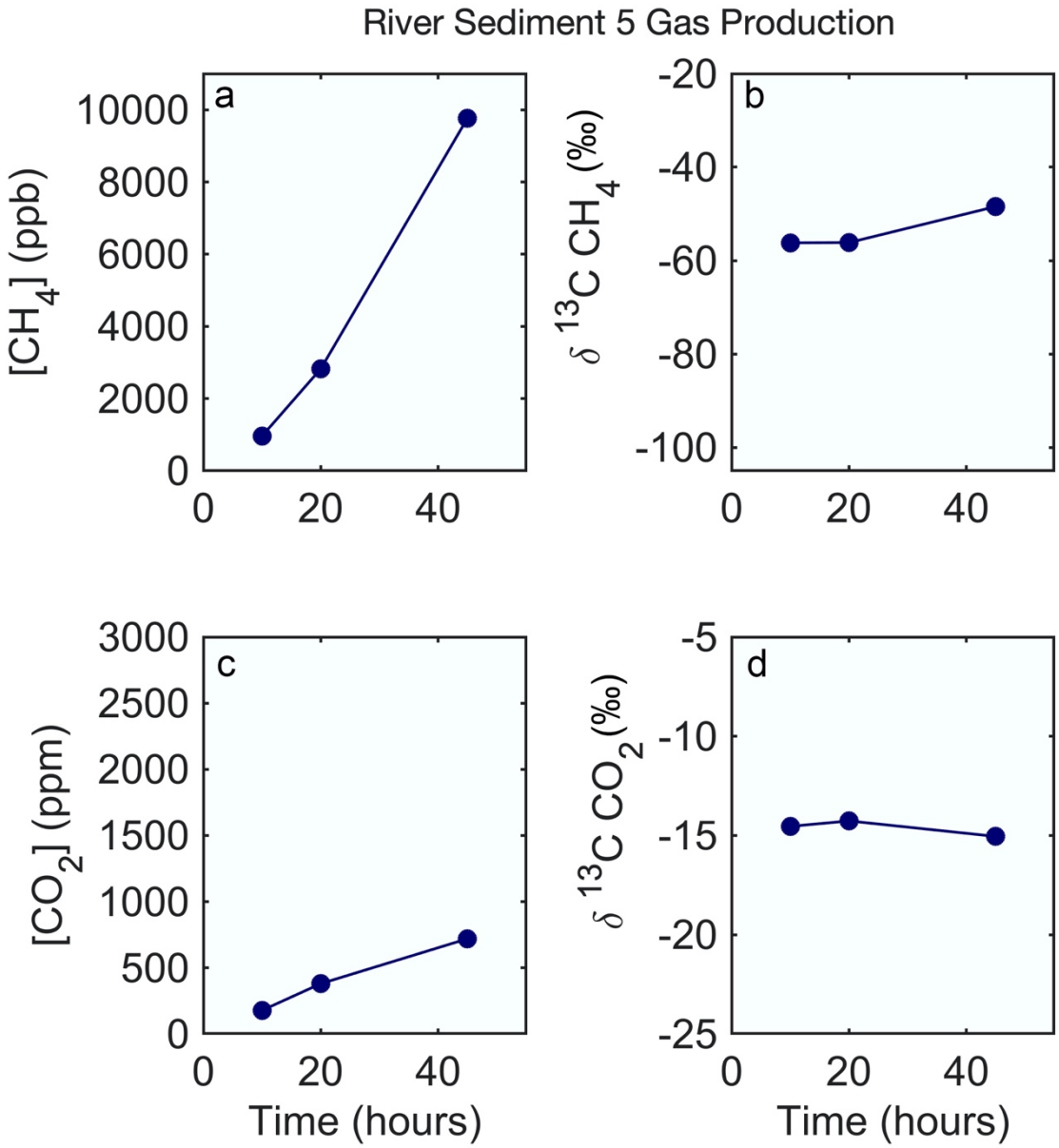

Figure 7.5.13: Gas production by Oldman River sediment sample 5 during anaerobic incubation, measuring (a) the concentration of methane and (b) its stable carbon isotope composition ($\delta^{13}C$), as well as (c) the concentration of carbon dioxide and (d) its stable carbon isotope composition over 45 hours. Note the y-axis on (a) differs from other individual sample figures.

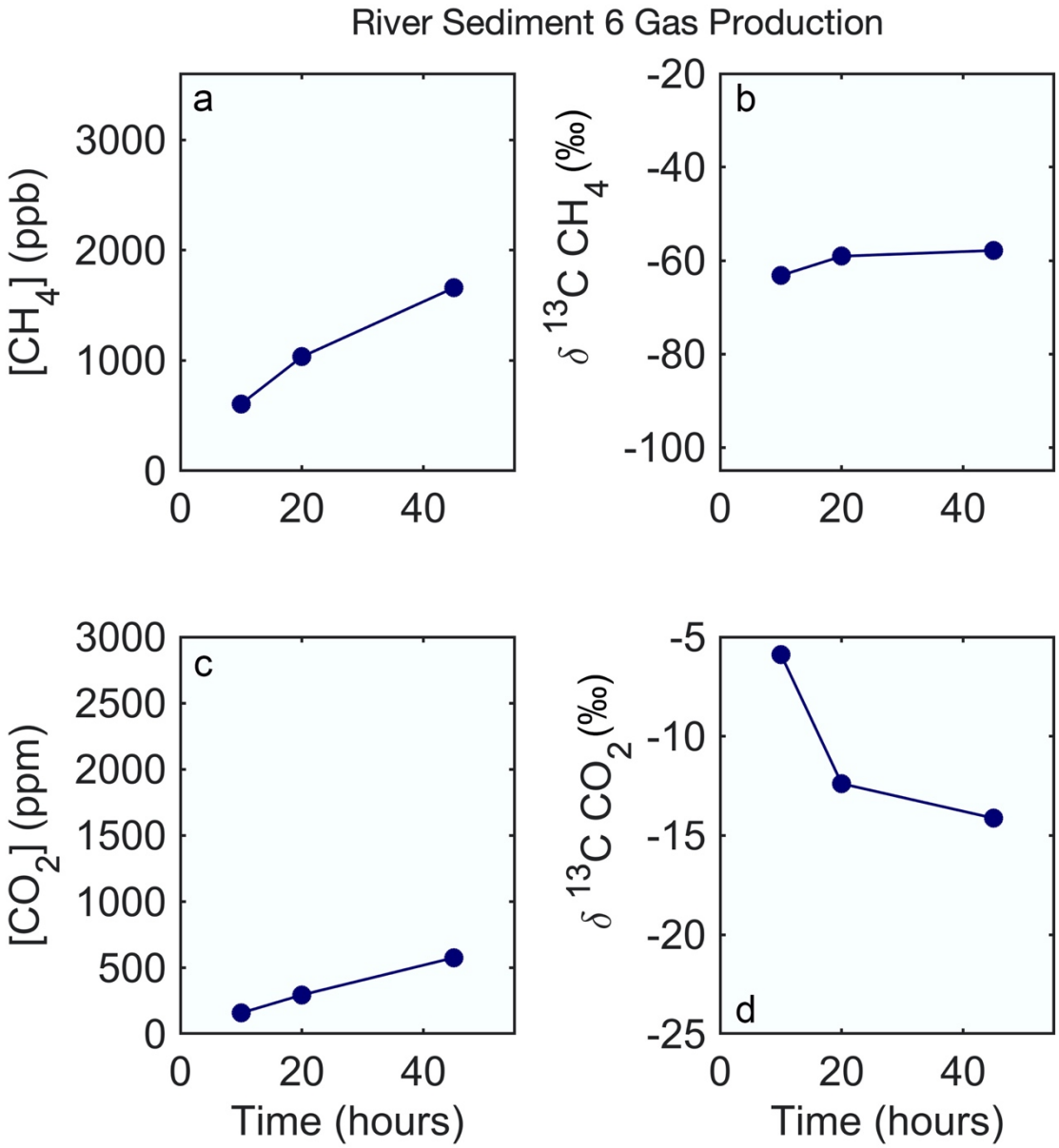

Figure 7.5.14: Gas production by Oldman River sediment sample 6 during anaerobic incubation, measuring (a) the concentration of methane and (b) its stable carbon isotope composition ($\delta^{13}C$), as well as (c) the concentration of carbon dioxide and (d) its stable carbon isotope composition over 45 hours

7.6 Methane production in heartwood and sapwood tissue in *Populus* tree stems

Incubation experiments and organic matter analyses were conducted as previously described (See section 2.2.3 to 2.2.5) on heartwood and sapwood samples to compare the metabolic pathways of methane production within these tissue types. Samples were collected in duplicate from 2 poplar trees cut down in the Elizabeth Hall Wetlands (49.704 N, -112.868 W), located parallel to the HSNR on the west side of the Oldman River (Fig. 2.1). The exposed cross section at the cut site was used to measure the length and distribution of heartwood, sapwood, cambium, and bark to use as a reference for separating tree core increments into pure tissue types. Following collection with an increment borer, the samples were laid on a sterile glove, and the cambium/bark layers were removed using a sterile razor blade and discarded. Heartwood and sapwood (0.5 cm length) along the rough boundary between these tissue types were removed and discarded to ensure pure tissue samples, which were then stored separately in 50 mL falcon tubes with sterile water. Wood samples broken into 8 pieces (1.485 ± - 0.035 g) were prepared for incubation experiments as previously described, with discrete gas samples taken after 20, 40 and 164 hours for analysis. Following incubation, samples were analyzed for % C_{org}, % N and $\delta^{13}C_{org}$ as previously described.

Heartwood and sapwood samples from cottonwood trees did not differ significantly in $\delta^{13}C$ C_{org}, carbon content, total organic carbon available, nitrogen

content or total nitrogen available (Table 7.6). Both tissue types were metabolically active, producing significant quantities of methane and carbon dioxide over the incubation period, with production not differing significantly between sample types (Fig. 7.6.1). The stable carbon isotope composition of methane produced from heartwood (-50.9 to -59.6‰) and sapwood (-44.4 to -70.2‰) were not significantly different after 185 hours of anaerobic incubation (Fig. 7.6.2). These results are consistent with previous reports of methanogens in heartwood and sapwood tissue of *Populus* trees in an upland forest (Yip *et al.*, 2019), and the heterogeneity in methane emissions from tree stems showing localized "hot spots" in both tissue types (Jeffrey *et al.*, 2020).

Table 7.6: Similar organic matter characteristics for *Populus spp.* heartwood and sapwood samples. Values represent the mean (n=4) ± SD. The $\delta^{13}C$ C_{org}, % C_{org} and % N values did not differ significantly with sample type, as determined by single-factor ANOVA. For $\delta^{13}C$ C_{org}, $F_{(1,6)}$=0.77, P=0.41, for % C_{org}, $F_{(1,6)}$=0.43, P=0.54, for total carbon, $F_{(1,6)}$=1.85x10^3, P=0.97, for total N $F_{(1,6)}$=0.17, P=0.69, and for % N, $F_{(1,6)}$=0.43, P=0.54.

	$\delta^{13}C$ C_{org}	% C_{org}	% N	Total C (mg)	Total N (mg)
Heartwood	-26.9 ± 0.3	46.6 ± 0.7	0.09 ± 0.02	167.8 ± 38.1	0.30 ± 0.08
Sapwood	-27.2 ± 0.6	46.2 ± 0.8	0.08 ± 0.01	168.7 ± 18.6	0.28 ± 0.04

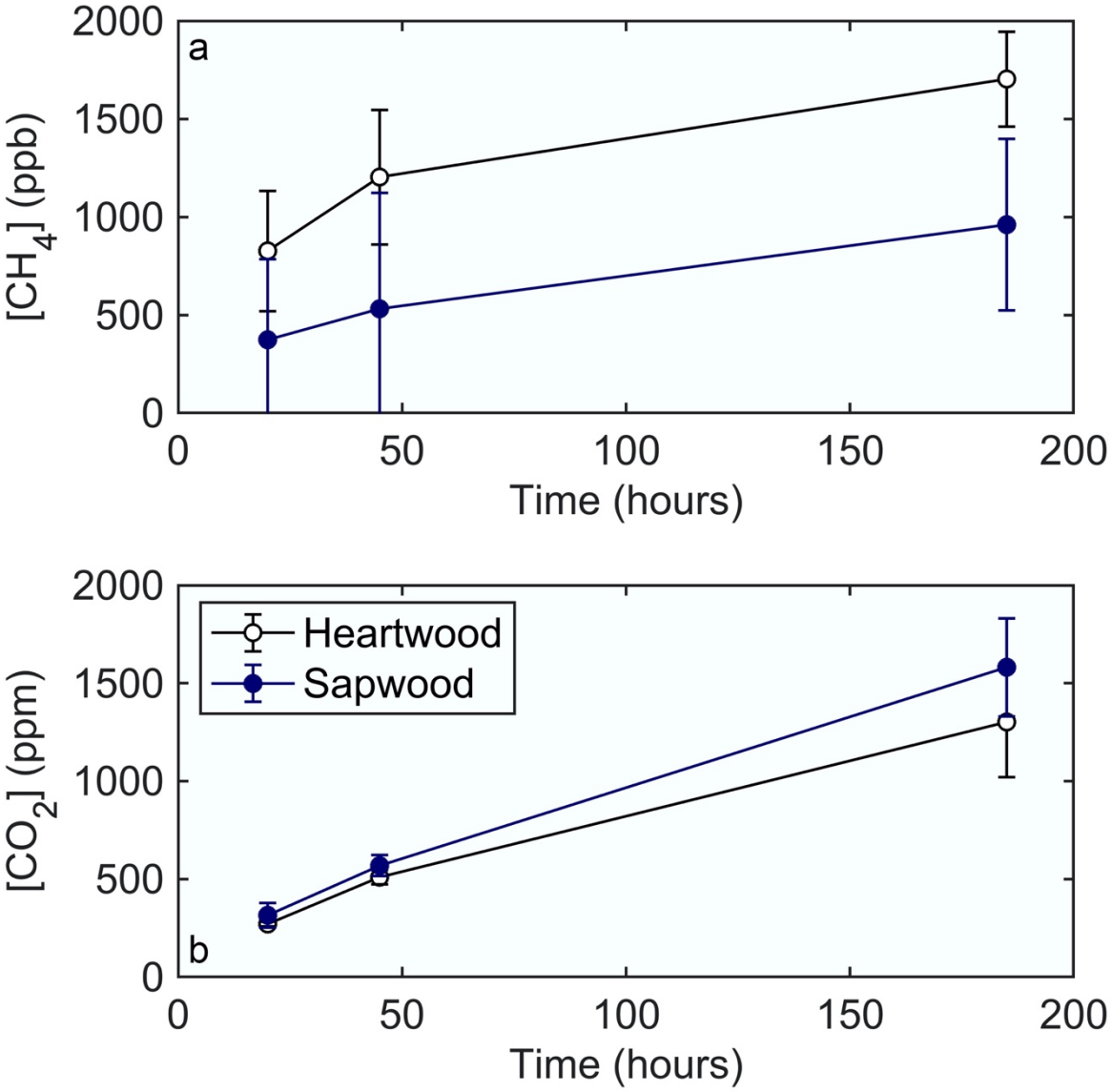

Figure 7.6.1: Production of (a) methane and (b) carbon dioxide by heartwood and sapwood during anaerobic incubation. Values represent the mean of heartwood and sapwood samples (n=4) ± SE. For both $[CH_4]$ and $[CO_2]$, time was a significant effect, whereas sample type and their interaction were not. Statistical significance based on a two-factor, repeated measures ANOVA (time is the repeated factor) for CO_2 and ln($[CH_4]$) values. Methane values were transformed due to non-normal distribution of sapwood $[CH_4]$ values at 20 and 40 hours, and heartwood $[CH_4]$ values at 164 hours based on Shapiro-Wilk normality tests. For ln($[CH_4]$), time effect, $F_{(2,12)}$=5.06, P<0.001, sample effect, $F_{(1,6)}$=3.00, P=0.13, and their interaction, $F_{(2,12)}$=1.08, P=0.37. For $[CO_2]$ values, time effect, $F_{(2,12)}$=28.6, P<0.001, sample effect, $F_{(1,6)}$=0.10, P=0.75, and their interaction, $F_{(2,12)}$=0.18, P=0.84.

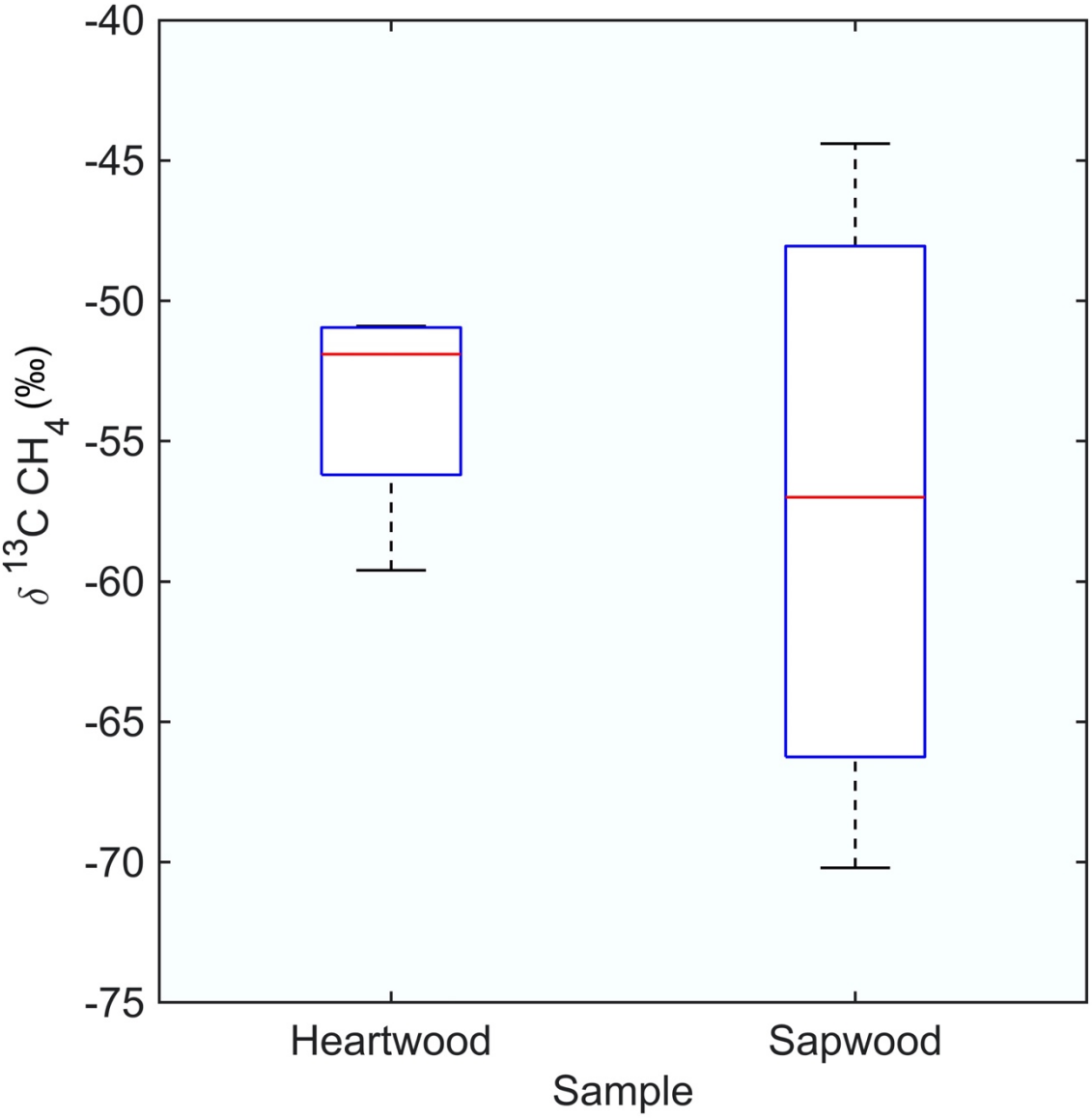

Figure 7.6.2: Box and whisker plots for the stable carbon isotope composition ($\delta^{13}C$) of methane produced by heartwood and sapwood following 185 hours of anaerobic incubation (n=4). $\delta^{13}C$ CH_4 values did not differ significantly for sample type, based on a Kruskal-Wallis test ($X^2_{(1,6)}$=0.33, P=0.56)

7.7 Effect of water content on the magnitude of methane production in tree cores

Incubation experiments were performed to investigate the role of water on methane production processes using tree core samples from the 9 trees of study within the HSNR (Fig. 2.2). Incubation experiments were the same as previously described (See section 2.2.4 to 2.2.5), using saturated tree cores (2.8 ± - 0.39 g broken into 8 pieces) with and without the addition of 60 mL sterile H_2O. Discrete gas samples were collected after 10 and 20 hours of incubation for analysis as previously described. Tree core samples submerged in water produced significantly greater quantities of methane than samples not submerged in water, with average methane concentrations over 13-fold greater at every time point measured (Fig. 7.7). Interestingly, the addition of water to tree core samples did not significantly change the rate of CO_2 production (Fig. 7.7). These results are consistent with previous studies, whereby the internal methane concentration in tree stems was significantly higher with greater water content (Wang *et al.*, 2017; Wang *et al.*, 2021). Increased methane production in tree stems with significant water content was attributed to decreased oxygen content providing more favourable conditions for methane production (Wang *et al*., 2017), however additional properties should be considered. Decomposition of organic matter relies on the molecules accessibility to enzymatic attack (Bertolet *et al.*, 2019), so low water content could hinder the rate of decomposition by limiting the diffusion of soluble substrates.

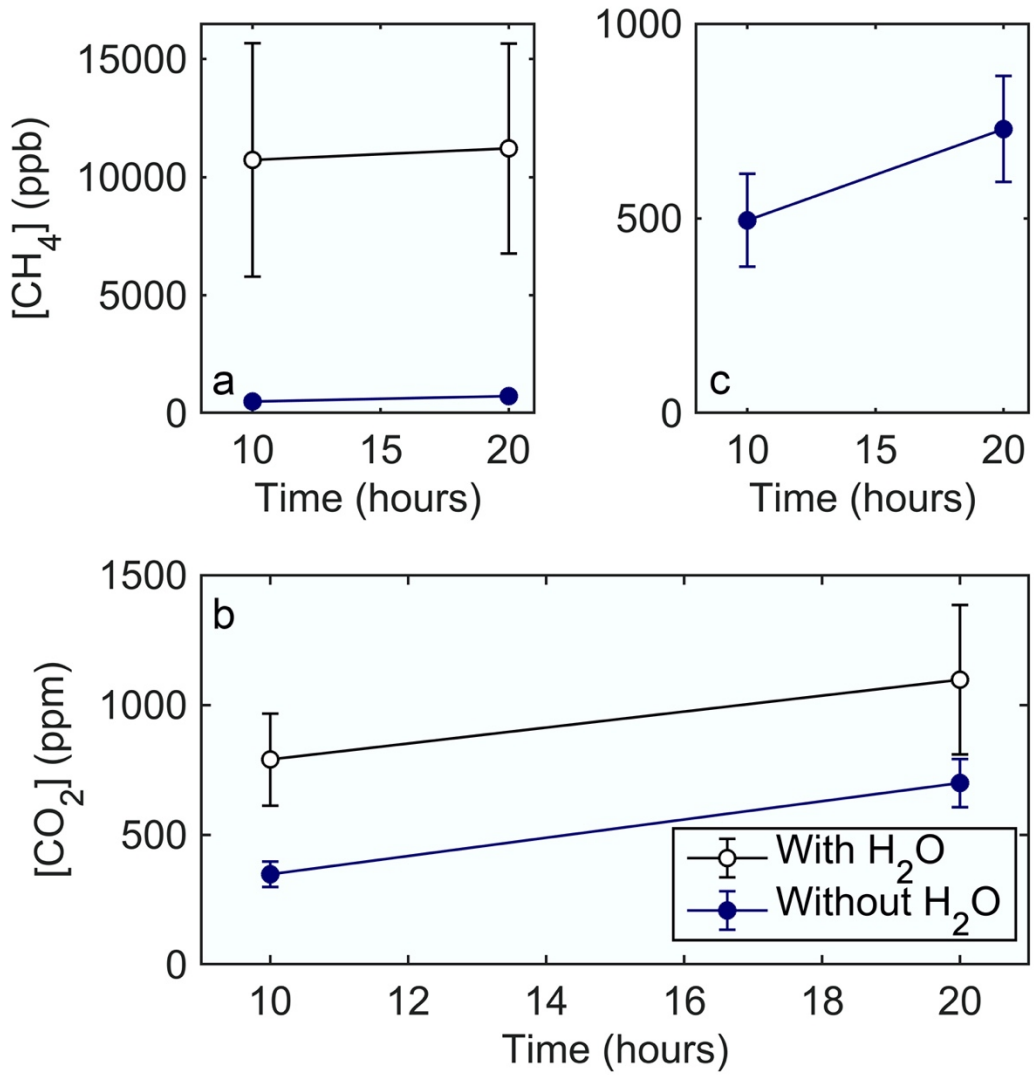

Figure 7.7: Gas production of (a & b) methane on different y-axis scales and (c) carbon dioxide by tree cores (*Populus spp.)* submerged and not submerged in water. Values represent the mean (n=4) ± SE. Sample type, time and their interaction were significant effects for [CH_4], while only time was a significant effect for [CO_2]. Statistical significance based on a 2-factor, repeated measures ANOVA (time is repeated factor) for [CO_2] and ln([CH_4]) values. Methane values were transformed due to non-normal distribution of water-soaked tree core [CH_4] values, based on Shapiro-Wilk tests of normality, and heterogeneity of variance. For ln([CH_4]), sample effect $F_{(1,16)}$=22.4, P<0.001, time effect, $F_{(1,16)}$=89.6, P<0.001, and interaction effect $F_{(1,16)}$=30.8, P <0.001. For [CO_2], sample effect, $F_{(1,16)}$=0.19, P=0.67, time effect, $F_{(1,16)}$=84.9, P<0.001, and interaction effect, $F_{(1,16)}$=1.39, P=0.08.

7.8 Comparison of LOESS models for data smoothing

LOESS is a nonparametric method used to smooth scatterplots by locally weighted regression and provide a relationship between two variables (Cleveland & McGill, 1984; Martinez & Martinez, 2002). The model chosen performs first degree polynomial local regression, and numerous smoothing parameters were attempted, choosing a model that most accurately fit the data (Fig. 7.8).

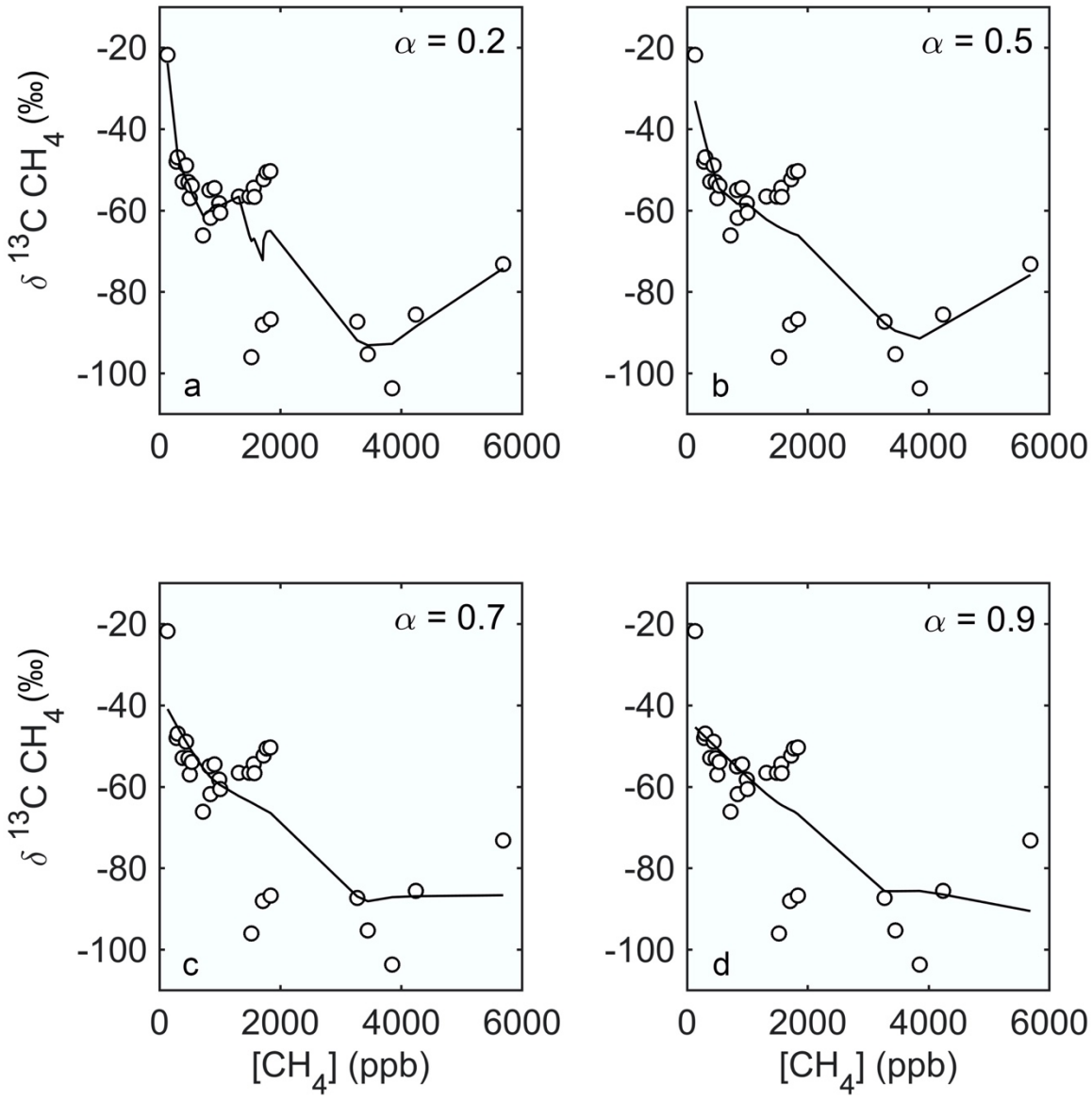

Figure 7.8: Representative comparison of smoothing parameters for linear LOESS models performed on tree core incubation data (see Fig. 3.10 b). The smoothing parameter (a-d) is shown in the top right corner (α). Root mean square error values for the loess models: (a) 9.87, (b) 10.8, (c) 10.8, and (d) 12.3. The α value of 0.7 was chosen for its low root mean square error, and absence of disproportionate effect elicited by values at the tail end of the curve.